FACULDADE DE ENGENHARIA DA UNIVERSIDADE DO PORTO

Development of Computational Methods for the Analysis of Neural Coding Mechanisms of Sensory Information in the Spinal Cord

Cristiana Raquel da Silva Carpinteiro

Mestrado Integrado em Bioengenharia

Supervisor: Paulo de Castro Aguiar

July 22, 2019

Development of Computational Methods for the Analysis of Neural Coding Mechanisms of Sensory Information in the Spinal Cord

Cristiana Raquel da Silva Carpinteiro

Mestrado Integrado em Bioengenharia

July 22, 2019

Resumo

A medula espinal é uma estrutura central do sistema nervoso que tem um papel chave na perceção sensorial. Patologias associadas a esta estrutura, como dor crónica e lesões vertebromedulares, são particularmente devastadoras. Para o desenvolvimento de estratégias de tratamento adequadas é necessário um conhecimento detalhado dos mecanismos de transmissão e integração de informação sensorial na medula espinal. A coluna dorsal está encarregue de processar a informação sensorial e transmiti-la para regiões supra-espinais. Contudo, a maior parte dos detalhes sobre os mecanismos por detrás destas funções são ainda desconhecidos. As recentes melhorias nas tecnologias de microeléctrodos (MEA), aliadas aos novos conhecimentos sobre como estimular, registar e descodificar atividade neuronal, têm possibilitado avanços importantes em neurociência e no estudo dos mecanismos acima mencionados. Desta forma, o principal objetivo desta dissertação consistiu no desenvolvimento de métodos computacionais para i) a análise dos mecanismos que alicerçam a codificação de informação sensorial nas vias ascendentes e ii) a análise dos circuitos espinhais. De modo a estudar as diferentes hipóteses de codificação, foi desenvolvido um modelo realista dos mecanismos de integração de informação nas vias ascendentes suportado por resultados experimentais. Este modelo foi capaz de simular a codificação de temperatura absoluta e a localização do estímulo na pele e apresenta flexibilidade para integrar outros mecanismos de codificação e modalidades de estímulo. O estudo dos circuitos neuronais foi possível graças à implementação e validação de uma metodologia de inferência de conectividade. As ligações funcionais foram detetadas usando um algoritmo implementado em Python - histograma de correlação cruzada filtrada e normalizada (FNCCH) - e filtradas para obter conexões biologicamente realistas. Foram desenvolvidas e validadas três visualizações distintas para evidenciar a estrutura da rede e possíveis ligações escondidas. A metodologia desenvolvida foi bem-sucedida na identificação de ligações funcionais concordantes com a estrutura imposta em experiências com microfluídica. Protocolos experimentais automatizados foram codificados e implementados no hardware de aquisição de dados com MEAs para lidar com a complexidade e volume de dados associados a experiências de análise de circuitos espinhais. Os programas personalizados permitiram a amostragem automática em fatias da medula espinal, usando ciclos controlados de estimulação e aquisição de dados. A medula espinal possui atividade espontânea reduzida pelo que a estimulação é absolutamente necessária para ativar os circuitos espinais.

Em suma, as ferramentas desenvolvidas - modelo computacional de integração de informação sensorial, algoritmo e visualização de inferência de conectividade e protocolos experimentais automáticos – melhoraram consideravelmente a aquisição/análise de dados em experiências de eletrofisiologia com MEAs, potenciando a compreensão da integração de informações sensorial na medula espinal.

Abstract

The spinal cord is an important structure of the central nervous system that plays a key role in sensory perception. Pathologies associated with the spinal cord, such as chronic pain and vertebral-medullary lesions, are particularly devastating. For the design of adequate therapeutic strategies, the thorough knowledge of the mechanisms behind spinal cord sensory information integration and transmission is of utmost importance. The dorsal horn has a central role in processing sensory information and transmitting it to supraspinal regions. Nevertheless, most of the details regarding the coding and integration mechanisms occurring in this structure are still unknown. Recent improvements in microelectrode arrays (MEAs) and new knowledge on how to stimulate, record and decode neuronal activity, have made possible important advances in neuroscience and in the study of these mechanisms. Hence, the main goal of this dissertation was to devise computational methods that allow i) for the analysis of the mechanisms behind sensory information coding in the ascending tracts, and ii) the analysis of spinal circuitry. A realistic model of sensory information integration and transmission was devised to study the different coding hypotheses based on experimental findings. The model successfully simulated the coding of absolute temperature and stimulus location and presents flexibility to integrate other coding mechanisms and stimulus modalities. The study of neuronal circuitry was achieved by implementing and validating a functional connectivity inference pipeline. Functional connections were detected through a Python implementation of the Filtered Normalized Cross-Correlation Histogram (FNCCH) algorithm. Three different visualizations were developed and validated to highlight hidden connections and more easily visualize the structure of the network. The developed pipeline successfully identified functional connections consistent with the structure imposed in experiments with microfluidic compartmentalization. Automated experimental protocols were coded and implemented in the electrophysiology MEA hardware to deal with the complexity and sheer volume of data associated with the circuit analysis experiments. The custom-made programming scripts allowed automated sampling in spinal cord slices, using controlled cycles of stimulation and recording from the MEAs. Spinal cord slices have very limited spontaneous activity, so stimulation is necessary to activate the spinal circuits.

Altogether, these developed tools - computational model of sensory integration, connectivity inference algorithms and visualization, and automated experimental protocols - greatly improve data acquisition/analysis of MEA electrophysiology experiments, potentially fostering our understanding of sensory information integration in the spinal cord.

Agradecimentos

Primeiro de tudo, queria agradecer ao meu orientador, o Dr. Paulo Aguiar, pela oportunidade, por todo o apoio e por tudo aquilo que me ensinou. Foi deveras um privilégio trabalhar no NCN e gostava de agradecer a todos os membros do grupo por me terem feito sentir que fazia parte desta equipa espetacular. Um obrigada especial ao Zé e ao Miguel por terem disponibilizado os dados das suas experiencias para eu poder fazer as minhas análises e ao Domingos por me ter ajudado a desenvolver o protocolo de estimulação ao som de boa música.

Numa nota mais pessoal, gostava de agradecer aos meus pais, que sempre acreditaram em mim em todas as etapas da minha vida, fossem elas boas ou más. A pessoa que sou hoje é mais forte por vossa causa e espero nunca vos desiludir. Ao meu irmão pelo exemplo de determinação e força de vontade e por todos os conselhos sinceros. Ao Tiago por me conseguir fazer rir sempre e por acreditar mais em mim do que ás vezes eu acredito em mim própria. Sou uma pessoa melhor por tua causa. Obrigada por tudo. Aos amigos da terrinha por tornarem Barcelos a cidade mais fixe de Portugal. Um especial obrigada à Leonor por todas as aventuras estúpidas ao longo destes anos e por ter estado lá para mim sempre que precisei. Ao Paulo, à Mariana, à Carolina, à Marina, à Lena, à Francisca, à Patrícia... Amigos que conheci na faculdade mas que levo para a vida. Obrigada Maggie e Joana por todas as pausas para café terapêuticas. Obrigada Maggie por me ajudares sempre independentemente de tudo.

Todas estas pessoas contribuiram para que terminasse esta etapa com sucesso.

Obrigada!

"Nothing is permanent, not even our troubles."

Charlie Chaplin

Contents

List of Figures

List of Tables

Abbreviations

ACSF	Artificial Cerebrospinal Fluid
API	Application Programming Interface
CNS	Central Nervous System
CM	Connectivity Matrix
DSP	Digital Signal Processor
DRG	Dorsal Root Ganglia
DIP	Dual In-line Package
DLL	Dynamic Link Library
ECAP	Electrically Evoked Compound Action Potentials
FNCCH	Filtered Normalized Cross-Correlation Histogram
HTMR	High-Threshold Mechanoreceptor
LCN	Local Circuit Neuron
LTMR	Low-Threshold Mechanoreceptor
MEA	Micro-Electrode Arrays
MEA-SG	256MEA Signal Generator
MCS	MultiChannel Systems
NE	Nerve Endings
PBS	Phosphate-Buffered Saline
PNS	Peripheral Nervous System
SNR	Signal-to-Noise Ratio
SCI	Spinal Cord Injury

Chapter 1

Introduction

The human nervous system possesses one of the most complex architectures ever known. In recent years, efforts to understand its mechanism have incited technological progress. In fact, artificial neural networks, a revolutionary computing system, were inspired in biological neural networks, drawing knowledge from the basis of neural communication.

The spinal cord is the main pathway of communication between the brain and the rest of the body, allowing for the collection signals from the outer world and the interaction with it. Spinal cord injury (SCI) interrupts this communication, compromising several fundamental body functions. Therefore, it is easy to understand why SCI is such a debilitating condition. Normally, it is caused by trauma, resulting from an accident, which means it strikes unexpectedly, transforming completely the lives of the ones who suffer it. According to the World Health Organization, between 250k and 500k people suffer a SCI, every year. Besides having their quality of life drastically reduced, patients with SCI are 2 to 5 times more likely to die prematurely [107]. Restoring spinal cord function is, thus, an appealing goal, yet very demanding. Beyond restoration of motor control, it is of fundamental importance to regain sensory function, this requires a thorough knowledge of the mechanisms behind information integration and transmission at the spinal cord level. Both pharmacological therapies and neuroengineering solutions, such as direct electrical stimulation of the spinal cord, demand the investigation about modulation and controlling methods of the electrical activity of neurons, the working units of the nervous system. The patterns of electrical activity of neurons encrypt information about the stimulus that triggered it. The search for a neural code, a language that describes the translation between stimulus and response, is the motivation behind neuroscience and requires the alliance of traditional (neuro)biology techniques with other areas of study to grasp the complexity of it.

The recent improvements in micro-electrode arrays (MEAs) technologies propelled the research in the neuroscience field. MEAs are devices that enable the simultaneous recording and stimulation of large populations of neurons in a non-invasive way for long periods of time, giving relevant information about population dynamics and the neural code [91].

The keyword to understand the nervous system is **information**. Thus, the future of neuroscience involves inevitably approaches in computational theory, signal processing, biophysics,

computational modeling, and simulation. For this reason, in this dissertation, neurons are viewed as biological units for information processing and transmission, going beyond the conventional neurobiological approach.

1.1 Motivation

The neurons from the dorsal horn play an essential role in the perception of changes both inside and outside the body, being responsible for the integration and processing of sensory information before its transmission to the brain. Despite its high importance, there is still no detailed description of how the sensory information is processed in the spinal neural circuits. The discovery of these mechanisms can give way to better therapeutic strategies to both restore spinal functioning in the context of SCI and tackle fundamental problems, such as chronic pain. Knowing the principles behind these processes, it is possible, for example, to design correct electrical stimulation protocols that mimic normal function, reestablishing the lost communication. This dissertation takes important steps towards the clarification of the coding and transmission mechanisms in the spinal cord, by developing specific computational tools to deal with the complexity in MEA data acquisition/analysis. These computational tools are created with the purpose of facilitating the process of identifying the governing principles of sensory information encoding in the ascending pathways.

1.2 Objectives

This work is framed in the recently funded FCT research project MindTheGap and its main goal is to devise computational methods to analyze the mechanisms behind sensory information coding in the spinal cord, with the purpose of answering the following research questions:

- How is peripheral sensory stimulation mapped in the spinal cord?
- What are the local circuits supporting sensory integration in this structure?
- How is sensory information encoded in the ascending tracts?

To fulfill these objectives, this work will encompass the development of a library for simulation of spinal sensory information integration and transmission using the NEURON simulation environment, the implementation of algorithms for automatic identification of functional connections in experimental data acquired with MEAs, and the design of a custom-made automated protocols for the stimulation and recording of spinal cord slices.

1.3 Challenges

The current electrophysiological methods to record neuronal activity still present challenges. MEAs excel in temporal resolution, however, the spatial precision is limited, so electrodes record

the activity of several neurons at the same time, which difficults data analysis. Moreover, neural activity is inherently noisy, making it hard to isolate the relevant information encrypted in the electrical signal. Furthermore, the existing coding hypotheses, especially for the processes occurring in the spinal cord, are incomplete. Models contemplate only a few stimulus modalities and significantly reduce the complexity of the nervous system. Also, coding schemes are not usually tested and simulated in a virtual environment, to assess its reliability. The present work tries to fill these gaps.

1.4 Document structure

This document is structured in 7 chapters. Background information and review of the literature is provided in Chapter 2. This Chapter first presents a description of the anatomical aspects of the spinal cord and, in more detail, of the dorsal horn and gives an overview of the pathologies that affect the spinal cord and the therapeutic potential of neuroprosthesis and spinal cord stimulation. Then describes the basic principles behind the generation of electrical signals and the methodologies used to record these, highlighting the importance of MEAs. Finally, approaches the different coding strategies in the nervous system and the current hypothesis for the coding in the spinal cord. Chapter 3 presents the fundamentals of the developed model, its structure and the functionalities implemented, and presents and discusses the results of the developed framework. Chapter 4 describes the connectivity analysis pipeline and discusses the results obtained for the testing of the algorithm in the different datasets. Chapter 5 details the experimental setup implemented to both stimulate and record activity in the spinal cord and examines the outcome of the experiment performed and the main obstacles. Finally, Chapter 6 draws the main conclusions about the work developed. Prospective future directions are presented at the end of the document.

Chapter 2

Literature Review

This Chapter explores the anatomical and physiological aspects of the spinal cord and, in more depth, of the dorsal horn and the ascending tracts. Additionally, it describes the methods and principles behind neural activity recordings, highlighting the importance of MEAs for the problem in hands. Furthermore, it reviews the state-of-the-art of coding strategies in the nervous system, mentioning the ones that prevail in the spinal cord.

2.1 The Spinal Cord

The spinal cord is the information highway of the nervous system, transmitting signals to and from the brain to the rest of the body. It is responsible for the perception of the outer world, its state and threats. Injuries in this structure break this connection, and consequently, the most basic functions of the body are compromised. Understanding the spinal cord in physiological conditions is fundamental to devise appropriate and effective therapeutic strategies for pathological conditions. In this chapter, it will be addressed the underlying mechanisms and anatomical principles that make this communication possible. As this thesis is focused on sensory information integration and transmission (and not on motor information), this chapter gives more attention to the spinal cord structure associated with the somatosensory system: the dorsal horn. As to better understand the anatomy (circuit architecture) and electrophysiology (dynamics) of the dorsal horn, this chapter starts with a general overview of neurobiology and the organization of the nervous system.

2.1.1 Principles of neurobiology

The building blocks of the nervous system are electrically excitable nerve cells, named neurons. These cells are responsible for the transmission and processing of information. The neuron is constituted by the cell body or soma, where the nucleus is located, dendrites, whose function concerns the transmission of the electrical impulses (action potentials) to the cell, and an axon, a long, slender projection that specializes in the conduction of electrical impulses, outward and away from the cell body towards the axon terminus. The length of an axon may vary: it can traverse large fractions of the brain or, in the peripheral nervous system, the entire body. Additionally, it

may be myelinated or unmyelinated, whether it possesses an electrically insulating layer, called myelin sheath, or not. Myelinated axons drive electrical impulses faster, since the propagation occurs from one node of Ranvier (gap between myelin sheats) to the next. In Fig.2.1 can be observed a real neuron with the detailed morphology pointed out.

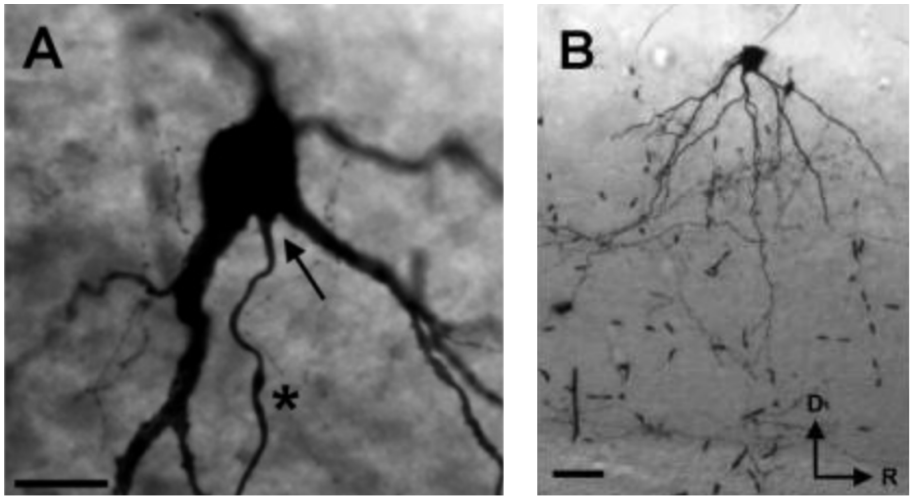

Figure 2.1: **(a)** General morphological features of the axon of local circuit neuron (LCN) from lamina I lumbar spinal cord. Main axon (asterisk), with origin in the soma (arrow). **(b)** Photomicrograph of the soma, dendrites, and axon branches of a typical flattened LCN in a sagittal spinal cord section. Adapted from [95].

As above stated, the fundamental goal of the nervous system is information processing. This is possible through the organized communication of neurons, which is mainly carried out by synapses. This process typically occurs between the axon of one neuron and the dendrites of the next. Synapses can be one of two kinds: electrical or chemical. Electrical synapses are less frequent than chemical ones. In electrical synapses, the membranes of the two communicating neurons are linked together by an intercellular specialization, called gap junction, allowing ionic currents to flow passively through the gap junction pores from one neuron to another [78]. On the other hand, chemical synapses occur through the diffusion of signaling molecules, known as neurotransmitters, to pass rapidly from one cell to the other. The complex branching structure of the dendritic tree enables the reception and compartmentalization of inputs from several other neurons.

In fact, based on the information they convey, neurons can be categorized in different specializations. Sensory neurons respond to one particular type of stimulus, such as temperature or touch, and converts it to an electrical signal. Motor neurons receive signals from the brain and spinal cord to control muscle contraction or glandular output. Finally, interneurons make the connection between two neurons, within the brain or spinal cord.

2.1.2 Organization of the nervous system

The nervous system can be divided into two major parts, the central nervous system (CNS), that consists in the brain and the spinal cord, and the peripheral nervous system (PNS), which connects the central nervous system to the rest of the body.

At a structural level, the central nervous system is organized in gray matter and white matter. Gray matter is made of neurons, embedded in neuroglia, a tissue specialized in nutrition and support of the central nervous system, while white matter refers to the areas that are mainly constituted by myelinated axons. In Fig. 2.2 can be observed a diagram portraying the organization of the nervous system.

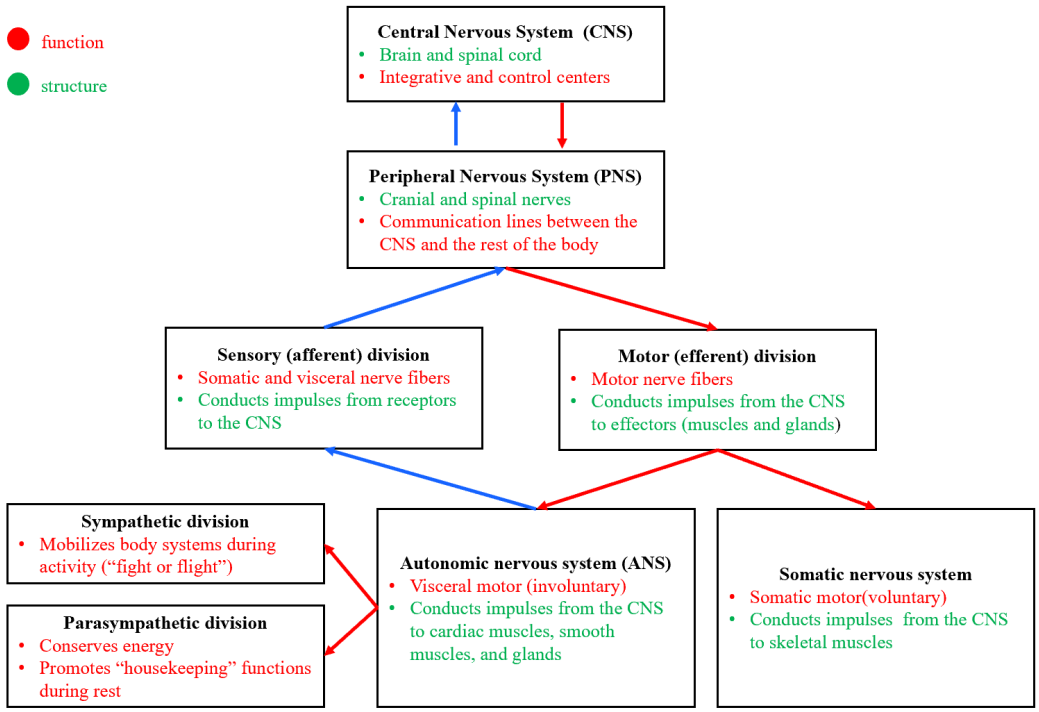

Figure 2.2: Diagram portraying the major divisions of the nervous system and its main functions and general structure.

The autonomic nervous system is responsible for involuntary control of the body, accounting for the innervation of involuntary structures, namely the heart, smooth muscle, and glands. There are two divisions of the autonomic nervous system – the sympathetic and the parasympathetic[15]. The sensory or afferent division carries sensory signals through afferent nerve fibers coming from receptors in the peripheral nervous system. It is constituted by the somatic and visceral divisions. The somatic sensory division carries signals from receptors in the skin, muscles, bones, and joints, while the visceral sensory division carries signals mainly from the viscera of the thoracic and abdominal cavities [63]. On the other hand, the motor (efferent) division carries motor signals by way of efferent nerve fibers from the CNS to effectors (mainly glands and muscles). It can be subdivided into somatic and visceral divisions. The somatic motor division carries signals to

the skeletal muscles. The visceral motor division, also known as the autonomic nervous system, carries signals to glands, cardiac muscle, and smooth muscle. It can be further organized into the sympathetic and parasympathetic divisions, which are responsible for the arouse and calming of the body, respectively [63].

2.1.3 Neuroanatomy of the spinal cord

The spinal cord is located inside the vertebral canal of the vertebral column. It is surrounded by three meninges, namely the dura mater, the arachnoid mater, and the pia mater, observed in Fig. 2.3. The cerebrospinal fluid gives extra protection and it is located in the subarachnoid space, surrounding the spinal cord. The spinal cord begins at the foramen magnum in the skull and terminates in the lumbar region [63].

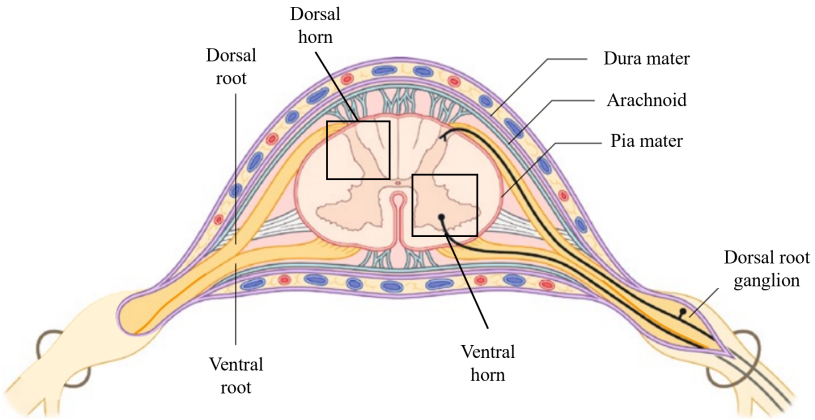

Figure 2.3: Spinal cord cross-section. The spinal cord is protected by a set of membranes: the pia mater, the arachnoid mater and the dura mater. The dorsal and ventral roots, emerge from the posterior and anterior columns of the spinal cord, respectively. Adapted from [15].

Along with its length, the spinal cord varies in size and shape, depending on whether the emerging motor nerves innervate the limbs or trunk. The spinal cord is organized in an inner core of gray matter surrounded by an outer layer of white matter.

From the spinal cord emerge 31 pairs of spinal nerves that link the spinal cord to muscles and sensory receptors in the skin. An area of the skin that is supplied by the same sensory nerve is called dermatome. The body can be divided into several dermatomes depending on the sensory nerve that supplies it, as seen in Fig.2.4. Each nerve has a sensory division that begins in the dorsal root and a motor division that rises from the ventral root. The dorsal roots carry sensory information into the spinal cord from muscles and skin. Different classes of axons coursing in the dorsal roots mediate sensations of pain, temperature, and touch. The cord also receives sensory information from internal organs. The ventral roots are bundles of the outgoing axons of motor neurons that innervate muscles. The motor neurons of the spinal cord comprise the *final common pathway* since all higher brain levels controlling motor activity must ultimately act through these

neurons in the ventral horn and their connections to muscles. Ventral roots from certain levels of the spinal cord also include sympathetic and parasympathetic axons [48].

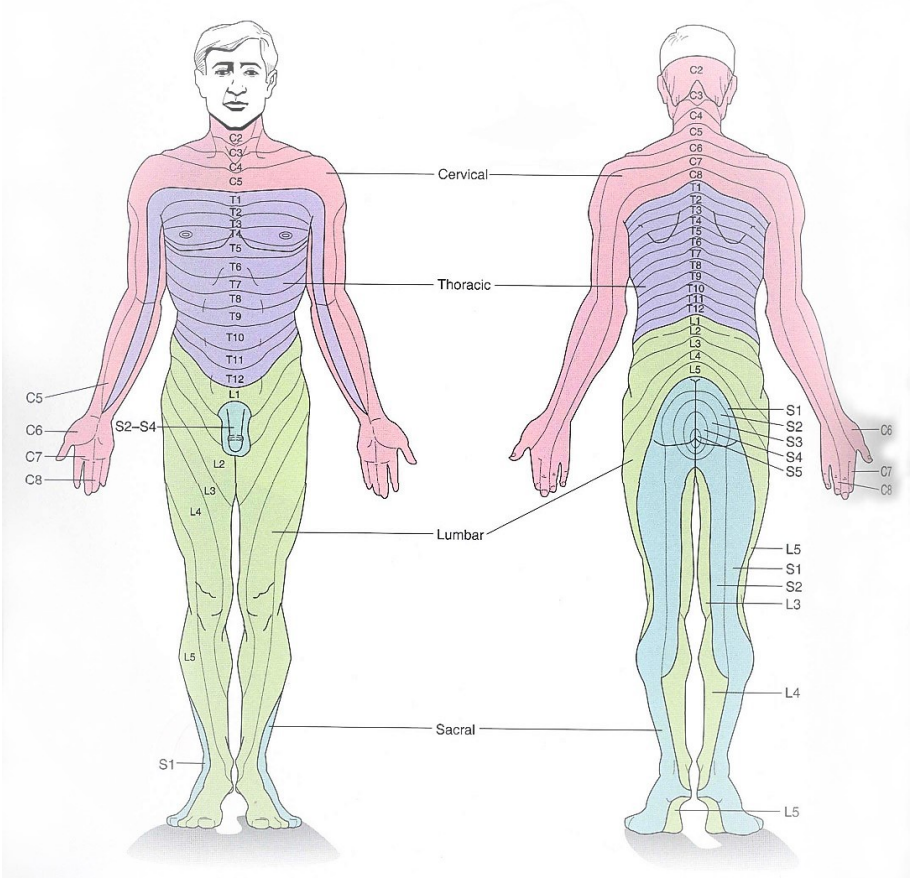

Figure 2.4: The area of skin supplied by a single spinal nerve is called a dermatome. In the trunk the dermatomes are roughly horizontal. In the limbs, dermatomes have been stretched out by the advancing limb bud during development. Adapted from [14].

Looking at the cross section of the spinal cord, Fig. 2.3, it is possible to observe a butterfly-shaped gray matter core. It is typically divided into dorsal and ventral horns. The dorsal horn contains an orderly arrangement of sensory neurons that receive input from the periphery, while the ventral horn contains motor nuclei that innervate specific muscles. The white matter is constituted by longitudinal tracts of myelinated axons that form the ascending pathways through which sensory information reaches the brain and the descending pathways that carry motor commands, and modulatory influences from the brain[48].

2.1.3.1 Dorsal horn architecture

The dorsal or posterior horn is further subdivided into 6 layers or laminae, in an organization that can be observed in Fig. 2.5. Their denomination is not only based on their topographic organization, with the lower numbers being towards the back of the spinal cord, but also on the types, and functions, of the neurons in each laminae.

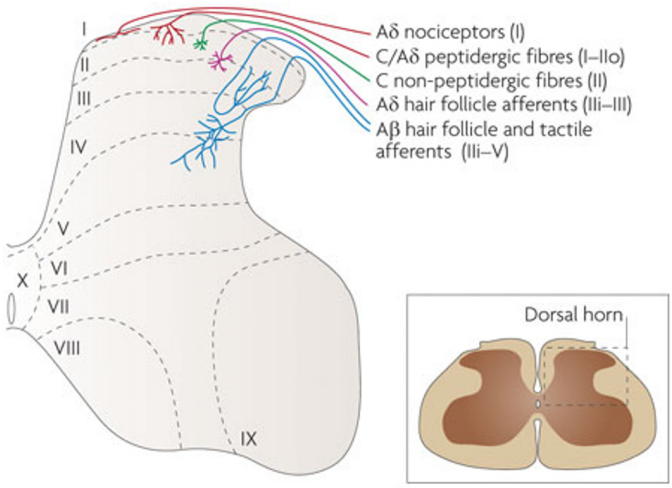

Figure 2.5: Laminar organization of the dorsal horn and primary afferent inputs. Primary afferents terminate in the dorsal horn in an organized way. Myelinated A tactile and A hair afferents end mainly in lamina III–V, with some ramifications to lamina IIi. A hair afferents branch in lamina II and lamina III, whereas A nociceptors terminate mainly in lamina I. C/A peptidergic afferents arborize mainly in lamina I and lamina IIo, while non-peptidergic C afferents terminate in the lamina II [66]. Figure adapted from [99].

Lamina I, also called the posterior marginal nucleus, locates at the outermost tip of the dorsal horn. Cells in this layer answer to primary afferent axons carrying information about pain and temperature sensations. Most of the neurons located here give rise to axons of the spinothalamic tract (further explained on subsection 2.1.3.2).

Lamina II, also called *substantia gelatinosa*, receives afferent fibers from Lissauer's fasciculus, conveying impulses important in transmission of pain, temperature and touch. It is primarily composed of Golgi II interneurons, which broadly project to secondary neurons in laminae I and V [38].

Lamina III and IV, also named *nucleus proprius*, include interneurons that receive touch and pressure stimuli. The dendrites of some of these neurons project into lamina II, while axons of certain neurons contribute to the spinothalamic tract.

Lamina V is situated at the neck of the dorsal horn. Neurons here receive input from afferent axons transmitting both harmfull and innocuos stimuli. Similar to what happens in laminae III and IV, axons of interneurons cross to the contralateral side and colaborate in the spinothalamic tract.

Lamina VI is located at the base of the dorsal horn in the cervical and lumbar enlargements and only conveys afferent input from central processes of primary sensory neurons [26].

Besides neurons from local circuitry and interneurons, the dorsal horn possesses also projection neurons that give rise to the different ascending tracts.

2.1.3.2 The ascending tracts

The ascending tracts refer to the neural pathways by which sensory information from the peripheral nerves is conveyed to the cerebral cortex. It is linked to the conscious perception of touch, pressure, pain, temperature, position, movement and vibration, coming from muscles, joints, skin, and fascia. It obeys three major functions: exteroceptive and interoceptive, which control response to external and internal stimuli, respectively, and proprioceptive, for the perception and control of body movement and balance [6].

Sensations detected in the periphery are forwarded through pathways via the spinal cord, brainstem, and thalamic relay nuclei to the sensory cortex in the parietal lobe over a 3-neuron system [3], as seen in Fig. 2.6. First, occurs the activation of primary sensory neurons whose cell bodies lie within the dorsal root ganglia (DRG) and cranial sensory ganglia. DRG neurons convert the physical and chemical state of the external and internal environment into neuronal activity [104]. DRG neurons are pseudounipolar, with one axonal branch that reaches peripheral targets, such as receptors located in the skin or muscles, and another axon that enters the spinal cord directly, without synapsing [6]. The total length of the processes of the primary neurons can reach over 2 meters (from receptors in the big toe to the medulla) [26]. At this point, the axon forms branches that either communicate with second-order neurons in the spinal cord gray matter or ascend to nuclei located at the junction of the spinal cord with the medulla [48].

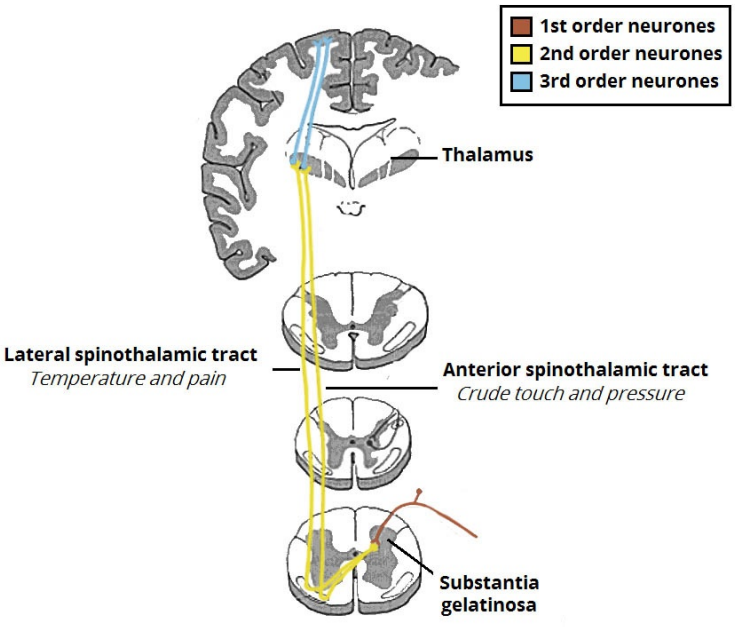

Figure 2.6: The spinothalamic tracts, which carry the sensory information of crude touch, pressure, pain and temperature. Adapted from [4].

The exteroceptive somatosensory system is specialized in the detection of harmful sensations. The perception of innocuous and harmful touch depends on special mechanosensitive sensory neurons that can be classified into two classes: low-threshold mechanoreceptors (LTMRs) and

high-threshold mechanoreceptors (HTMRs), that respond to innocuous and harmful mechanical stimulation, respectively [6].

The ascending branches are conveyed to lower brain regions (location of third-order neurons) where they are processed. In case of fast responses, the processed information may be dispatched directly to a motor system. But, when a thorough analysis is necessary, the information is transmitted to higher brain regions for additional processing. The sensory input reaches then the forebrain where the perception of complex patterns occurs. Fibers coming from the lower part of the body project to the superior aspect of the cortex, while fibers from the thoracic and cervical regions end in the more inferior aspect of the cortex. This fiber arrangement leads to an inverted representation of the body in the cortex identified as homunculus [26].

Differently tuned sensory pathways are uniquely activated by distinct stimuli modalities and the corresponding sensation depends on which pathway is activated, according the labeled line theory [104].

The ascending tracts can be organized into different tracts, which denomination is based on the trajectory of the nerve fibers, from the site they start (spinal cord) to the site they terminate, thalamus and cerebellum, respectively. Although this thesis will focus on the spinothalamic tract, for completeness a detailed list of the ascending tracts is provided.

The Anterolateral System

The anterolateral system consists of two separate tracts: the lateral and anterior spinothalamic tracts.

The lateral spinothalamic tract conveys sensations of pain and temperature from receptors throughout the body (except the face) to the brain. Free nerve endings, projected from processes of primary neurons, are sensitive to molecules indicative of cell damage and are, therefore, the principal receptors. The central processes of the primary neurons enter the Lisauer's fasciculus and ascend at least one segment before entering the dorsal horn to synapse with the secondary neurons (interneurons) [48]. Secondary neurons of the spinothalamic tract are mostly found in laminae I, IV, V and VII. Interneurons from laminae I and V ascend in the lateral spinothalamic tract, through the brainstem, reaching the thalamus. The third order neurons in the thalamus will, then, project to various regions of the somatosensory cortex [48].

On the other hand, the anterior spinothalamic tract conducts impulses related to sensations of light, poorly localized touch.Axons of the primary neurons drive impulses of soft touch from receptors in the hairless areas of the skin to the cell bodies located in the DRG. The central processes of these primary neurons reach into the dorsal horn, through laminae IV to VII. Here, they synapse with secondary neurons, whose axons cross in the anterior white commissure and turn rostrally to form the anterior spinothalamic tract in the anterolateral part of the spinal white matter. In the medulla, this tract merges with the lateral spinothalamic tract. Finally,they reach the posterior region of the thalamus [74]. This tract is phylogentetically newer in mammals, contributing to more precise sensations of pain and temperature [26].

The Spinocerebellar Tracts

Within the spinocerebellar tracts, there are four individual pathways: the anterior and rostral spinocerebellar, the posterior spinocebellar and cuneocerebellar tracts.

The anterior and rostral spinocerebellar tracts convey impulses related to movement and position sense from tendon organs and muscle spindels to the cerebellum. The information conducted in this pathway may contain information regarding an entire limb. Peripheral processes of the primary neurons of the anterior spinocerebellar system approach their cell bodies in the DRG of lumbar and sacral spinal nerves. The central processes of these neurons enter the cord at these levels and synapse with interneurons in the bases of the posterior and anterior horns.The axons of these secondary neurons then cross to the contralateral side and turn rostrally to form the anterior spinocerebellar tract. Finally, the tract ascends the brain stem to enter the cerebellum.

On the other hand, the rostral spinocerebellar tract is the equivalent of the anterior tact for the upper limbs. The central processes of the primary neurons enter the cervical cord, synapsing with secondary neurons. The axons of these neurons remain uncrossed and join the rostral spinocereberllar tract, entering the superior cerebellar peduncle [48].

The posterior spinocerebellar tract conveys muscle spindle or tendon organ related impulses from the lower half of the body, while the cuneocerebellar tract transmits such impulses from the lower part of the body. The axons conducting impulses from the lower half of the body are large Ia, Ib, and II fibers, the cell bodies of which are in the spinal ganglia of spinal nerves below C8. Primary neurons below L3 deliver their processes into the laminae of the dorsal horn. These processes, then, bend and ascend in the laminae to the L3 level. From L3 up to C8, incoming central processes and those in the dorsal columns project to the medial part of lamina VII. At this point, the central processes of primary neurons synapse with secondary neurons, the axons of which are, then, rerouted to the leateral funiculi as the posterior cerebellar tracts. Finally, they ascend and communicate with the cerebellum. Fibers of this tract are among the most rapidly conducting elements of the central nervous system.

Similarly to the posterior spinocerebellar tract, the cuneocerebellar tracts conduct impulses from muscle spindels, tendon organs and skin but of the upper part of the body. The primary axons enter the spinal cord above C8 and the secondary axons run rostrally as the cuneocerebellar tract [48].

2.1.4 Spinal cord pathologies

The spinal cord carries in a small cross-sectional area nearly the whole sensory input and motor output of the trunk and limbs. Thus, diseases in this part of the nervous system cause more damage than in any other [31]. The diversity of pathologies associated with the spinal cord's sensory components are vast. This chapter focuses on spinal cord injury and chronic pain.

When the spinal cord is lacerated, it starts neurological damage in the spinal cord that is usually named *primary injury*. The mechanical injury produces a cascade of biological events, described as *secondary injury*, which results in additional neurological damage. Finally, there is the chronic

phase, which can occur days to years after the injury, leading to neurological impairments, including in brain regions. The chronic phase involves events such as white matter demyelination, exemplified in Fig. 2.7, gray matter dissolution, connective tissue deposition and reactive gliosis that lead to glial scar formation [88].

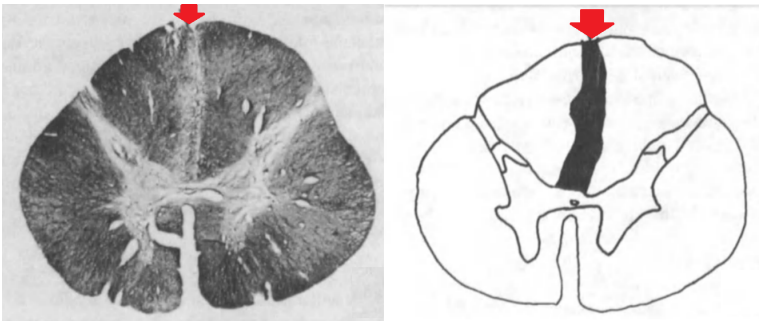

Figure 2.7: On the left, photomicrograph of cross section of the spinal cord just above the level of the lesion. The spinal cord section was stained for myelin, and the arrow shows a region of demyelination that demarcates the extent of the lesion, which interrupts the fasciculi gracilis bilaterally for a short distance on either side of the midline. On the right, ba drawing representing the extent of the demyelination. Adapted from [106].

The disability associated with irreversible spinal cord damage is determined primarily by the level of the lesion and by whether the disturbance in function is complete or incomplete [31]. A complete spinal cord injury (SCI) produces a total loss of motor and sensory function below the level of the injury, producing paraplegia or quadriplegia[31]. On the other hand, an incomplete injury causes damage in a limited section of the spinal cord, which leads to different disabilities depending on the areas affected. For example, anterior cord syndrome is associated with deficits referable to bilateral anterior and lateral spinal cord columns, which translates in loss of touch sensation, pain, temperature, and motor function below the level of the lesion. The posterior column functions of proprioception and vibratory sensation remain intact, though [9].

Other spinal cord syndromes include Brown-Sequard syndrome, which is caused by the damage to one half of the spinal cord, and central cord syndrome, the most common form of cervical SCI, causing loss of motion and sensation in the arms and hands.

Long-term complications after SCI may include respiratory, cardiovascular, urinary and bowel complications, spasticity, pressure ulcers, osteoporosis and bone fractures [84].

Despite the loss of sensory function, many patients with spinal cord injury experience chronic pain. The hyper-excitability of the sensory neurons of the dorsal horn is presented as the major causing factor [88].

2.1.5 Neuroprosthesis and the therapeutic potential of spinal cord stimulation

Neuroprosthesis have the potential to improve the quality of life of patients that have seen their mobility compromised either by a trauma or a disease in the spinal cord. By applying controlled electrical stimulation to paralyzed nerves and muscles, neuroprosthesis may restore part of their

function [7, 101, 10]. This is particularity important in patients where the conventional pharmacological approaches do not produce the intended results.

Contrary to what happens in the CNS, peripheral nerves when transected, exhibit regenerative abilities to a certain extent. Nevertheless, this process is slow and the target area may atrophy. By recording the electrical activity from the proximal nerve stumps, peripheral interfaces can produce motor commands for a neuroprosthesis, replacing central motor control. Furthermore, information can be translated into electrical impulses to excite the nerve, simulating tactile and proprioceptive sensation, thus, mimicking ascending pathways [7].

Clinical applications range from the control of micturition to activation of lower extremity motion and reduction of pain [68, 22]. Regarding the latter, investigation has increased rapidly, since the first paper on pain inhibition by electrical stimulation, almost 50 years ago [86].

Currently available spinal cord simulation systems for the treatment of chronic pain aim to replace the pain sensation with paresthesia, a comfortable tingling sensation. These techniques usually deliver electrical impulses with a fixed frequency to the dorsal columns. Nevertheless, this method is compromised by shunting of energy by the cerebrospinal fluid (CSF) or lead migration. As a result, in recent years a new type of stimulation has risen, which consists in the direct stimulation of the dorsal root ganglia associated with the pain generating area. This method was linked with a greater quality of life [108].

The aforementioned methods deliver an electrical input to the neural target without sensing or automatically adjusting to the nerve fibers' response to stimulation (open-loop stimulation) [82]. For this reason, the efficacy diminishes over time [49], since 29 % of patients develop tolerance [57], due to the plasticity of the nervous system. In response to tolerance development, the amplitude of the stimulus is increased to achieve the same analgesic effect. Additionally, patients' discomfort may increase with change in body positioning and current stimulation therapies do not adjust their settings accordingly [93].

As a result, there has been a development of techniques that aim to adapt the stimulus to the electrophysiological response of targeted neurons (closed-loop stimulation) [82].

A closed-loop system uses measured ECAPs (electrically evoked compound action potentials) as a feedback control mechanism to automatically maintain the desired recruitment levels. The ECAP amplitude is compared to a set point determined by the patient, in a feedback algorithm, and calculates a new stimulus amplitude by changing the input current. This process is repeated for every stimulus, resulting in a continuously adjusted current that maintains constant ECAP amplitude [82]. Thus, a more consistent and improved pain relief is provided, allowing for stimulus adaptation to both prevent tolerance development and discomfort in position change [93].

Furthermore, present stimulation methods use extremely basic protocols, with very poorly defined spatial targets, and elementary temporal profiles (based sinusoidal signals limited to amplitude and frequency definition). If we compare neurons in the dorsal horn to musicians in an performing orchestra, we are trying to restore proper dynamics using a maestro that attempts to coordinate the intricate spatiotemporal activity by blowing a horn. It is paramount to uncover the sensory integration circuits of the dorsal horn and the coding strategies in the ascending tracts in

order to devise effective and long-term therapeutic strategies (based or not in electrical stimulation) for spinal cord pathologies.

2.2 Electrophysiology

Electrophysiology concerns the study of the electrical activity of living cells and tissues. It is considered the main tool in neuroscience investigation, since it can capture a wide spectrum of neural events, from the electrical activity of a single neuron to the behavior of small populations, allowing for the decoding of intracellular and intercellular messages [20].

The recording of neuronal activity is only possible due to the electrical properties of the neuron and the dynamic behavior of its membrane, which enable the propagation and transmission of electrical impulses. These signals can be detected using electrodes, even at a distant source [69].

Electrophysiological approaches to record neuronal activity can be broadly separated into extracellular and intracellular recording techniques [105]. Intracellular methods, such as the patch clamp, expose in detail the cell's membrane dynamics and electrical properties. However, compromise the cell's structure and, for that reason, prevent long duration recordings. Conversely, extracellular techniques monitor the neuronal activity from outside the cell, measuring patterns of action potentials from neuronal populations, allowing for the examination of population behavior and the study of pathologies. Extracellular methods include electroencephalography and, at a smaller scale, multi-electrode arrays. This dissertation concerns the development of computational tools for study of spinal local circuitry, thus only small-scale recording methods, such as the patch clamp and MEAs, will be addressed. But, first, as to fully comprehend the principles behind electrophysiology recording methods, this chapter begins with an overview of neuronal membrane dynamics.

2.2.1 Neuronal membrane dynamics

Neurons are highly specialized cells, both in morphology, as described in section 2.1.1, and in physiology. In fact, the neuron's membrane possesses a wide variety of ion channels. Structures that allow ions, predominantly sodium (Na^+), potassium (K^+), calcium (Ca^{2+}) and chloride (Cl^-), to move through the cell's membrane, giving it a semipermeable character. Ion channels control the flow of ions across the cell's membrane by opening and closing in response to voltage changes and both internal and external signals [24].

The flow of ions across the membrane causes a difference in the distribution of charges in the exterior and interior of the cell, generating an electrical field across the membrane. Any structure that keeps electric charges separated by a fixed potential, can be modeled as a capacitor. So, the cell's membrane can also be viewed as one. This uneven distribution of charges leads to a difference in electrical potential across the membrane, that is, under resting conditions, -70 mV, since the interior of the cell is negative.

Ionic flow across the membrane can be attributed both to voltage changes and concentration gradients. When positive ions move to the exterior of the cell, the membrane's potential decreases. This phenomenon is called hyperpolarization. On the other hand, when the current is negative, the membrane potential increases, in a process named depolarization [26].

Action potentials or spikes occur when the membrane potential at a specific location suddenly rises and, then, falls, characteristic pattern. This is, a depolarization followed by a hyperpolarization, which translates in an electrical potential fluctuation of roughly 100 mV, that lasts about 1ms [35]. They occur following a stimulus, when there is a sudden change in the permeability of the membrane, that causes the ions to flow across it [26].

After that, there is a refractory period, in which Na+ channels are inactive. Therefore, any stimulus given to the cell will not trigger another action potential, no matter how strong it is.

2.2.1.1 Hodgkin-Huxley model

The Hodgkin-Huxley model describes the generation and propagation of action potentials. It was first proposed in 1952 [45], and is still used nowadays as the basis for computational neuroscience modelling. This model assumes that the cell membrane can be represented as an electrical circuit, as described in Fig. 2.8. The explanation, hereafter presented is based on [92]. The mem-

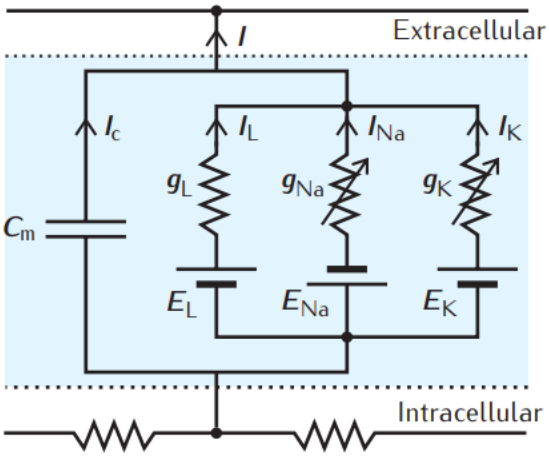

Figure 2.8: The Hodgkin–Huxley equivalent electrical circuit, representing the cell's membrane. Adapted from [92].

brane is, therefore, characterized by a capacitor, C_m, and three ionic currents: a sodium current, I_{Na}, a potassium current, I_K, and a leakage current, which represents the sum of some factors that contribute to the total membrane current that can be assumed to be relatively constant [24]. Each ionic channel is described as a battery in series with a resistance. The current can be calculated using equation 2.1, where the sodium, potassium and leak conductances are represented by g_{Na}, g_K and g_L ,respectively, and E_{Na}, E_K and E_L are the corresponding equilibrium potentials. g_L is constant, whereas g_{Na} and g_K change with voltage.

$$I_x = g_x(V - E_x) \tag{2.1}$$

The equation that corresponds to the circuit drawn is given by 2.2. Where I_i corresponds to the sum of the ionic currents and I_c represents the capacitive current.

$$I = I_c + I_i = I_i + C_m \frac{dV}{dt} \tag{2.2}$$

For the description of the ion currents, it is assumed that the membrane contains a number of gates, which can be either closed to the passage of all ions or open to the passage of potassium ions. Each gate is controlled by a number of gating particles, that can be either in a closed or open conformation. The transition between one state and the other is dictated by the membrane potential. Considering that the particles are independent of each other, the probability of the entire gate being open is n^x, where n is the probability of a single potassium gating particle being in the open state and x is the number gating particles in the gate. Therefore, the membrane conductance for potassium can be calculated by 2.3, considering the probability of it being open and the maximum membrane conductance g_k. Experimentally, the number of gating particles was found to be equal to 4.

$$g_k = \bar{g}_k n^x \tag{2.3}$$

However, the same behaviour is not observed for the sodium ion. The sodium conductance decays, after it reaches a maximum, even when applying voltage to the membrane. This phenomenon is called inactivation. To discriminate the inactivation level of the gate particles, the variable h was introduced. Variable m identifies the sodium activation, similarly to the variable n for the potassium activation. Experience shown that the number of gating particles can be approximated to 3. This way, the conductance for the sodium ion can be observed in equation 2.4.

$$g_{Na} = \bar{g}_{Na} m^3 h \tag{2.4}$$

Thus, combining equation 2.3, 2.4, 2.2 and 2.1, one can deduce the Hodgkin and Huxley equation to describe the membrane potential, equation 2.5, where I_{LC} corresponds to the contribution of the axial current from the vicinity regions of the axon.

$$C_m \frac{dV}{dt} = -\bar{g}_L(V - E_L) + \bar{g}_{na} m^3 h (V - E_{Na}) + \bar{g}_k n^4 (V - E_K) + I_{LC} \tag{2.5}$$

The Hodgkin-Huxley model can also describe the propagation of an action potential along an axon, however, to do so a multi-compartment model, which can describe spatial variations in the membrane potential, must be developed [24].

2.2.2 Instrumentation

The available tools to record neural activity depend on the scale one intends to observe it. In spite of patch clamping enabling the accurate recording of electrical activity, it only does it for a few neurons. In contrast, methods such as functional magnetic ressonance imaging detect activity in

large brain regions, but cannot assign it to a single neuron. In recent years, progresses in imaging and electrophysiology led to the possibility of analyzing neural circuitry at the cellular level [12].

Although electrical recording is the standard, other techniques, namely optical methods, can be used to study neural activity at a cellular resolution, such as calcium imaging [69].

The main disadvantage of calcium imaging in comparison to electrophysiology resides in the temporal domain; currently available calcium indicators possess rise and decay rates of tens to hundreds of milliseconds. Additionally, the extraction of specific action potentials from calcium signals is dependent on image quality and on the neuronal firing patterns. In fact, at high firing rates, the calcium indicators behave in a nonlinear way, difficulting the said extraction [36].

The possibility of tracking neural activity in real-time is the main advantage of electrophysiology, when comparing with imaging techniques. Even though calcium imaging is capable of following action potentials, electrodes identify the actual underlying activity. In fact, the calibration of optical signals relies on electrophysiological recordings. Intracellular electrodes used for calibration can only monitor small sets of neurons, thus, researchers have focused on extracellular electrodes, which can profile hundred of neurons at the same time [12].

2.2.2.1 Patch-clamp

The patch-clamp recording technique was originally developed in the 1970s and it is still the most broadly used to study the electrophysiological properties of biological membranes. This method allows for the low noise measurement of currents passing through the low conductance ion channels, by isolating a small portion of the membrane, which sometimes can contain a single channel [110]. It has been commonly applied to the study of current and potential changes in isolated cells, cultured cells and brain slice preparations. However, in recent years, there has been a growing interest in using this technique for in vivo recordings, with the objective of studying intact brain regions in living animals [96].

The membrane potential is measured by attaching a hollow glass electrode filled with a conducting electrolyte to a neuron and comparing the recorded potential with a reference electrode located in the extracellular medium. Patch electrodes have a wide tip, which is sealed tightly to the surface of the membrane, by applying suction. After the patch electrode seals, the membrane under its tip is either broken or perforated, leading to the electrical contact with the interior of the cell [24]. This way, all ions fluxing the membrane patch flow into the pipette and are recorded by an electrode connected to a highly sensitive electronic amplifier. Then, current injections through the electrode repeatedly excite the neuron, which permits to extract fundamental biophysical parameters, such as input resistance, membrane capacitance, and reverse potential. The described functioning can be observed in Fig. 2.9.

However, recording and stimulation sessions have limited time to be performed, since perfusion of the cytoplasm modifies the intracellular composition of the cell. Moreover, the use of patch electrodes for parallel recording presents technical limitations, as the micromanipulation of the electrode tips to target cells entails the use of rather bulky micromanipulators. For these

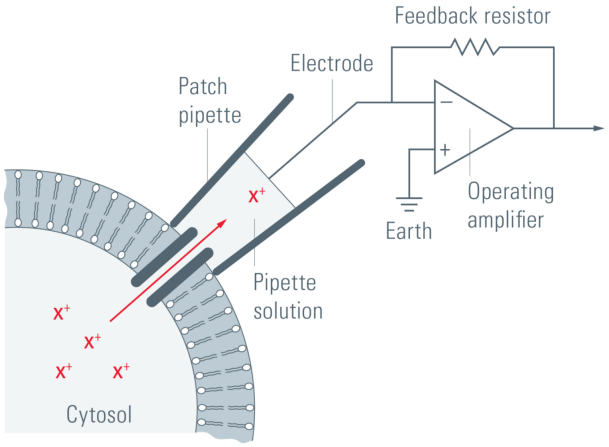

Figure 2.9: General principle of patch-clamp recordings. A glass pipette containing electrolyte solution is tightly sealed onto the cell membrane and thus isolates a membrane patch electrically. Currents fluxing through the channels in this patch hence flow into the pipette and can be recorded by an electrode that is connected to a highly sensitive differential amplifier. In the voltage-clamp configuration, a current is injected into the cell via a negative feedback loop to compensate changes in membrane potential. Recording this current allows conclusions about the membrane conductance. Adapted from [103].

reasons, it is impossible to record and stimulate large sets of neurons simultaneously using this method [40].

Conversely, the use of noninvasive extracellular microelectrode arrays allows investigators to record and stimulate large populations of excitable cells for days and months without compromising the cell's membrane [40].

2.2.2.2 MEAs

The understanding of synaptic transmission and modulation processes at the network level in both physiological and pathophysiological states is of uttermost importance for the unraveling of the mechanisms behind spinal cord function [58]. This is the underlying motivation for the development of microelectrode arrays (MEAs) for multisite recordings.

Currently, MEAs are the cutting edge instrumentation for the investigation of neuronal network dynamics [62]. These devices contain multiple microelectrodes, through which stimulation is delivered or neural signals recorded, in a non-invasive manner. The electrodes are connected with a contact pad by thin contactors to carry the captured signals to an amplifier [50]. The available products in the market vary in the number of electrodes they possess, ranging from 60 to 5000 [2]. Fig. 2.10 shows the design of a planar MEA with 60 electrodes.

Unlike the patch-clamp, microelectrode arrays detect signals from all possible sources around each sensor, so, they can only detect field potentials generated by action potentials or, in rare cases, synchronized synaptic potentials in highly ordered neuronal networks [40]. Thus, it is difficult to track the source of the electrical signals recorded.

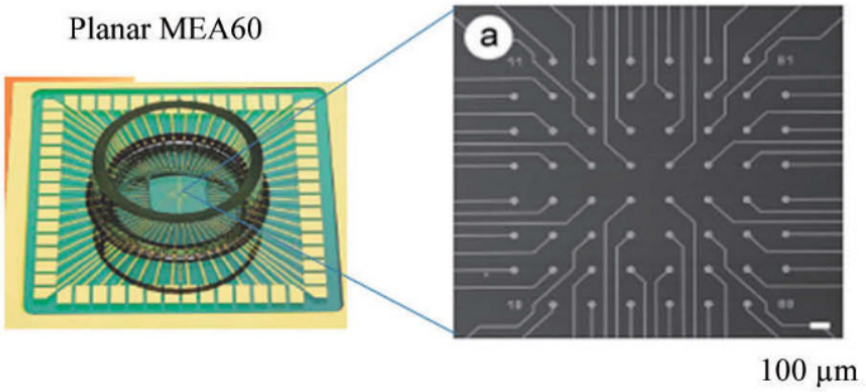

Figure 2.10: Planar MEA. On the left, overview of the MEA60 chamber; on the right, design of MEA60, where it is possible to see the 60 microelectrodes connected to strip conductors that the recording field is composed of 60 microelectrodes connected to strip conductors. Adapted from [58].

Multielectrode arrays excel in time resolution, yet, they have low signal-to-noise ratio and their spatial resolution is limited by the areal density of electrodes. The maximal distance between a neuron and an electrode, that permits action potentials to be picked up, must be smaller than 50–70 μm although this depends on the recording setup and the respective preparation. However, for traditional, commercially available MEAs, the inter-electrode distance is usually larger (60–200 μm), making it impossible to detect the activity of the same single neuron on multiple electrodes [34]. Bearing this, high-density MEAs, with thousands of electrodes, have been developed [46]. These devices have cellular and subcelular spatial resolution, giving way to 1 : 1 coupling, when one neuron is plated over the surface of each electrode, and to the possibility of recording the activity of individual neurons by multiple electrodes[47] [46]. From the signal processing point of view, this technological development is beneficial, since this recording setup greatly increases the performance of neural decoding algorithms [34].

To overcome the limitations of the method, researchers have been combining it with different techniques. For example, the combination of electrophysiology with two photon calcium imaging, provides access to structure and genetic labels, while maintaining the high time resolution[12].

2.3 Neural Coding

The neural code concerns the study of the representation of information in the nervous system. Neurons represent and transmit information about the sensory input by firing sequences of spikes in various temporal and spatial patterns. To understand how the information is coded in these firing patterns, it is necessary to uncover the link between stimulus and neuronal activity. Neural encoding refers to the map from stimulus to neuronal activity, while, neural decoding concerns the reverse map, from the neuronal activity to the stimulus, and the reconstruction of the stimulus.

The most simple neural code, proposed in the early 20th century, is the rate code and is still a prevailing theory. According to it, the intensity of a stimulus is correlated with the firing rate (the number of spikes a neuron fires per unit of time) of the sensory neuron activated by it. The hypothesis of a universal code for information processing in the nervous system is appealing since it has the potential to explain the integration of different inputs and the conversion from sensory input to motor output, by admitting that all neurons use the same language to communicate. This hypothesis may not be correct however, and different regions of the nervous systems (with different functional constraints, or originated at different evolutionary stages) may have very distinct strategies to encode, transmit and process information.

The present work will contemplate the information encoding in the spinal cord, namely how somatic sensations (nociception, touch, temperature) are encoded and conveyed to the brain. The first step involves the translation of the different kinds of inputs into sequences of spikes. After that, the information is conveyed to the spinal cord. But, how does the integration of information at the spinal level occur? How does the nervous system deal with great quantities of information? How are different stimuli written in the neural language? To answer these questions, in this chapter, the current neural coding hypothesis will be presented.

2.3.1 Stimulus-response relation

The characterization of the relation between stimulus and patterns of neuronal activity is a difficult process, since neuronal responses are complex and variable. First, the stimulus needs to be translated into electrical signals, this process is called transduction and is carried out by specialized receptor cells, such as mechanoreceptors which sense mechanical stimuli and photoreceptors that sense light. Then, the neuronal response is translated into a complex spike sequence, that reflects the temporal features of the stimulus and the dynamics of the neuron itself. Thus, hypothetically, the relationship between stimulus and neuronal response can be uncovered if all possible input patterns could be presented and the resulting responses recorded [64]. However, the number of possible inputs is too large to be experimentally feasible. Additionally, neural responses vary from trial to trial even if the same stimulus is presented and the isolation of its features is challenging due to the time scale (the same order as the interval between spikes) at which the changes occur. The inherent variability of neural responses can be attributed to randomness associated with biophysical processes that potentiate neural firing and the effect of other processes occurring concurrently with the trial[24].

As a result and given our current understanding of the nervous system, the deterministic prediction spike sequences is unfeasible. Instead, the triggering of a spike sequence by a certain stimulus is modeled as a probability. One approach to address this probabilistic nature is to use functional models. Functional models address directly the computation that the neuron performs on its inputs, without regard for the biological processes that generated the response [89].

The sequence of spikes a neuron fires, named spike train, contains information about the stimulus that triggered it. Despite the fact that action potentials differ in their amplitude and duration, in neural encoding studies, these variables are deprecated and action potentials managed as identical stereotyped events [24]. Thus, the information is encoded, for instance, based on the number of spikes the sequence includes or on the precise timing they occurred. In mechanoreceptores, features such as the intensity of the stimulus, are encoded by the rate at which the neuron fires. This relationship can be observed in Fig.2.11, where the encoding of mechanical force is attributed to three types of mechanoreceptors reacting to distinct intensity ranges: T cells for touch, P cells for pressure, and N cells for strong, noxious skin stimulation [55]. This relationship is almost linear, with the number of spikes fired being proportional to the amplitude of the mechanical forces.

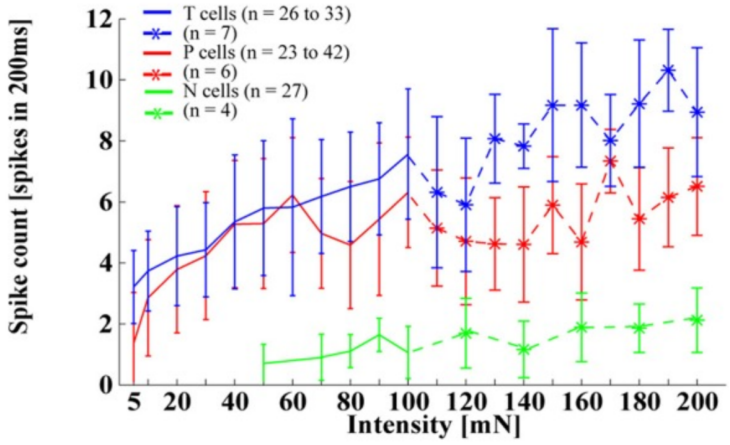

Figure 2.11: Spike count for T cells (blue), P cells (red) and N cells (green) responding to tactile stimuli with intensities of 5–200 mN applied at 0. Stronger pressure intensities (> 100 mN) were tested with fewer cells (see legend). Adapted from [103].

Neuronal responses depend on many attributes of the stimulus, namely its amplitude, location, duration and modality. This last feature concerns the type of energy the receptor is specialized in, for example, thermal receptors are activated by changes in temperature, whereas mechanoreceptors are triggered by sheer physical activity [106]. The most basic mechanism to identify the modality of the sensory input is via labeled lines principle, that is, input from a specific nerve is always interpreted by the brain as a given input. For example, optic nerve is always interpreted as a visual input [48]. On the other hand, the intensity of sensation is determined by the amplitude of the stimulus. The lowest stimulus strength a subject can detect is termed the sensory threshold. Thresholds are normally determined statistically by presenting a subject with a series of stimuli of random amplitude. The sensory threshold for a modality is limited by the sensitivity of receptors.

The threshold energy is related to the minimum stimulus amplitude that generates action potentials in a sensory nerve [48]. The duration of a stimulus is estimated from the onset of the neural response and its duration. Typically there are neurons in sensory systems that only respond to the onset of a stimulus- these are generally referred to as phasic responders and they are good for estimating the time of occurrence of a signal. There are other neurons that respond throughout the stimulus presentation- tonic responders- these signal stimulus duration [48].

Moreover, the same stimulus can trigger many neurons, thus it is necessary to study the behaviour of the population of neurons to thoroughly understand the stimulus features. For this reason, one needs to scrutinize, in addition to the firing pattern of each neuron, the relation of the individual firing patterns with each other [24].

2.3.2 Receptive fields and tuning curves

The spatial dimension of the neural code can be described by estimating a neuron's receptive field, that is, the peripheral area that influences its response; for instance, the receptive field of a primary touch afferent neuron is the area of the skin where stimulation causes its activation. On the other hand, the receptive fields of dorsal horn neurons are the combination of the receptive fields of the primary afferent neurons with which they communicate, as seen in Fig.2.12. Receptive fields on cells of lamina V are larger than in other laminae, since lamina IV excites its neurons, according to Wall (1967) [106]. More, the size of receptive fields of lamina I neurons range from 1 mm_2 on the fingertips to 1000 mm_2 on the back and hip [13, 106], meaning that perception in the fingertips is more precise. Finally, the receptive fields of tactile- sensory related cortical neurons are even larger and can be influenced by injury in sensory nerves or experience. In spite of its large size, cortical neurons are able to discriminate fine detail due to patterns of excitation and inhibition relative to the field that leads to spatial resolution. Dorsal horn neurons have both excitatory and inhibitory receptive fields. Normally, the inhibitory receptive field surrounds the excitatory one (strong stimuli applied to this area can produce inhibition of postsynapitc potentials), whereas stimulation in the excitatory area produces excitation. Thus, one can conclude that the size and pattern are fundamental properties of receptive fields, since they characterize both the convergence of primary afferent nerves and the features of the stimuli applied. This leads to the idea that neurons can be *feature detectors*, signaling the presence of specific pattern elements, coded by the distribution of activity across a neuronal population [90].

Furthermore, sensory neurons are tuned to different aspects of the stimulus. The contribution of individual neurons to sensory function is evaluated by measuring its responses to an appropriate set of stimuli. This description is accomplished by plotting the average firing rate of the neuron, across several trials, as a function of relevant stimulus parameters - the neuronal tuning curve [18]. These plots allow for the determination of the stimulus attributes to which a given receptor produces the greatest response and, hence, to which it is optimally tuned, its selectivity. The optimal stimulus is, commonly, identified by determining the peak of the tuning curve, that is, the stimulus that produces the highest firing rate. This approach is effective, because high firing rates are easily distinguishable from background noise. However, nearby stimuli are most easily

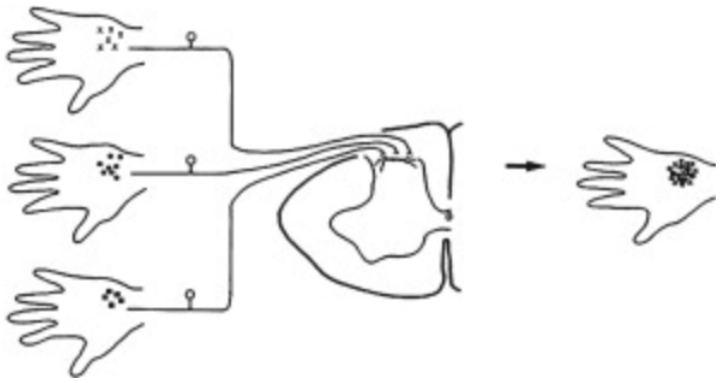

Figure 2.12: Diagram of mechanisms of integration of nociceptive inputs in lamina I neurons. Left panel indicates the receptive fields of three mechanical nociceptors with overlapping receptive fields. The three primary afferents terminate on the same lamina I neuron in the middle panel. The right panel indicates the resulting receptive field. The receptive field is somewhat larger, and more responsive points are found within the responsive area. Thus, unlike primary afferent receptors, spinal nociceptive neurons have nearly continuous receptive fields with less unresponsive regions between responsive spots. Adapted from [13].

distinguished in high-slope regions of the tuning curve, because, in these areas, small variations in the stimulus translate in the greatest changes in firing rate [24, 83]. From this point of view, the peak of the tuning curve is an insensitive region of the neuron's response because the slope at the peak is zero. Both these interpretations can be correct depending on the experimental context and level of neuronal variability [18]. Tuning curves can assume different shapes. Figure 2.13 represents a common tuning curve of a neuron, that can be approximated to a Gaussian function of a specific stimulus parameter, characterized by a mean firing rate and a standard deviation. Other shapes include half wave rectified cosine functions or sigmoidal tuning curve. Mechanoreceptors response to pressure can be modelled as the latter mentioned curve.

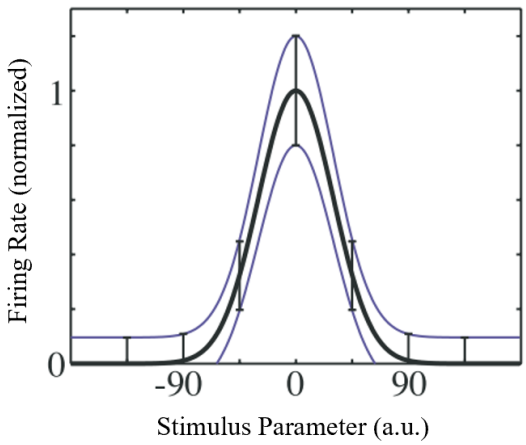

Figure 2.13: Typical tuning curve of a neuron, with mean firing rate (thick line) and standard deviation (thin lines) shown as a function of the stimulus parameter h. Adapted from [18].

2.3.3 Coding strategies in the nervous system

Locally signals can be conducted by analog and electrical mechanisms, however, across large distances, information ought to be transmitted by the spatiotemporal patterns of spike trains generated by a set of neurons. How this information is encoded, either by the precise timing of individual spikes or the time-scale of the neural code, and the role of noise and trial-to-trial variability are still questions of debate [109]. In fact, there is not an universal code for the coding of information in the nervous system, there are multiple hypothesis, as observed in Fig.2.14. It is assumed that individual neurons code simple features whereas the encoding of complex features requires the coordination of thousands or hundreds of thousands of neurons [54].

2.3.3.1 Rate coding

The most common notion of a neural code follows the paradigm described in section 2.3.2, when explaining the concept of tuning curves, which is that information is encoded by the frequency at which spikes are fired. For that reason, the only variable of interest is the total number of action potentials emitted by a neuron in a relatively long time period of several hundred milliseconds or even seconds [54]. In a rate code the precise timing of the occurrence of spikes is not relevant, two spike trains with the same spike frequency contain the same information.

2.3.3.2 Spike-count rate

The spike count rate is calculated by simply dividing the total number of action potentials fired during a trial divided by the duration (T) of the trial. It can be calculated from a single trial. The duration of the trial depends on the neuron recorded and the type of stimulus, but, typically T ranges from 100 ms to 500 ms. This process is called temporal averaging. It can fully describe cases where the stimulus is constant or slowly varying, such as to convey information about the strength of a touch stimulus [48] or the force exerted during voluntary contraction of muscles [30]. However, neurons respond strongly to rapid changes in the stimulus, in fact a fly can react to a stimulus and change its course of flight in just 40ms [80].

2.3.3.3 Spike-triggered average

Sensory systems make numerous adaptations to adjust to the average level of stimulus intensity. To study these adaptations a new concept is introduced, the spike-triggered average, the average value of the stimulus a time t before a spike is fired. It can be calculated using equation 2.6 In other words, it provides a tool to study the response of a neuron using the spikes emitted in response to a time- varying stimulus [24].

$$C(\tau) = \left\langle \frac{1}{n} \sum_{n}^{i=1} s(t_i - \tau)) \right\rangle \tag{2.6}$$

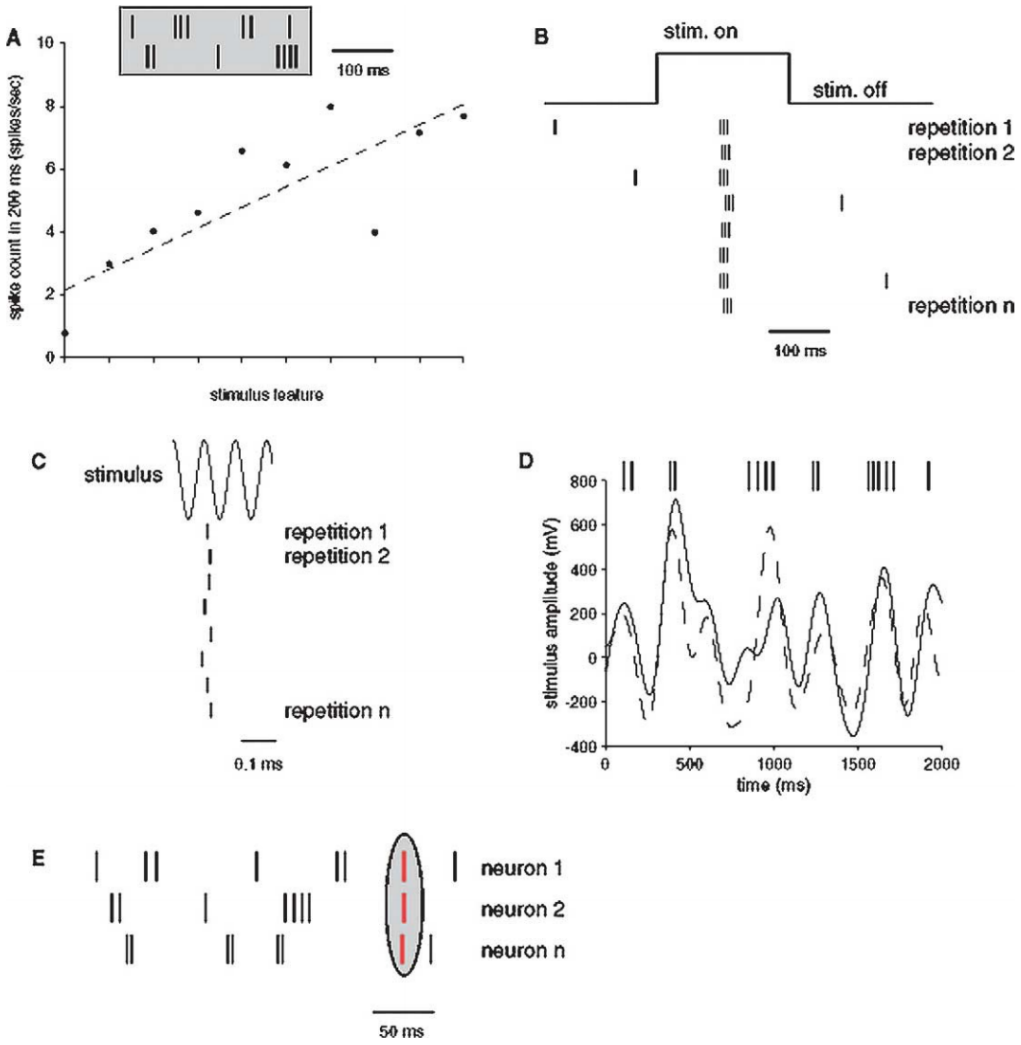

Figure 2.14: Schematic illustration of different coding schemes and their corresponding temporal resolutions. **(a)** In a rate coding scheme, the number of spikes in windows of several hundred ms correlates with some stimulus feature. The two spike trains shown on the top part are considered to be equivalent for a rate code since they carry the same number of action potentials in spite of the different temporal patterns. Although a linear trend is illustrated here, the relationship between stimulus and the spike count may be non-linear. **(b)** In a sparse representation, the neuron shows a very low spontaneous activity. The neuron reliably fires a single burst of spikes at a particular time from stimulus onset during multiple repetitions of the same stimulus. **(c)** A neuron shows very precise spike timing, with a trial-to-trial variation which can be less than 1 ms. **(d)** A time varying signal (solid trace) is represented by a neuron that can follow the rapid changes in the stimulus (top, action potentials). The stimulus can be reconstructed (dashed trace) from the instantaneous firing rate of the neuron. **(e)** In this example, the synchronized activity of multiple neurons (symbolized by the spikes marked in red) constitutes the code to represent information. Adapted from [18].

A code based solely on the time-dependent firing rate can be considered an independent-spike code. This means, that the generation of each spike is independent of all the other spikes in the train.

2.3.3.4 Correlation coding

Correlation codes refer to spike trains where individual spikes do not encode independently of each other. The correlation between spike times may contain additionally information. An example of a correlation code is when stimulus information is carried by interspike intervals. Since studies found that the information conveyed by the correlation between two or more spikes is rarely larger than 10 % of the information carried by spikes considered independent, most works on neural coding assume spike independence [24].

2.3.3.5 Temporal coding

When precise spike timing or high-frequency firing-rate fluctuations are found to carry information, the neural code is often identified as a temporal code [24]. A number of studies have observed that the temporal resolution of the neural code is on a millisecond time scale, thus, the precise spike timing is a major player in neural coding. Through the perspective of rate coding models, high-frequency fluctuations of firing-rates are noise, while temporal coding models propose that they encode information.

Latency coding

The latency of firing of a neuron, the latency time between stimulus onset and first action potential, can vary greatly depending on input parameters [102]. This idea is in the foundation of *Time to first spike* coding. In the most purist view of this coding scheme, each neuron only needs to fire one spike to convey information. After it fires, it is inhibited until the onset of the next stimulus. Thus, latency may be identified as one way for signal encoding in the nervous systems. The main advantage over rate coding, is the speed with which it allows information transmission and processing. To assure the efficiency of latency coding, the precise timing of spike generation is imperative. Therefore, the performance of latency coding may be corrupted by noise-induced fluctuations in discharge times. The quantification of the contribution of this effect is essential to discuss the efficacy of latency coding and its possible advantages over other neural codes [37]. Touch sensors in the finger tip use latency coding to encode the strength and direction of the touch [6].

2.3.3.6 Phase coding

One can apply the concept of time to first spike also to the situation where the reference signal is not a single event, but a periodic signal, an oscillation. In the hippocampus, information such as the body's spatial position is conveyed using phase coding. Action potentials do not lock to the timing of external inputs (onset and offset), instead are referenced internally to the oscillatory rhythm of the neuronal population at theta frequencies [67, 21].

2.3.3.7 Population coding

The methods discussed focus on the information coded by single neurons, however, information in many brain regions is represented in a distributed way by the activity of populations of neurons. It is generally accepted that this distributed representation allows the nervous system to surmount the challenges of trial-to-trial variability in single neuron responses, giving strength to the representation. Due to the noisy nature of neurons, population coding is necessarily probabilistic [85, 11]. When studying population coding, it is important to analyze whether individual neurons act independently or if the correlation between different neurons provides further information. The easiest interpretation and the most commonly used is independent-neuron coding when neurons are considered statistically independent [24]. Several experimental parameters, such as the stimulus itself and the state of the animal, may influence the level of independence. Moreover, the correlation in the firing of two neurons may depend on the distance between them, due to the fact that putting two electrodes very near each other may present some difficulties, and the connectivity may be such that it may be very challenging to find two neurons that are connected or have common input [54].

The neural response features contributing to a population code [71] are:

1. *Diversity of single-neuron firing rates:* Neurons with different stimulus preferences can each add complementary stimulus information as they each vary in terms of stimulus preference or tuning width.

2. *Relative timing:* In a neuronal population, informative response patterns may comprise the relative timing between neurons.

3. *Network state modulation:* Neural responses depend not only on sensory inputs but also on large-scale brain states that change on time scales slower than the transient responses to individual stimuli.

4. *Periods of silence:* Neural populations also encode information by the absence of firing of some neurons.

Correlation-based coding

The spike patterns of a neuronal population can be viewed as an additional source of information [53]. Its degree of synchrony or the rate at which the patterns are generated can be stimulus modulated, and consequently, the degree of correlations in the spike trains is stimulus modulated [28]. Yet, the study of correlation presents several challenges, since its computation requires a large amount of data recorded simultaneously from multiple neurons and the interpretation of raw correlation values can be complex. Nevertheless, the emergence of new recording techniques, such as multielectrode arrays and two-photon imaging, has facilitate the obtaining of such recordings.

Correlation is a normalized measure of covariation, normally, of two different events. It can be calculated in several ways, as pointed out in table 2.1. It may be used to assess tuning similarity, measured as the correlation in the mean responses of two neurons to an ensemble of stimuli (named signal correlation) or the co-fluctuations in the responses of a pair of neurons over different timescales, from the precise temporal alignment of spikes (that is, synchrony) to slower changes in excitability. The timescale over which correlated activity modulates the responses of neurons is unknown, but membrane time constants suggest that it occurs over tens of milliseconds or less [33].

Table 2.1: Types of correlation between spike patterns. Adapted from [23].

Types of correlation
Signal correlation measures the correlation coefficient between mean responses to different stimuli. It is frequently employed to quantify the extent to which a pair of neurons has similar tuning or other functional properties. Decreases in this type of correlation, such as through adaptation or contextual modulation, can produce sparsening of population responses.
Spike count correlation (also called noise correlation) is the Pearson's correlation coefficient of spike count responses to repeated presentations of similar stimuli, under the same behavioral conditions. Spike counts are typically measured over the timescale of a stimulus presentation or a behavioral trial, which range from a few hundred milliseconds to several seconds. Spike count correlations are proportional to the integral under the spike train cross-correlogram.
Synchrony measures the degree to which the timing of spikes is precisely aligned, typically on the timescale of one or a few milliseconds. It is typically quantified using the sharp peak of in the cross-correlogram. Dependencies in the timing of individual spikes can also be measured in the frequency domain, using spike-spike coherence.
Long-timescale correlation measures the extent to which a neuron's response to one trial is correlated with a second neuron's response to trials in the future or past. It is used to quantify the influence of slow fluctuations in responsiveness on spike count correlation. When measured, the long-timescale correlation has been found to be close to 0.

In the simplest approaches to neural coding, the noise in the output of a neuron is assumed to be independent of that in other neurons, since noise makes the output less precise, and consequently, difficult the coding process. However, some neural systems display correlation in the variability of the output of a population of neurons in response to a given stimulus, this is, noise correlation or spike count correlation [33]. Noise correlation tends to be higher between pairs of neurons that are near each other and have similar tuning and functional properties.

The source of correlation is often associated with shared or common inputs. But, this relationship is not trivial, since shared inputs do not necessarily produce high correlations. For example, in randomly connected networks of excitatory and inhibitory neurons (balanced networks), fluctuations in the excitatory drive are followed rapidly by fluctuations in the activity of inhibitory neurons. When two neurons receive correlated excitatory drive, correlated inhibitory signals (i.e., inhibitory inputs that are correlated with each other and with the excitatory pool) largely cancel their impact on postsynaptic responses [53].

Correlations can also provide important information about the functional architecture of neuronal networks [23]. In fact, correlations can be used to infer functional connectivity from measurements of the spiking activity [100]. Indeed, the correlation of spike timing activity has been used to infer the anatomical connection of pairs of neurons, namely between neurons of the thalamus and the cortex [23].

Rank order coding

Rank order coding is a simple, computationally inexpensive, coding scheme that is based on the relative timing of spikes across a population of cells. The principle behind it rejects the precise timing information, and focus on the specific order in which the spikes arrive, and, therefore, were generated. This way, the first spike of the population corresponds to the most activated neuron, the second spike to the next most activated neuron, etc. Since there are factorial N possible orderings, a rank order code can transmit up to $log_2 N!$ bits of information under conditions where each input neuron can only emit one spike. Besides its capacity of conveying information, a further advantage of rank order coding is its invariance to changes in both input intensity and contrast. This is, when these changes occur, there are no changes in the rank ordering of the units. This automatic normalization of inputs is an additional advantage of rank order coding that is difficult to achieve using other coding schemes [102, 98].

Sparse coding

Sparse coding relies on the principle that information is represented by a relatively small number of simultaneously active neurons out of a large population. For each stimulus, this is a different subset of all available neurons. Sparseness may be focused on the temporal domain [51] or on the sparseness in an activated population of neurons. In fact, it constitutes a general principle of sensory coding in the nervous system [70]. This was first observed in the visual cortex, where population responses to natural stimuli may be the result of a sparse approximation of images. These populations are typically very overcomplete, allowing for great flexibility in the representation of a stimulus. Using this flexibility to achieve sparse codes may offer many advantages to sensory neural systems, including enhancing the performance of subsequent processing stages, increasing the storage capacity in associative memories, and increasing the energy efficiency of the system [81].

Combinatorial coding

Combinatorial coding relies on the principle that different features of sensation are processed separately in specialized assembles of neurons and then combined to form a unified perceptual experience. A given feature of the object is coded by units that are considered to be either active or passive; combining N units there is a total of c=2>N possible combinations. Thus, combinatorial

coding is based on the activation of specific combinations. The number of active units depends on the stimulus. This coding scheme differs from sparse coding, where the number of active units is small compared to their total number [32].

2.3.4 Coding strategies in the spinal cord

The predominant theories for the encoding of somatic sensations rely on two competitive views: the labeled line theory (or specificity theory) and the pattern theory. As above mentioned, the labeled lines theory proposes that each sensory modality is processed along a fixed, direct line communication system from the skin to the brain. This means that, for instance, nociceptors are only activated by noxious stimulation and this activation encodes pain; other primary afferent neuron types respond to other stimuli and their activation is the basis for the perception of other modalities [76]. This is supported by the existence of specific spots in the human skin whose activation correlates with a specific sensation: cool, warm, touch, pain, or itch [59], and the existence of primary sensory neurons and spinal relay neurons that respond to that same stimulus. On the other hand, pattern theories suggest that sensations are generated by a summation of inputs from various primary sensory afferents. However, the most plausible hypothesis is, in fact, a combination of the two referred theories, since the coding of somatic sensations involves both specificity and complex activation patterns. This synergistic approach is a form of population coding, more specifically, combinatorial coding [60, 77].

Gate control theory, a pattern-based theory, states that low and high-threshold afferents converge on unspecialized central neurons and that strong enough activation of those central neurons encodes pain. This theory originally denied the existence of specific labeled lines, but subsequent, research showed that the encoding of pain may coactivate several primary afferents from different labeled lines in distinct patterns, suggesting, instead a population coding scheme.A modification of this theory, a Leaky gate model, was the proposed [94]. This model emerged from the discovery that a subset of second-order neurons participates both in the coding of itch and pain sensations (suggesting that different labeled lines crosstalk in the spinal cord). Another feature of the population is the intensity-dependent coding of pain, due to the fact that upon strong gastrin-releasing peptides indirectly inhibit pain via the recruitment of the endogenous opioid system.

Table 2.2 presents the most recent studies related to the coding of different modalities in the spinal cord. From the analysis of the gathered data, it is possible to assert that polymodality, the presence of neurons that encode different sensations, is a prevalent phenomenon in afferent neurons. While polymodality is considered a flaw according to the specificity theory, it supports the combinatorial coding hypothesis. In fact, it was suggested that dorsal root ganglion (DRG) neurons encode cold sensation using a combinatorial strategy [104]. On the other hand, heat is encoded in a graded fashion both at population and single-neuron levels, that is, as the temperature increases more heating-sensitive neurons are activated and most individual neurons respond more strongly. Different coding schemes in the dorsal horn were also observed [79]: in the heating range, spinal dorsal neurons encode absolute temperature, whereas, in the cooling range, neurons encode temperature change. However, how the ‘modality-specific’ coding at the periphery is

Table 2.2: State-of–the-art coding hypothesis in the spinal cord.

Source	Year	Animal Model	Modality	Population of Neurons	Coding Hypothesis
[39]	2019	Rat	Temperature, nociception	Dorsal horn neurons	Differential encoding of innocuous and noxious thermal and mechanical stimuli
[104]	2018	Mouse	Temperature	DRG neurons	Polymodality; graded heat coding; combinatorial coding for cool/cold temperatures
[42]	2018	Mouse	Nociception, temperature	Dorsal horn neurons	Polymodality: heat and cold are coded through the recruitment of both shared and unique spinal cord neuron types.
[94]	2017	Mouse	Nociception, itch	Spinal second-order Grp labeled neurons	Leaky gate model; polymodel interneurons respond both to itch and pain; intensity-dependent coding of pain
[79]	2016	Mouse	Temperature	Spinal cord OGB-labeled neurons	Populations that respond both to cold and heat stimulus, different coding schemes for heat and cold
[29]	2016	Mouse	Nocipetion	dorsal root ganglion	85 % of the dorsal root ganglion are modality specific
[75]	2016	Leech	Touch	Primary afferent neurons	Multiplexed population coding
[55]	2016	Leech	Touch	Primary afferent neurons and spinal interneurons	Multiplexed encoding of touch location and force intensity
[17]	2015	Mouse	Itch	Spinal cord interneurons	Spinal cord inhibitory pathway that gates the transmission of mechanical itch
[27]	2014	Mouse	Nociception	Populations of spinal excitatory and inihibitory neurons	Population coding: hybrid theory between specificity and pattern theory
[52]	2013	Mouse	Temperature	TRPM8 neurons of DRG	Labeled line for cold coding
[87]	2013	Rat	Nociception	Deep dorsal horn neurons	Intensity coding and spatial summation

transformed into the continuously distributed activation temperature thresholds in the spinal cord remains an outstanding question. Spinal neurons receive convergent innervation from direct or indirect DRG inputs. The relative strengths of different DRG inputs or local inhibition onto the spinal neurons may play important roles [79]. Despite polymodality being a reality, 85% of the dorsal root ganglion is modality specific [29].

Concerning nociception, intensity coding and spatial summation have been proposed as the coding mechanisms for noxious stimuli in the deep dorsal horn neurons [87]. It was observed that greater stimulation areas activate peripheral zones of neighboring receptive fields of spinal neurons. The recruitment of additional nociceptors and the increase in stimulus intensities produced greater firing of spinal neurons.

On the other hand, multiplexed population coding was suggested as the general mechanism of touch encoding [56]. Multiplexing relates to the simultaneous encoding of different stimulus properties by distinct neuronal response features, each mechanoreceptor neuron of the leech varies spike count and response latency to both touch intensity and location. While a rigorous experimental verification of the multiplexing hypothesis is difficult to accomplish in a complex vertebrate system, it is feasible for a small population of individually characterized leech neurons, with similar results to primates.

Chapter 3

SensorySimLib

Sensory information detected in the periphery is forwarded through the ascending pathways via the spinal cord, brain-stem, and thalamic relay nuclei to the sensory cortex over a 3-neuron system. As the information about the stimulus travels the spinal cord, it is integrated and the level of abstraction over the stimulus features increases. This way, the information that reaches the sensory cortex is only a general representation of the main stimulus features: its modality, location and intensity. How these attributes are individually coded and integrated to produce a representation of the stimulus is still a question of debate, which requires knowledge about the local circuits of the spinal cord and the coding strategies used to integrate the neuronal information at the different levels of the 3-neuron system. Given the complexity of this system, progress in the understanding of its mechanisms can be achieved through the construction and analysis of mathematical/computational models. This approach was taken in this thesis, with the development of a model (and simulation tools) which objective was to create a realistic representation of the ascending tracts that can be manipulated and extended to test different coding hypotheses in the spinal cord. Experimentally, understanding how the entire spinal circuitry orchestrates and represents information requires recording from a large number of neurons and delivering stimuli in a precisely controlled manner. The creation of the computational model tries to ease this process by offering a method for studying hypotheses that may arise from experimental findings, refining the experiments that need to be performed.

This chapter first overviews the foundations that underpin the model and then explores the library structure and the mathematical formulations behind the model created.

3.1 Model fundamentals

The model focuses on the coding of thermal stimuli. DRG neurons are the first afferent neurons in the somatosensory system, as they convert a physical/chemical state into electrical activity - the state that they encode is determined by their biophysical properties, namely their ion channels dynamics. For example, TRPV1+ dorsal root ganglions are associated with the coding of intense cooling [79]. DRGs can be viewed as feature detectors, as they encode a specific attribute of

the stimulus within their receptive field. This specific preference can be translated into a tuning curve, that describes the activity of a sensory neuron as a function of a certain stimulus attribute. The model developed represents this selectivity through its tuning curve instead of focusing on its biophysical properties, as it offers a higher level of abstraction and is in concordance with the characterization made by Wang et al. [104]. For these same reasons, the geometry of neurons is not relevant, since it doesn't constrain the electrical response of the neuron. With this in mind, cells were modeled using a simple ball-and-stick model. How the neural ensembles communicate with the interneurons to represent the whole stimuli continues to be subject of debate, being the specificity theory and combinatorial coding the prevailing theories [59]. With the objective of simulating the different theories, DRGs were divided into subsets according to the stimulus features they encode. This offers flexibility to test different hypotheses on how the DRGs communicate with the interneurons. From a structural point of view, the skin does not have boundaries and so the receptive fields of the DRGs do not. This constraint had to be taken into account when designing the model.

3.2 NEURON simulation environment

The NEURON simulation environment is one of the most widely used tools in computational neuroscience. It can be used to test hypotheses, estimate experimentally inaccessible parameters and illustrate brain mechanisms. NEURON enables the creation of biologically realistic quantitative models of the nervous system's mechanisms, in which the investigator has power over which details to include or omit, not being restricted by the simulation program [44]. The user can deal directly with familiar neuroscience concepts - biophysical properties, network architecture, and synaptic communication - without the need for reformulating the model to fit the requirements of the simulator.

The program focuses on the simulation of the equations that describe nerve cells, being capable of handling problems in which membrane properties are spatially inhomogeneous and where membrane currents are complex. NEURON simulates these equations efficiently because its computation relies on the implementation of implicit integration methods optimized for complex structures. This way, the program is capable of simulating large networks (with up to 10k neurons) with fast run times. NEURON has been widely used in literature - as of September 2017, more than 1900 scientific articles and books have reported work that was done with NEURON - making it a reliable and validated tool for the simulation of neuronal activity [5].

Most of the programming behind NEURON has been done with hoc, an object-oriented language with C-like syntax that has been extended to include functions specific to the domain of modeling neurons and implementing a graphical interface. Python can be used as an alternative interpreter. All hoc variables, procedures, and functions can be accessed from Python, and vice-versa. This increases the flexibility of the simulator for setting up the anatomical and biophysical properties of models, defining the appearance of the graphical interface, controlling simulations, and plotting results.

3.3 Library structure

SensorySimLib extends the functionalities of the NEURON simulation environment for the context of models of sensory integration in the spinal cord, by using Python as an interpreter. The library focuses on the construction of a high-level anatomically correct network model of the ascending tracks and provides a variety of custom-made visualizations of the neuronal activity in different stages of information integration. The library is built to facilitate the construction of these models. The base class - *Cell* - implements NEURON's methods to define biophysical parameters and cell structure, based on the ball-and-stick model. *DorsalRootGanglia* and *Lamina* classes inherit methods from the base class to construct neural networks with distinct methods to simulate the mechanisms of integration of information specific to these populations. On the other hand, the class *ConnectLayers* implements the information transmission mechanisms between the different populations of neurons. Finally, the *Stimulation* class emulates the different stimuli which may be applied to the skin, permitting to apply single cell stimuli and to simulate time varying and spatially uneven stimulation patterns applied to the whole skin surface.

3.4 Individual neuron modelling

Neurons are the fundamental unit of the nervous system and, thereby the building blocks of the model. In NEURON, the construction of the biophysical cell model is made by parts because it makes debugging, extending, and translating to parallel implementations simpler [19].

The parts of the cell model are:

- Sections - the cell sections (e.g. soma and axon)
- Topology - The connectivity of the sections
- Geometry - The 3D location of the sections
- Biophysics - The ionic channels and membrane properties of the sections
- Synapses - Optional list of synapses onto the cell

Taking into account that the purpose of the model is to study the transmission of information and not the biophysical properties of individual cells, individual cells were modeled with the ball-and-stick model. In this representation, neurons are formed by only two sections: a soma connected to a single dendrite. The diameter of the soma was considered to be 12.6 microns, whereas the diameter of the dendrite was set to 1 micron. Each section has its own discretization parameter *nseg*, which dictates the number of internal points at which the discretized form of the cable equation is integrated. For the dendrites, this parameter was set to 5, whereas soma has only one segment. The cell is further characterized by its 3D location, which is determined according to the characteristics of the population to which the cell belongs.

The cell's membrane biophysical aspects were defined according to the Hodgkin and Huxley equations, described in Chapter 2.2. The axial resistance was set to 100 $Ohm \cdot cm$ and the

membrane capacitance was valued to 1 $\mu F/cm^2$. More, the sodium conductance was set to 0.08 S/cm^2 and the potassium conductance to 0.02 S/cm^2 and the threshold adjustment parameter was $V_{Traub} = 55mV$, in concordance with [8]. All compartments contained a leakage (passive) conductance with a reversal potential of 65 mV and a maximum value of 0.042 $mS/cm2$. All cells have a synaptic profile modeled as conductance changes following an exponential waveform defined by a decay time constant, $\tau = 5ms$. The synapse is later connected to a target, according to the structure described by the model. SensorySimLib extends the cell model by implementing the concept of receptive field.

3.4.1 Receptive field

The receptive field is the area in the sensory periphery where stimuli can influence the electrical activity of the cell. The receptive field of a primary afferent neuron is the area of the skin where stimulation affects its activation. On the other hand, the receptive field of dorsal interneurons is the combination of the receptive fields of the primary afferent neurons with which they communicate. The neuron's activation is influenced by the position of the stimulus within its receptive field: stimuli closer to the receptive field's center cause greater activation than stimuli applied to the periphery. Thus, one can model the influence that a stimulus applied to the position x has over the neuron i as a Gaussian function of the distance to the neuron's receptive field's center, μ_i, as described in equation 3.1, where σ is the standard deviation, and n is the scalling factor. This way, for each neuron, every location of the layer to which it is connected has a weight that represents the contribution that a stimulus applied to that point can have over the total activation of the neuron - which represents its receptive field. The sum of all receptive field's weights is 1.

$$RF_i(x) = e^{-\frac{1}{2\sigma^2}(x-\mu_i)}/n \tag{3.1}$$

3.5 Population modeling

In SensorySimLib, a population of neurons is defined by its dimension, dim, and the 3D position of the center of the distribution of the cells that make the population. Cells are created and positioned in cylindrical geometry: somas are placed on the surface of the cylinder with a predefined spacing and dendrites are oriented radially, pointing to the center of the cylinder. The cylindrical organization is a more anatomically correct representation and complies with the infinity boundaries constraint. This way, the location of the somas can be defined in cylindrical coordinates, following equation 3.2, where δ is the spacing between neighbor cells and i, j belong to $[0, dim]$. This mathematical simplification makes the projection of the cell's receptive field on the surface of the skin easier, however, three discontinuities emerge: two on the edges of the cylinder and one when $\theta = \pi/2$. The discontinuities in the edges of the cylinder are solved by considering that the upper edge communicates with the inferior one and vice-versa. On the other hand, the discontinuity at $\theta = \pi/2$ is solved by translating the receptive field to fill the unrealistic values. The total

number of cells in a population is $dim \times dim$.

$$\begin{cases} z = i \cdot \delta \\ r = \frac{\delta \cdot dim}{2\pi} \\ \theta = j \cdot \frac{2\pi}{dim} \end{cases} \tag{3.2}$$

3.6 Model for spinal sensory information transmission – a 2-neuron layered system

The information transmission in the ascending tracts was envisioned as a 2-layer neuron system, where the first layer represents the dorsal root ganglia, whereas the second layer the interneurons (Fig.3.1). The DRG layer can be further subdivided into two layers: the nerve endings located in the skin and the thermoreceptors themselves. As the information flows through the layers, the level of abstraction over the stimulus features increases. The library allows for the test of different connection hypotheses between layers to justify the different coding strategies for heat and cold observed in the literature. The design of this model involved the articulation of several neuroscience concepts.

3.6.1 Dorsal root ganglia

In SensorySimLib, dorsal root ganglia are defined by the modality of the stimulus they encode. In the experiments performed, only thermal stimuli were considered, however, the code presents flexibility to implement other modalities. The individual DRG populations are further defined by their tuning curves - the stimulus attribute to which they respond optimally. The DRG model is constituted by a skin model and the associated thermoreceptor.

3.6.1.1 Skin model

The skin is represented by the nerve endings (NE) dedicated to temperature sensing, which are distributed uniformly over a cylindrical surface, similar to the population model, equation 3.2, using a receptor density of $250/mm^2$. Considering this density, the spacing between the nerve endings, δ, was set to $0.063mm$. The NE's were organized in a regular grid with a location jitter of 5 % over the whole surface of the cylinder, within an area of $81.8mm^2$. This quasi-uniform distribution is consistent with the actual distribution of mechanoreceptors nerve endings, as reported in [72]. Thus, each receptor is fully described by its cartesian coordinates, r_x, where $i\varepsilon\{1,...,20449\}$. When a stimulus is applied at a given location w of the skin patch, the mechanic and conductive properties of the skin extends the effect of the stimulus to nearby locations, such that the responses of any receptor is given by:

$$s_x(w) = e^{-\frac{1}{2}\|w-r_x\|} \tag{3.3}$$

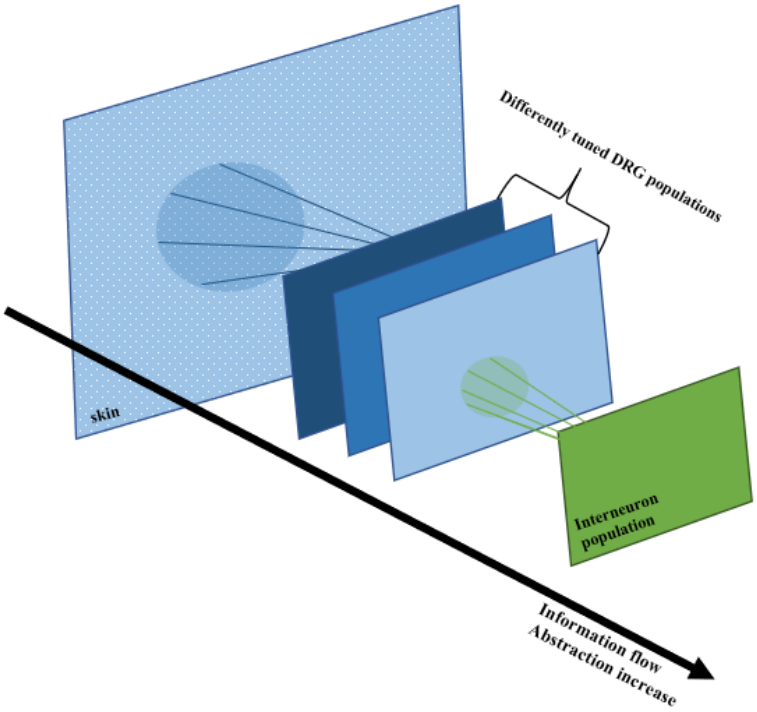

Figure 3.1: Model architecture. The stimulus information is transmitted through a series of layers. The first layer represents the DRG nerve endings located on the skin - doted plane, each dot represents a nerve ending. There are differently tunned DRG populations that sense stimuli applied to the skin. Each DRG receives information from a specific area - its receptive field - represented by the blue circle on the first layer. Interneurons are activated by the DRGs within its receptive field. As the information flows through the layers, the level of abstraction over the stimulus features increases.

For thermal stimuli the equation can be altered as follows:

$$s_x(w) = T_0 - (T_0 - T_x)e^{-\frac{\tau}{2}\|w-r_x\|} \tag{3.4}$$

Where T_0 is the room temperature, T_x is the temperature at location x and τ is a scaling factor determined empirically.

Considering that the size of one DRG receptive field on the fingertip is about 1 mm^2 and that the stimulus intensity within the receptive field follows a Gaussian profile, the standard deviation, σ, of DRG neurons' receptive field was considered to be $0.25mm$. Bearing this in mind, the considered skin patch is sensed by a population of 81 DRG neurons.

3.6.1.2 Neural tunning

Wang et al. [104] described that distinctly shaped tuning curves support different coding strategies for heat and cold so, to explore the cellular basis behind these strategies, thermoreceptors were subdivided into two categories (non-monotonic and monotonic) according to the shape of

their tunning curves. Normally, tuning curves are obtained by plotting the average firing rate of the neuron as a function of relevant stimulus attributes. However, given that the relation between firing frequency and the current injected in rat somatosensory cortex neurons is approximately linear [97], one can approximate the relationship between the stimulus attributes and the injected current using the mathematical association found with the tuning curve. A non-monotonic tuning curve is characterized by an increase and eventual decrease as temperature moves away from neutral. Non-monotonic tuning can be modeled as a Gaussian function of temperature, as follows:

$$I_{non-monotonic}(T_i) = A_{max} e^{-0.5 \cdot (\frac{T_i - T_{optimal}}{\sigma_{tunning}})^2} \tag{3.5}$$

Where T_i is the temperature sensed by neuron i, A_{max} is the maximum activation that can be produced, $T_{optimal}$ is the optimal tuning temperature - the temperature at which the response of the neuron is maximum - and, $\sigma_{tunning}$ is the standard deviation, which controls the rate at which the activation decreases as the temperature changes.

A monotonic tuning curve is described by an increase and no subsequent decrease in response to temperature change and its shape can be approximated to a sigmoidal function, through equation 3.6, where λ controls the slope of the curve.

$$I_{monotonic}(T_i) = A_{max} \frac{1}{1 + e^{\lambda (T_i - T_{optimal})}} \tag{3.6}$$

A_{max} was found empirically, $A_{max} = 0.0003$, so that the maximum current injected produces a firing frequency compatible with biologically observed firing rates for leech mechanoreceptors [56].

3.6.1.3 DRG total activation

Bearing all the concepts introduced and combining equations 3.1, 3.4 and equation 3.6 or 3.5 if the tuning curve is monotonic or non-monotonic, respectively, one can calculate the activation of DRG neuron i, as follows:

$$\begin{array}{cc} & A_i = I(T_i) \\ c & where \\ & T_i = \sum_{x=1}^{x=N} RF_i(r_x) \cdot S_w(r_x) \end{array} \tag{3.7}$$

Where $S_w(r_x)$ corresponds to the response of receptor x (x varies from 1 to N, t which is the number of individual nerve endings) to a stimulus positioned at w, or in the case of thermal stimuli, to the temperature that is sensed by receptor x if a thermal stimulus is located at w; $RF_i(r_x)$ is the influence that the response of receptor x has over neuron i. Thus, $\sum_{x=1}^{x=2044} RF_i(r_x) \cdot S_w(r_x)$ can be interpreted as the sum of the individual nerve endings responses within the receptive field of DRG neuron i, more specifically, it gives a measure of the temperature sensed by the cell - T_i. This temperature is then converted to current, through the tuning curve that characterizes the neuron. The current is then used to stimulate the NEURON simulated DRG to produce a biologically realistic response.

3.6.2 Interneuron Population

Projection neurons receive the input of different DRGs and produce a response that corresponds to the integration of the information conveyed by the DRG population to which they are connected, their receptive field. Similarly to what happens in the first layer of the model, the different neurons connected to the interneuron have distinct weights over its activation. These weights are determined by the position of the DRG within the receptive field, according to equation 3.1, and determine the synaptic weight, and consequently the quantity of information that is transmitted in the connection between the DRG and the interneuron.

DRG neurons encode specific modalities and stimulus features, however, how the information coming from all the DRGs connected to a single interneuron is integrated and translated into a neuronal response remains a challenging question. Different connection hypotheses were tested to answer this problem and to assess which coding strategies are used to code temperature.

Three hypotheses were tested:

1. Each population of singly tuned DRGs is connected to a distinct interneuron;
2. Each interneuron is connected to all types of singly tunned DRGs;
3. Each interneuron is connected to a different combination of singly tunned DRGs.

In this way, the interneuron response is modulated by the activation of the different populations of DRG to which they are connected.

3.7 Results

A model for the simulation of cold coding in the ascending pathways was built, making use of SensorySimLib. The construction of the model's DRG layer was based on the recent work published by Wang et al. [104], which contemplates a thorough description of mice's heat and cold responding DRG populations. The response of the DRGs was measured using Calcium imaging since it yields sufficient sensitivity to resolve all sensory modalities in DRGs. From the analysis of the data acquired, Wang et al. concluded that heating- and cooling-sensitive neurons have distinct tuning curves. In the cool range, monotonic and non-monotonic DRGs were activated in equal proportions. Three different tuning temperatures were identified: 15°C, 17.5°C, and 20°C. Considering this characterization, it was established that the model's DRG layer is constituted by 6 DRGs populations with the same number of neurons: 3 sub-layers of non-monotonically tunned DRGs with different optimal temperatures (15°C, 17.5°C, and 20°C) and 3 sub-layers of monotonically tunned DRGs with the same optimal temperatures. The standard deviation of the non-monotonic tuning curves was set to 2.25°C, whereas the slope of the monotonic tuning curves, λ, was set to 1.8. The DRGs receptive fields were considered to have the same size and were distributed evenly across the surface of the skin model.

The 3D arrangement of the nerve endings and their influence on the different DRG receptive fields is depicted in Fig.3.2(a). Fig.3.2(b) illustrates the cylinder's surface, where it is evident the Gaussian profile of the different receptive fields, which were organized in a hexagonal geometry so that the whole surface of the skin is covered.

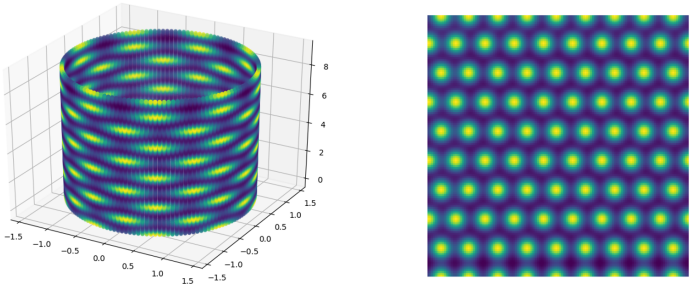

(a) **(b)**

Figure 3.2: Representation of the organization of the nerve endings and influence on DRGs receptive field. **(a)** Cylindrical arrangement of the nerve endings and their influence on the different DRG receptive fields. **(b)** Cylinder's surface projection, where the hexagonal geometry of the DRGs receptive field is evident.

The temperature distribution across the skin caused by the application of a thermal stimulus with 10°C at the nerve ending 10000 can be observed in Fig.3.3. Applying this same stimulus for 2 seconds, the population of DRGs non-monotonically tunned for 20°C produces the activation pattern shown in Fig.3.4, where each square represents the maximum firing rate registered by the DRG during the total course of the experience. The instantaneous firing rate was calculated by

convolving each spike train with a Gaussian window with 100 ms. The distribution of the DRGs in the representation of Fig.3.4 resembles the distribution of the respective receptive field in the skin.

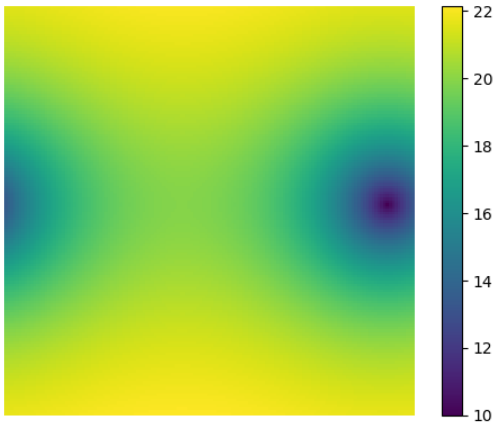

Figure 3.3: Temperature sensed on the skin, resulting from the application of a stimulus with 10°C at nerve ending 10000. The temperature rises exponentially as the distance to the stimulus application point increases. The maximum temperature is 22 degrees - the room temperature.

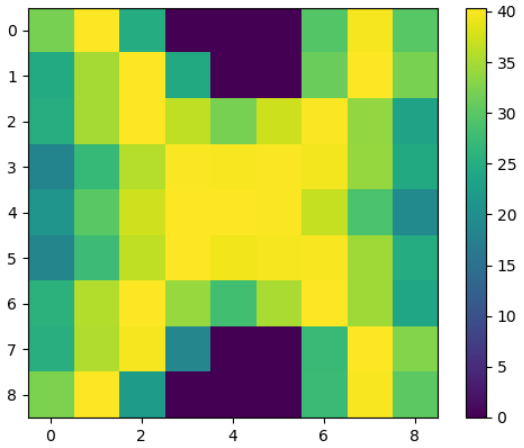

Figure 3.4: Activation pattern of DRG non-monotonically tunned for 20°C population, resulting from the application of a stimulus with 10°C at nerve ending 10000 during 2 seconds. Each square represents a DRG. The activation of the individual neurons is measured as the maximum firing frequency registered during the total course of the experience.

The response of the different DRG populations to a linear, spatially uniform temperature increase (from 12°C to 23°C) can be observed in Fig.3.5(a) and (b). Fig.3.5(a) features the responses of monotonic neurons, whereas in Fig.3.5(b) the responses of non-monotonic neurons are evident.

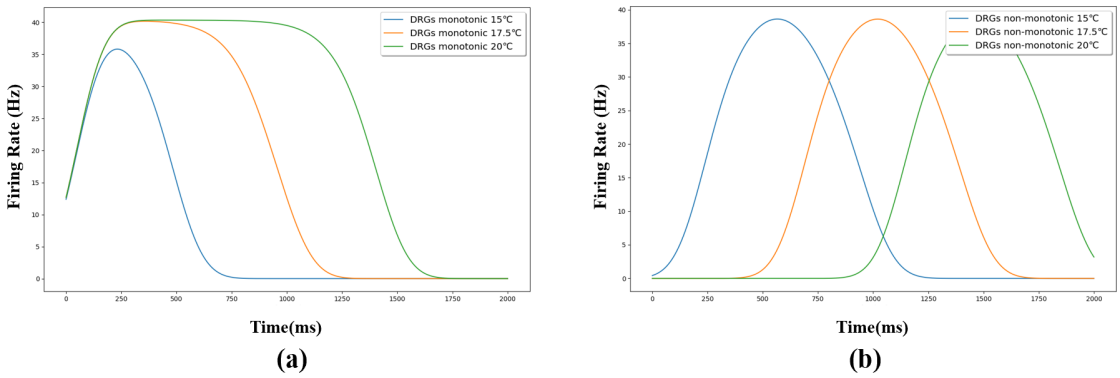

Figure 3.5: Differently tunned DRGs responses to a linear, spatially uniform temperature increase (from 12°C to 23°C). **(a)** Monotonic tunning curves of the DRGs tunned for different temperatures (15°C, 17.5°C, 20°C). **(a)**Non-monotonic tunning curves of the DRGs tunned for different temperatures (15°C, 17.5°C, 20°C).

For the testing of the different connection hypothesis between DRGs and internuerons proposed in section 3.6.2, a spatially even stimulus with a temperature profile similar to the one tested in Ran et al. [79], seen in Fig.3.6, was employed during 16 s, in order to test whether the proposed architecture can explain the experimental results observed in the literature. An overlay of the resulting interneurons responses with the temperature trace of the cooling stimulus (blue line) is depicted in Fig.3.7.

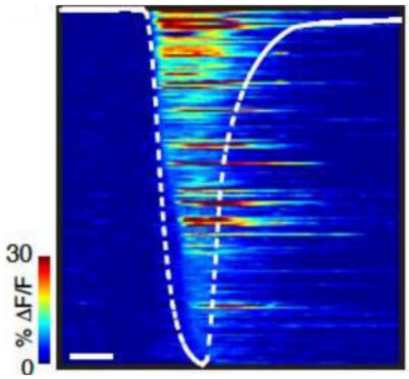

Figure 3.6: An overlay of the temperature trace of a cooling stimuli (white, from 32°C to 16°C) with neuronal responses during this stimulus - heatmap. Adapted from [79].

Furthermore, employing a spatially uneven stimulus, illustrated in Fig.3.8 (a),the response of the interneurons connected to non-monotonically tunned for 15°C and monotonically tunned for 20°C DRG populations is observed in Fig.3.8 (b). Image (b) represents the response of the 9 interneurons whose receptive fields cover the whole surface of the skin. The organization of the squares mimics the organization of the receptive fields. The firing rate differs across the population of interneurons, meaning that the model is capable of coding stimulus location with small spatial resolution at the interneuron level. This decrease in resolution results from the integration of

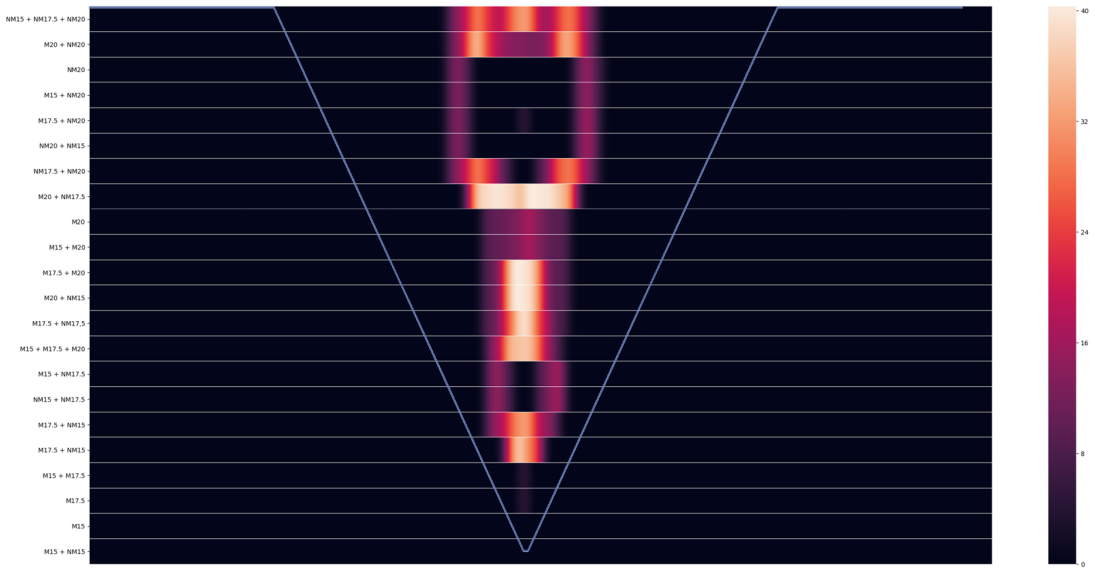

Figure 3.7: Overlay of heatmap of the activity of the different interneurons populations and the temperature trace. The different interneurons populations are distinguished by the DRGs to which they are connected. In the graph NM stands for connections with non-monotonically tunned DRGs, whereas *M* stands for connections with monotonic neurons. The blue line represents the temperature trace during the course of the experience. The maximum temperature is 32°C, while the starting temperature is 16°C.

neuronal information within the receptive field of the interneurons.

Each interneuron communicates with a subset of DRGs and the strength of the connection is determined by the relative position of the DRG to the interneuron receptive field center on the DRG layer, as seen in Fig.3.9.

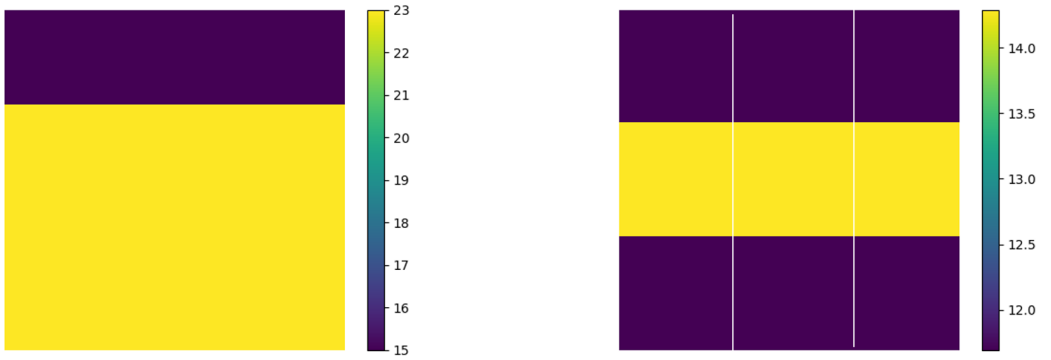

Figure 3.8: Interneurons responses to a spatially uneven thermal stimulus applied to the skin. **(a)** Temperature distribution across the skin's surface. **(b)** Population of interneurons connected to non-monotonically tunned for 17.5 degrees and monotonically tunned for 20 degrees DRG populations responses. Each square represents the response of an interneuron.

In Fig.3.9, it is shown the structural organization of the different layers of the model, which are disposed in a concentric geometry. Black spheres represent individual DRGs monotonically tunned for 15 degrees, while the different colored spheres represent distinct interneurons.

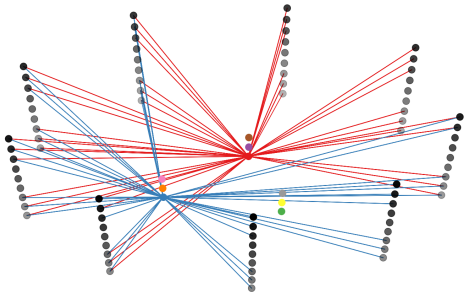

Figure 3.9: Representation of the connections between DRGs monotonically tunned for 15 degrees and two different interneurons. Black markers represent the different DRGs, whereas the different colored markers portray the different interneurons. The connections between the two layers are represented by lines, whose color identifies with which interneuron the connection is made.

The library further provides an interface to target individual cells for stimulation. Fig.3.10 shows how the user interacts with the interface: first, it sets the number of active cells and then, identifies which cells are going to be stimulated and at which moment, finally, a visualization of the active cells is produced. More, it is possible to define the individual spike times for each cell.

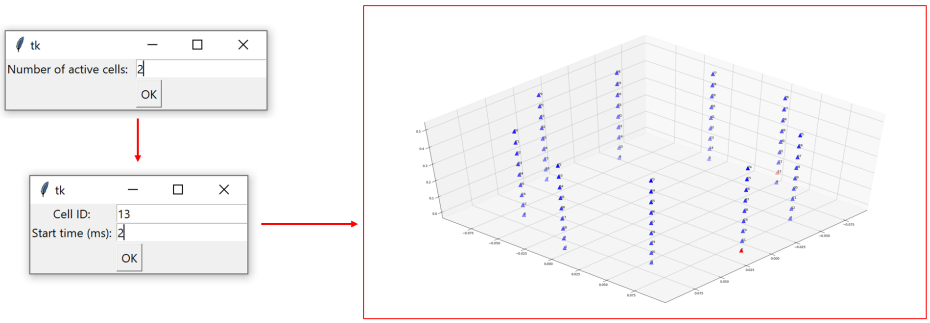

Figure 3.10: Targeted stimuli interface. First, the user sets the number of active cells and then, identifies which cells are going to be stimulated and at which moment, finally, a visualization of the stimulated neurons is produced.

3.8 Discussion

SensorySimLib provides a three dimensional model of the skin's surface and the DRG temperature sensing. The DRGs receptive fields are organized in a hexagonal geometry to cover the entire skin surface. This organization is a simplification of the human skin because, in reality, the different DRG receptive fields overlap and have different sizes. The skin model complies with the no boundaries constraint since the receptive fields located on the bottom of the cylinder have continuity to the top border and the indetermination for $\theta = \pi/2$ is not present.

The proposed architecture is capable of coding stimulus location at the DRG layer since different DRG responses are produced according to its tuning and the temperature sensed within its receptive field. This way, the pattern of activity of a population of DRGs tunned for the same feature can code a spatially uneven stimulus. The resolution with which this encoding is made is determined by the size of the receptive fields because individual DRG responses are determined by the weighted sum of the temperature sensed by each nerve ending of the DRG: large receptive fields encompass a greater number of nerve endings which sense a greater area. The maximum firing rate was 40 Hz which is a value compatible with the observed in the literature for mechanoreceptors.

The coding strategy used to code absolute temperature in the DRG layer is determined by the proportion of monotonic and non-monotonic DRGs. In the framework built, these proportions are equal and the monotonic curves are steep. This way, individual DRGs are activated at different temperature thresholds and the absolute temperature is coded with a combinatorial strategy, compatible with the experimental findings for cold coding in Wang et al. [104]. Increasing the proportion of monotonic graded DRGs, the model would be capable of simulating graded strategies for heat coding.

In the interneuron layer, it is evident this same kind of response: different interneurons are activated at distinct temperature thresholds, according to the DRGs to which they are connected. In fact, neuronal responses only appear after the temperature decreases below 22 degrees. The activation of the different interneurons changes and one interneuron does not suffice to represent the cooling stimuli, hinting for the existence of a combinatorial code in this layer. This way, it is possible to conclude that the model is successful at simulating the results obtained for the coding of absolute cold temperature in the literature and it proved that the strategies proposed by Wang et al. for the coding of temperature in the dorsal root ganglia are compatible with the experimental findings of Ran et al. [79] for the cold coding of temperature in the dorsal horn.

However, experimentally it is observed that cold responding dorsal neurons further respond to temperature change in other temperature ranges, which the model is not capable of simulating. This is, it was found that the responses of cold-responding neurons peak during the cooling stage and rapidly adapt to steady cold stimuli. The modeling of this kind of neuronal response requires the integration of special membrane channels that respond directly to continuous stimulation.

All in all, SensorySimLib provides a framework to test different model architectures and sensory information integration mechanisms, based on experimental findings. The model developed

focused on the coding of thermal stimuli in the cooling range, however, the library presents flexibility to implement other stimulus modalities. Even though the spatial resolution decreases as the layers stack, it was proven that the model is effective in coding stimulus location at the different levels of information integration. On the other hand, stimulus' intensity is coded by the combination of the neural responses of differently tuned neurons. The model can, therefore, code absolute temperature, but does not have the capacity of coding temperature change in other temperature ranges. SensorySimLib can easily be extended to add specific coding mechanisms, without the need for redesigning the whole model structure. More, the library can convert the temperature applied in the skin model into a neuronal response, but can also be put to the test with real spiking data, allowing for the testing and refining of specific experience parameters.

Chapter 4

Functional Connectivity Inference

For the understanding of the structure and function of neuronal networks, its dynamics, and operational principles, it is of critical importance to study the interaction between neurons. The discovery of the wiring diagram behind neuronal circuits can help predict network behavior in novel situations, which has both technological and medical applications [25]. The characterization of neuronal interaction can be studied through functional and effective connectivity. Effective connectivity refers explicitly to the influence that a neuron exerts on another one, either at a synaptic or a populational level. It can be inferred by perturbing the activity of a neuron and measuring the changes on another one. On the other hand, functional connectivity is defined as statistical dependence among measurements of neuronal activity. The present work will focus on the latter.

Functional connectivity can be assessed using correlation-based (model-free) methods or model-based methods. Model-free methods are based on descriptive statistics without any assumption about the process that generated the data, while model-based approaches rely on the premise that a certain mathematical model generated the data and try to infer the parameters and structure of the model. Correlation-based methods are the most used due to its intuitiveness - the output of these algorithms is a weight that can be interpreted as the strength of the connection between the pair of studied neurons. Other model-free techniques to infer functional connectivity are based on Granger causality and Information Theory tools. After the connectivity matrix is obtained it is often filtered to remove weak and non-significant connections.

This work will focus on correlation-based methods to assess the functional connectivity of neuronal networks, namely on the filtered normalized cross-correlation histogram (FNCCH), a novel algorithm proposed recently by Pastore et al. [73]. This algorithm is capable of efficiently infer both functional excitatory and inhibitory links with a low computational cost. The resulting connectivity matrix(CM) can then be filtered to obtain realistic biological connections. Several new visualization techniques were produced to assure that the representation of the functional connections is intuitive and informative.

4.1 Filtered normalized cross correlation histogram

The FNCCH algorithm [73] builds on the standard definition of the cross-correlation 4.1. In theory, cross-correlation is capable of detecting the increase and decrease of synchrony between spike trains of interconnected neurons. However, in real experimental data, the cross-correlogram exhibits an irregular behavior, difficulting the detection of small peaks and troughs and limiting the detection of inhibitory links. Therefore, to better the performance of the algorithm in the said situations, the cross-correlation is normalized and, then, filtered - a process that can be viewed as simple post-processing to the cross-correlation histogram (named Filtered and Normalized Cross-Correlation Histogram, FNCCH).

$$C_{xy}(\tau) = \frac{1}{\sqrt{N_x N_y}} \sum_{s=1}^{N_x} x(t_s) y(t_s - \tau)) \tag{4.1}$$

Equation 4.2 presents the mathematical formulation of the absolute peak of the FNCCH calculated between a reference spike train x and a target train y, where W is the time window in which the FNCCH is calculated.

$$FNCC_{xy} = C_{xy}(\tau)|\tau = argmax \left\{ \left| C_{xy}(t) - \frac{1}{W} \sum_{v=-\frac{W}{2}}^{v=\frac{W}{2}} C_{xy}(v) \right| \right\} \tag{4.2}$$

The filtering procedure comprises the subtraction of the mean value of the cross-correlogram (in the time window W) from the values of the normalized cross-correlogram $C_{xy}(v)$, $v \in [-W/2, W/2]$. The peaks are detected by considering the absolute values, allowing for the detection of the highest peak (positive or negative). This peak reflects the strength of the estimated functional link between the two electrodes in evaluation. The distinction between peaks and troughs is possible by considering the original signal - excitatory links have a positive value, while a negative value refers to an inhibitory one.

The output of the algorithm is a full $n \times n$ connectivity matrix (CM) where each element (i,j) represents an estimation of the strength of the functional link between the electrode i and electrode j.

For the sake of reduction of computational time, electrodes with no significant electrical activity during the total duration of the experiment were discarded and not considered for the computation of the CM. Also, the FNCCH may produce unreliable results in these situations, since strong connections between electrodes with no significant activity may be identified. This way, electrodes with a basal activity inferior to 0.1 Hz were discarded.

4.2 Connectivity matrix spatio-temporal filtering

The functional CM was further filtered to remove biologically unrealistic connections. The implemented method to do so was based on [61]. It consists of filtering the CM with a distance-dependent latency threshold. The threshold for each element of the CM, $t_{(i,j)}$, is determined by

assuming a maximum propagation velocity of $400mm/s$ [16] and by calculating the distance between the electrode pair (i,j) using the Euclidean distance 4.3. This way, if a functional connection has a temporal delay lower than the latency threshold is dismissed. The CM was further filtered with a minimum delay of $1ms$, compatible with fast excitatory AMPA synaptic transmission [73]. In experiments that deal with intracellular action potential propagation, the maximum velocity threshold was set to $3m/s$ and minimum delay threshold was set to 0.001 ms.

$$t_{(i,j)} = v_{max} * \sqrt{(x_i - x_j)^2 + (y_i - y_j)^2} \tag{4.3}$$

The CM was then redefined by removing all the connections that do not respect these thresholds.

4.3 Hard thresholding

The FNNCH gives an estimation of the strength for every pair of electrodes in the CM. Thus, a thresholding procedure is necessary to remove the values that refer to noise and do not represent real functional connections [73]. The simplest thresholding technique is to use a hard threshold, defined by equation 4.4, where μ and σ are the mean and standard deviation, respectively, computed across all elements of the CM.

$$\varepsilon = \mu + n \cdot \sigma \tag{4.4}$$

There are other more sophisticated procedures based on shuffling methods, however, the added complexity makes them computationally expensive. Thus, a simple threshold equal to $\mu + 2\sigma$ was applied for the identification of excitatory connections and for inhibitory ones the threshold was set to $\mu + \sigma$.

4.4 Connectivity map visualization

The visualization of the results of functional connectivity detection algorithms can often be confusing and misleading. In order to make this step more informative and its interpretation easier, three different visualizations were developed, each one providing a distinct perspective on the results.

All the visualizations have a common background - the electrode matrix displayed in the same configuration as the hardware. Electrodes that were previously regarded as non-significant (with no significant electrical activity) were shaded gray, whereas active electrodes were colored yellow, as observed in Fig.4.1. The functional links are represented by a line drawn between the pair of interacting electrodes. The color of the line encodes the strength of the connection: stronger links are colored red, whereas weaker ones are colored blue, following a jet colormap.

In the standard visualization, the connections between the electrodes are represented by straight lines. However, lines may overlap and hide links, for example, when there are several connections between pairs of electrodes of the same column. To avoid this, it was developed a visualization

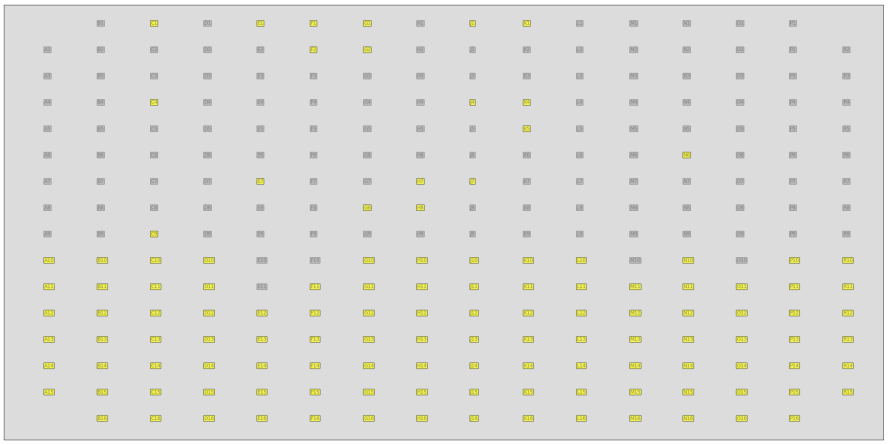

Figure 4.1: Background of visualization. Electrically non-significant electrodes are shaded gray, while active electrodes are highlighted in yellow.

in which the bonds are represented by curved lines. The curves were computed using Bezier's interpolation method with 3 control points: the coordinates of the pair of electrodes and a third point located on the line perpendicular to the straight line connecting the two electrodes.

Finally, a 3D visualization was devised, in which the third dimension corresponds to the cluster coefficient. This metric is a measure of the degree to which an electrode is interconnected with its neighbors and it is defined by equation 4.5, where e represents a generic electrode (or node) ; v_e is the total number of nodes adjacent to e (including e) - its neighbors; u is the total number of edges (connections between the neighbors of e).

$$C_e = \frac{2u}{v_e(v_e - 1)} \tag{4.5}$$

The different visualizations of the CM can be observed in Section 4.6.

4.5 Synthetically generated data for algorithm validation

Spike trains can be simulated by using a Poisson point process, a stochastic process that generates a sequence of events statistically independent. The Poisson distribution, equation 4.6, describes the probability of k events occurring within the observed interval λ.

$$f(k;\lambda) = \frac{\lambda^k e^{-\lambda}}{k!} \tag{4.6}$$

The connectivity analysis was performed in two different configurations: between totally independent spike trains and between totally dependent spike trains. The totally independent spike

trains were generated with independent Poisson processes with different λ, whereas the totally dependent spike trains were created by delaying the first spike train by a specific delay.

4.6 Results

The connectivity inference pipeline was tested in four different sets: in synthetically generated data, in data from hippocampal cultures grown on top of the MEA, in recordings from microfluidic compartmentalized hippocampal cultures and, finally, in data recorded from the stimulation of spinal cord slices. The first test is a validation step, which is necessary to assure the correct functioning of the pipeline. It is achieved by putting the algorithm to the test in controlled situations and evaluate if it performs as expected: the algorithm predicts functional connections when effectively they exist.

4.6.1 Algorithm validation - results in synthetically generated data

Four spike trains were synthetically generated and assessed with the FNCCH algorithm to search for functional links between them. Two spike trains, spike train 1 and 2, were generated with independent Poisson processes, with λ equal to 100 ms and 50 ms, respectively. Spike train 3 was obtained by delaying spike train 1 by 1 ms, to simulate a functional connection with maximum strength. Finally, Gaussian noise was added to the third spike train to produce spike train 4, to mimic the inherent noise of biological signals.

The results of the functional connectivity analysis on the synthetically generated data are shown in Table 4.1.

Table 4.1: Results of functional connectivity assessment on different pairs of synthetically generated spike trains. The FNCCH output can be interpreted as the strength of the connection between the spike trains. When FNCCH is valued at 1, the spike trains are fully correlated and a link with maximum strength is identified. On the other hand, when FNCCH equals 0, no connection is identified. The delay corresponds to the value within the time window (25 ms) where the FNCCH was evaluated where the maximum correlation is registered.

Pair of spike trains	FNCCH	Delay(s)
1&1	1.000	0.000
1&2	0.019	-0.012
1&3	1.000	-0.001
1&4	0.209	-0.001

The FNCCH algorithm was evaluated in a time window of 25 ms for all spike trains combinations. For fully synchronized spike trains (1&1), it was predicted a functional connection with strength 1 and delay equal to zero. On the other hand, for spike trains created with independent Poisson processes (1&2) a weaker connection ($FNCCH < 0.1$) was detected. Between spike train 1 and 3 a functional connection with maximum strength, 1, and delay of 1 ms was identified. The connection between spike train 1 and 4 had also a delay of 1 ms but lower strength, 0.2.

4.6.2 Unconstrained cell cultures connectivity inference results

A hippocampal neuronal culture was grown on top of an MEA and its electrical activity measured after 12 days in vitro (DIV). For the connectivity analysis of the data acquired, the maximum velocity threshold was set to 400 mm/s and the minimum delay threshold to 1 ms. The standard visualization of the resulting excitatory CM is depicted in Fig.4.2.

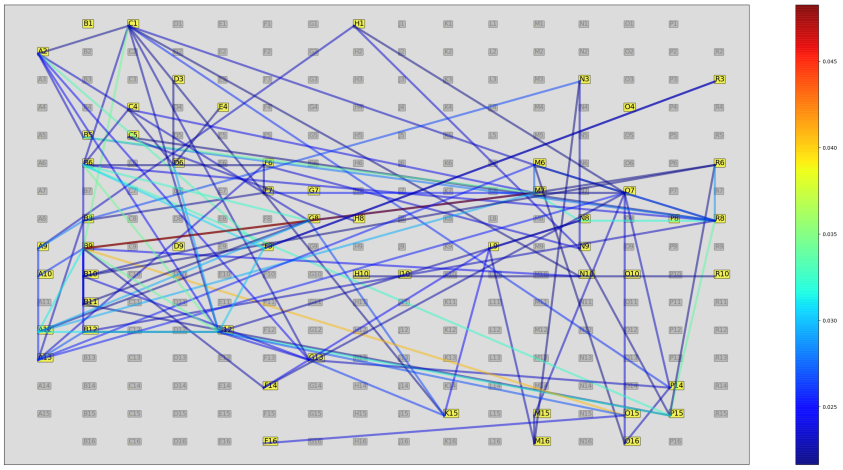

Figure 4.2: Standard visualization of the excitatory connectivity map of hippocampal culture at 12 DIV. Connections are colored according to its strength. The maximum strength among the detected connections is 0.050.

The probability histogram of the connections' strength is depicted in Fig.4.3(a). The average strength of the biologically realistic connections detected is 0.026 and 97.2% of them have strength below 0.035. The distribution of the length and delay of the links are illustrated in Fig.4.3 (b) and (c), respectively. The average length of the links is 0.71 mm, whereas the average delay is 6.2 ms. On the other hand, Fig.4.4 shows the 3D view of the links. Electrode N10 presents the maximum clustering coefficient and the average clustering coefficient of the network is 0.13. No inhibitory connections were detected.

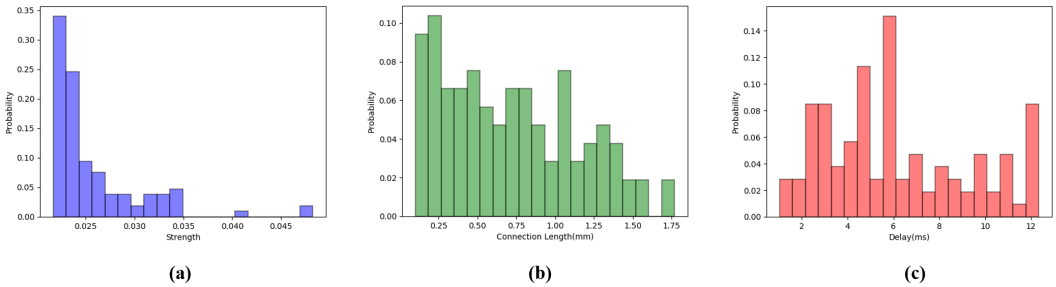

(a) **(b)** **(c)**

Figure 4.3: Characterization of the functional connections detected in hippocampal culture at DIV 12. **(a)** Probability histogram of the connections' strength, where 97.2% of the links have strength below 0.035. **(b)** Histogram of connections' length. The average length is 0.71 mm. **(c)** Histogram of connections' delay. The average delay is 6.2 ms.

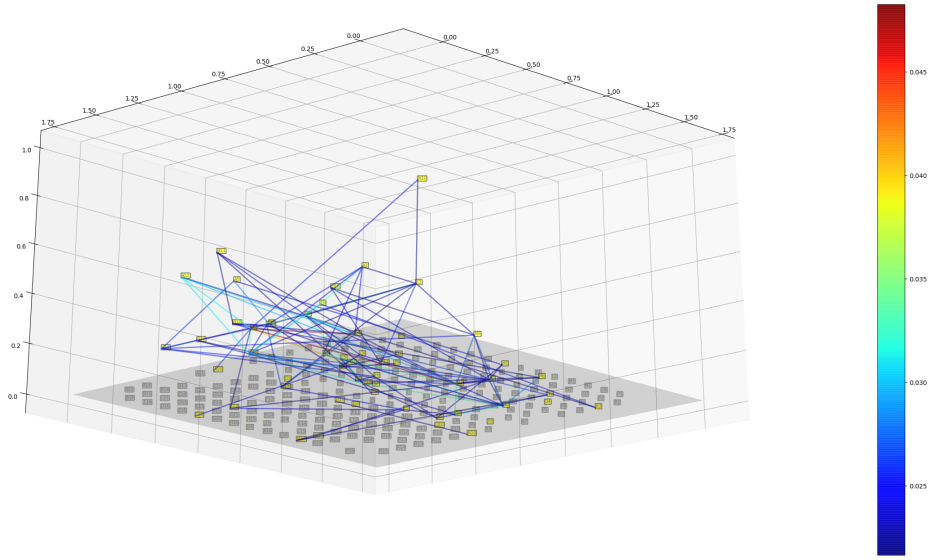

Figure 4.4: 3D visualization of excitatory links detected with the FNCCH algorithm for hippocampal culture at DIV 12. The third dimension of the graph represents the electrode's clustering coefficient, which is valued between 0 an 1. The clustering coefficient is a measure of the degree to which elements in a network tend to cluster together.

The algorithm was further tested in a different hippocampal culture also at DIV 12. The average length of the detected links is 0.71 mm, whereas the average delay is 5.8 ms, and the average strength was 0.025. The histograms of the connections strength, length, and delay are depicted in Fig.4.5(a), (b) and (c), respectively. The connections length is distributed over a wide range, between 0.1 and 1.75 mm. The maximum length possible is 0.21. On the other hand, the strength of the links is concentrated in the 0.020 to 0.030 spectrum. The standard visualization of the excitatory connectivity map is illustrated in Fig.4.6. The 3D view of the functional links is shown on Fig.4.7. Electrodes N1, A10 and D6 present maximum clustering coefficients and the average clustering coefficient of the network is 0.20. No inhibitory connections were detected.

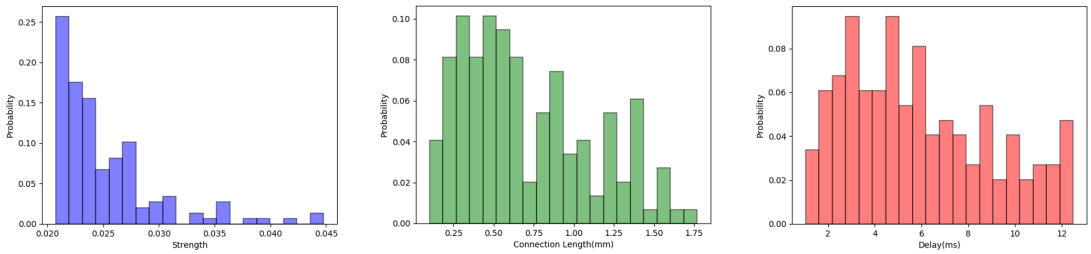

(a) **(b)** **(c)**

Figure 4.5: Characterization of the functional connections detected in the second hippocampal culture at DIV 12. **(a)** Probability histogram of connections' strength. The strength of the links is concentrated in the 0.020 to 0.030 spectrum. **(b)** Probability histogram of connections' length. The average length of the links is 0.71 mm. **(c)** Probability histogram of connections' delay. The maximum delay is 12 ms.

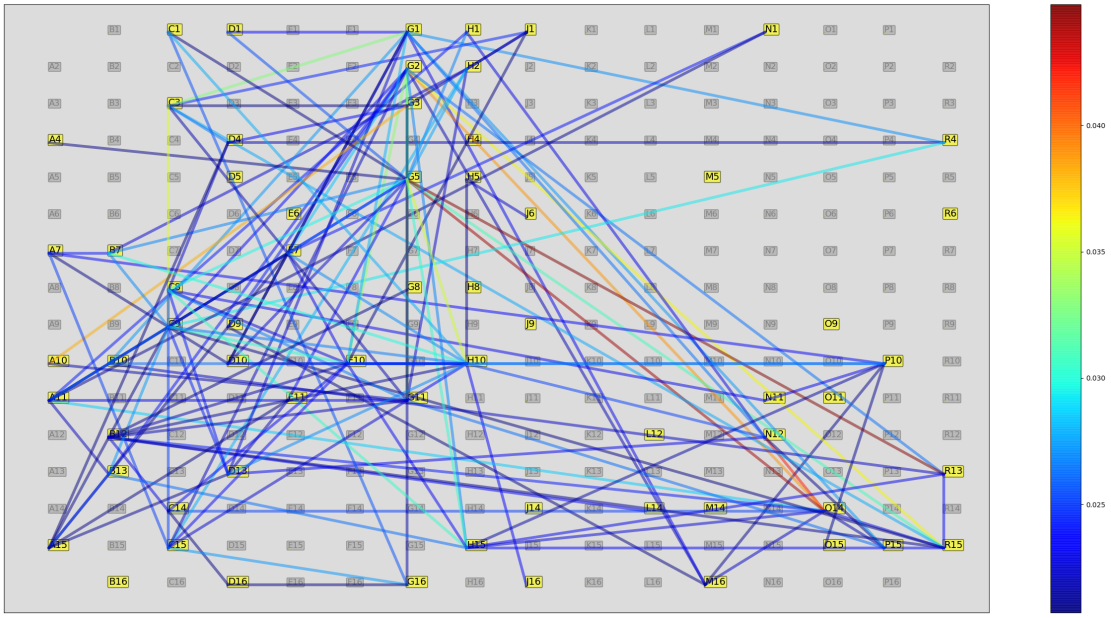

Figure 4.6: Standard visualization of the connections detected in the second hippocampal culture at DIV 12.

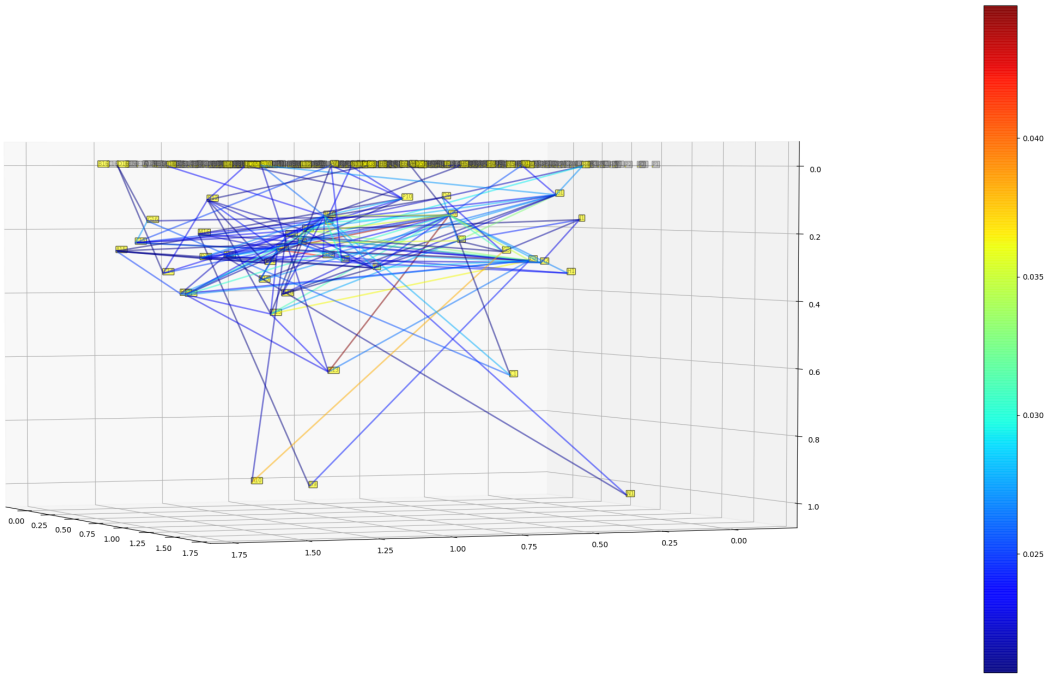

Figure 4.7: 3D visualization of the excitatory links resulting from the connectivity analysis of the second hippocampal culture at DIV 12. Electrodes N1, A10 and D6 present maximum clustering coefficients.

4.6.3 Connectivity inference in compartmentalized cell cultures in microfluidics

By interfacing microElectrode arrays with microFluidics (EF devices), it is possible to compartmentalize neuronal cultures with a specified alignment of axons and microelectrodes [43]. This setup allows the extracellular recording of spike propagation with a high signal-to-noise ratio over the course of several weeks. Recordings obtained with this method were analyzed with the developed pipeline. As the experiments deal with intracellular action potential propagation, the maximum velocity threshold was set to $3m/s$, while the minimum delay threshold was set to 0.001 ms - values compatible with the maximum axonal spike propagation velocity observed in the literature.

The excitatory connectivity map obtained from the analysis of microfluidic compartmentalized hippocampal cultures at DIV 11 is pictured in Fig.4.8(a) and (b). Fig.4.8(a) depicts the standard view of the CM, while Fig.4.8(a) illustrates the curved lines visualization. The connectivity inference analysis was performed without prior knowledge about the structure imposed by the microfluidic compartmentalization, which Fig.4.9, obtained with confocal microscopy, reveals. The vertical grooves of the microfluidic structure, seen in the figure, are aligned with the MEA's electrode columns from index 10 to 16. Additionally, the electrode marked red - electrode C9 - is close to an agglomerate of neurons. In the standard view of the CM, one can observe that a great deal of connections leave this electrode. In the curved lines visualization, Fig.4.8(b), the interconnections between electrodes of the same column - links that are hidden in the standard visualization - are exposed. The network's structure can be further studied in the 3D visualization, Fig.4.10. Electrodes that participate in the connections inside the microgrooves present maximum clustering coefficient. The average clustering coefficient is 0.55.

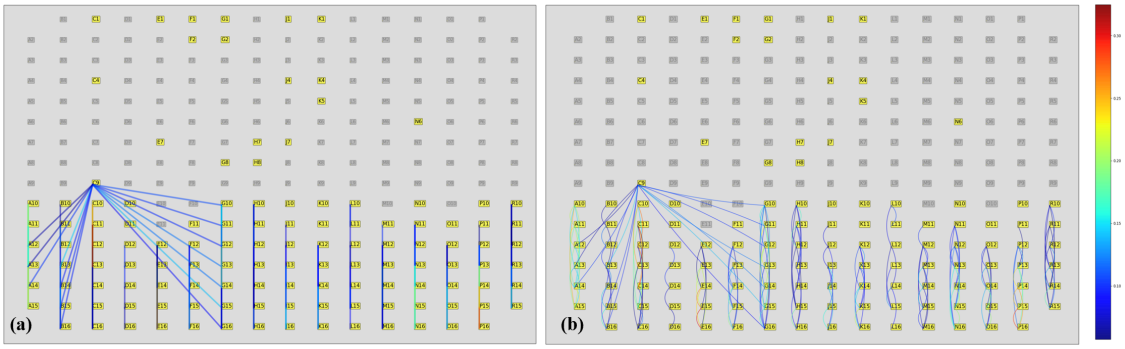

Figure 4.8: Visualizations of the excitatory connectivity map detected in microfluidic compartmentalized hippocampal cultures at DIV 11. **(a)** Standard visualization of excitatory connectivity map. The majority of the connections detected is parallel to the MEA's electrode columns. **(b)** Curved Lines visualization. This view of the CM allows fof the identification of hidden connections between electrodes of the same column.

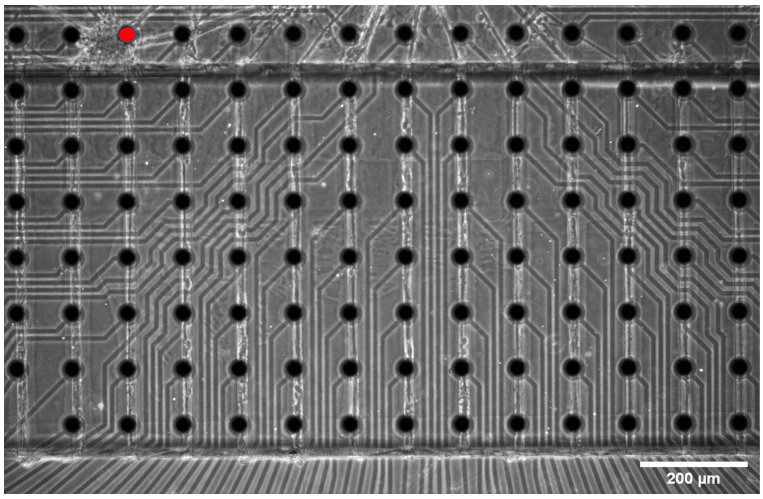

Figure 4.9: Confocal microscopy image (10x magnification) of microfluidic compartmentalized hippocampal culture at DIV 11, where the microfluidic structure is evident. The vertical grooves of the structure are aligned with the MEA's electrode columns from index 10 to 16. The electrode marked red - electrode C9 - is positioned near an agglomerate of neurons, which may explain the high number of connections coming from this electrode detected with the connectivity inference pipeline.

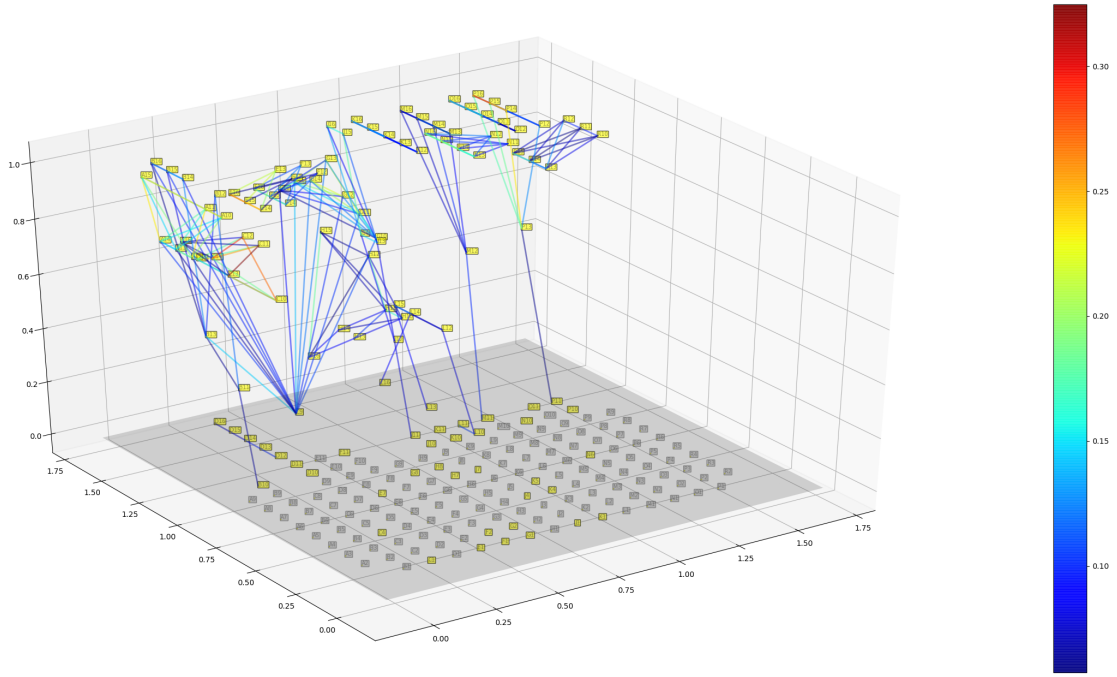

Figure 4.10: 3D visualization of the excitatory links identified in microfluidic compartmentalized hippocampal culture at DIV 11. The majority of the electrodes that participate in the links between electrodes of the same column present maximum clustering coefficient.

In Fig.4.11(a), one can observe the probability histogram of the connections' strength. The most frequent strength is 0.1 and the average link strength is 0.13. On the other hand, in Fig.4.11(b),

it is visible that most of the links have a delay below 0.5 ms, which is consistent with intracellular spike propagation. Finally, the majority of the links have a connection length between 0.1 and 0.2 mm, as observed in Fig.4.11(c), which indicates that most of the links are between neighbor electrodes. The mean link length is 0.25 mm, whereas the average connection delay is 0.46 ms.

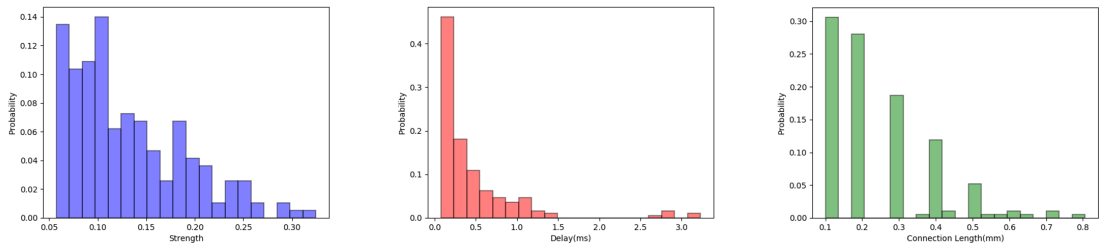

Figure 4.11: Characterization of the functional excitatory links detected in microfluidic compartmentalized hippocampal culture at DIV 11. **(a)** Probability histogram of connections' strength. The most frequent strength is 0.1. **(b)** Probability histogram of connections' length. The average link length is 0.25 mm. **(c)** Probability histogram of connections' delay. The average connection delay is 0.46 ms.

The number of inhibitory connections detected was significantly lower - inhibitory links represent only 3.5% of all connections discovered. The inhibitory connectivity map is exhibited in Fig.4.12. All inhibitory connections have the same delay (12.5 ms) and present low strength, inferior to 0.0001.

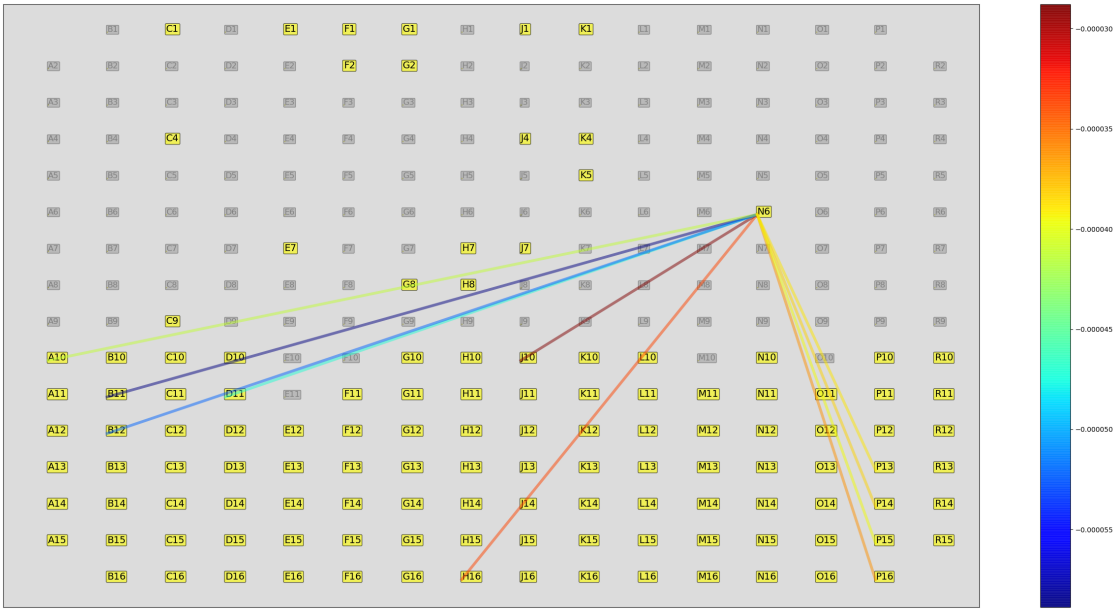

Figure 4.12: Standard visualization of the inhibitory connections detected in microfluidic compartmentalized hippocampal culture at DIV 11. All connections have strength inferior to 0.0001.

Axotomy is the process of cutting or otherwise severing an axon. It is often performed to study nerve regeneration [41]. The previously analyzed culture was subjected to this process - the axons growing inside the microgrooves were cut - and its electrophysiological activity recorded 12 hours after axotomy. The excitatory and inhibitory connectivity maps resulting from the connectivity inference analysis are depicted in Fig.4.13(a) and (b), respectively. The structure identified in the excitatory CM is different from the one identified before axotomy: the number of parallel connections to the electrode columns reduced substantially. In the 3D visualization of the excitatory CM, Fig.4.14, it is evident that the electrodes that participate in the parallel connections still present high clustering coefficients, however the average clustering coefficient of the network decreased to 0.23. The probability histogram of the connections delay, seen in Fig.4.15(b), presents a similar distribuition to the one obtained before axotomy, with the majority of the links having a delay below 0.5 ms. The average delay is 4.3 ms. Most of the links are short-range - connection length under 0.2 mm, as illustrated in Fig.4.15 (c). The histogram of the linking strength, Fig.4.15 (a), is distributed over a larger range of values, with a significant amount of links stronger than 0.25. The average link strength is 0.20.

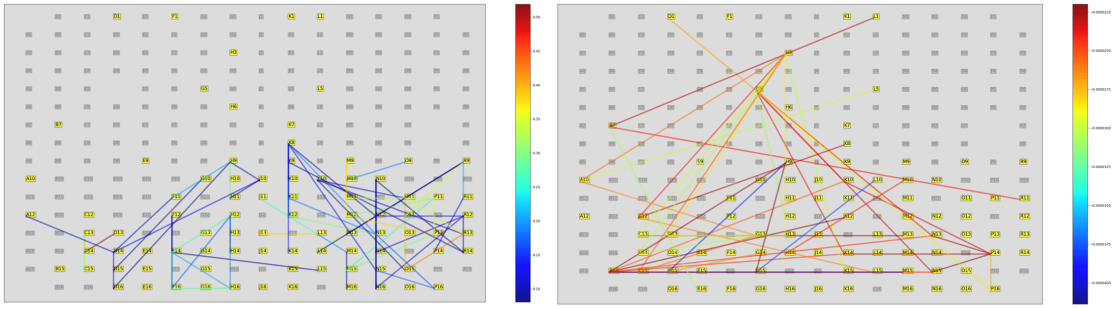

(a) (b)

Figure 4.13: Visualizations of the excitatory connectivity and inhibitory connectivity maps detected in microfluidic compartmentalized hippocampal cultures at DIV 12 after axotomy.**(a)** Standard visualization of the excitatory connectivity map. The number of connections parallel to the electrode columns reduced significantly after axotomy. **(b)** Standard visualization of the inhibitory functional connections detected. Most of the links are long - range.

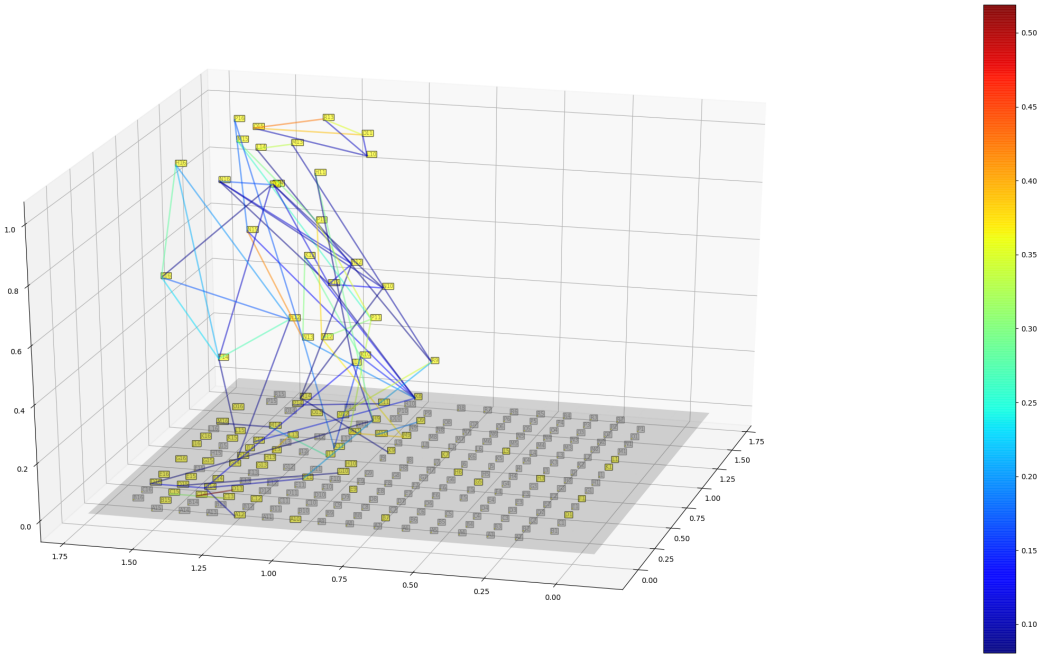

Figure 4.14: 3D visualization of the excitatory links identified in microfluidic compartmentalized hippocampal culture at DIV 12 after axotomy. The number of electrodes with maximum clustering coefficient significantly reduced, in fact, the overall clustering coefficient decreased to 0.23.

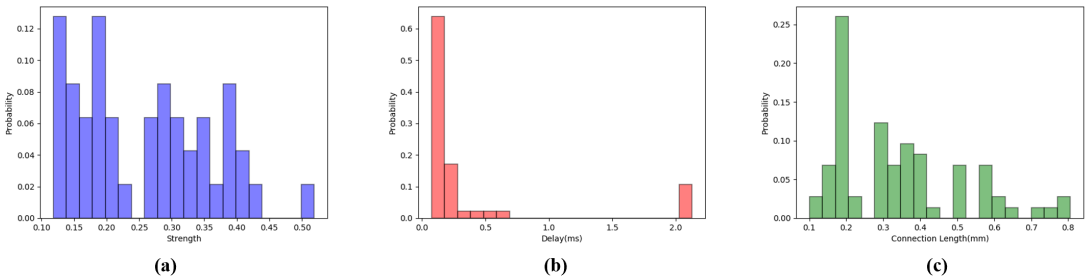

Figure 4.15: Characterization of the functional excitatory links detected in microfluidic compartmentalized hippocampal culture at DIV 12, 12 hours after axotomy. **(a)** Probability histogram of connections' strength. The average connection strength is 0.2. **(b)** Probability histogram of connections' length. Most of the links are short-range - the most frequent length is 0.2. **(c)** Probability histogram of connections' delay. The average delay is 4.3 ms.

The inhibitory connections are, on average, longer than the excitatory ones, as seen in the histogram comparison of the connections' length, in Fig.4.16. All inhibitory connections present the same delay - 12.5 ms.

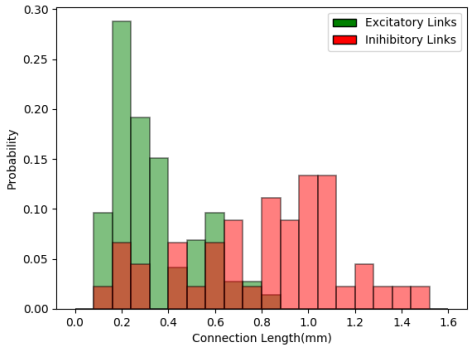

Figure 4.16: Histogram comparison of the excitatory and inhibitory connections' length. Inhibitory connections are on average longer.

4.7 Discussion

The results obtained for the connectivity inference in synthetically generated data are in agreement with what was expected since maximum strength connections were identified between spike trains fully synchronized and low strength connections were detected between spike trains independently generated. Also, the delay of the detected links was concordant with the data generation process. The algorithm is, therefore, capable of detecting and correctly characterizing functional links. The results obtained in synthetic data can be used as a solid baseline for the interpretation and comparison of the real data connectivity inference analysis results. In fact, comparing the strength of the excitatory links detected in the unconstrained cell cultures with the baseline, it is possible to classify them as weak since their average strength is significantly smaller than the strength of synthetic biological connections and approximates to the linking strength of spike trains independently generated. The weakness of the links may be explained by the fact that the neuronal cultures grew unconstrained so, the likelihood of having a neuron placed directly above a microelectrode is low. The signal picked up has, therefore, a low signal-to-noise ratio since it is a sum of local field potentials generated by transient imbalances in ion concentrations in the space outside the cells. The unconstrained cultures grew freely with no imposed structure. The CMs obtained for the analysis of the electrical activity of these cultures reflect the randomness of the networks connections since no apparent organization is perceptible. In the same way, the flat appearance of the connections' delay and length histograms shows the diversity of connections identified.

In contrast, the connections detected in the microfluidic compartmentalized cultures are strong: the average strength of the excitatory links has the same order of magnitude as the strength of the biologically simulated links. The detection of strong connections is related to microfluidic

structural imposition. The axons are aligned with the electrode columns, which allows for the acquisition of high signal-to-noise ratio extracellular recordings. The majority of the connections are short-range, between neighbor electrodes, for the same reason. The excitatory CM of the culture before axotomy reveals the structural architecture imposed since the presence of parallel connections and the absence of transversal links to the electrode columns is evident. These connections are located in the same location where the microfluidic was placed, revealing the success of the microfluidic compartmentalization process. After axotomy, the presence of parallel connections is reduced, which may be explained by cell death. In fact, the global clustering coefficient also decreases, indicating that the aggregation of the network was reduced. Before axotomy, the electrodes that participated in the connections inside the grooves presented maximum clustering coefficient, meaning that they were tightly interconnected. After axotomy, only a few of those electrodes present maximum clustering coefficient, suggesting that the spike propagation inside the grooves was impaired.

The results obtained for the detection of inhibitory connections were inconclusive since the linking strength of the identified connections was close to zero. More, all the connections detected had the same delay, which is not biologically realistic and is most probably a result of hardware noise.

The different CM's visualizations allow for the thorough inspection of the structure of the discovered network. The curved lines view of the CM may uncover hidden connections. On the other hand, the three-dimensional visualization is interactive and can be rotated to observe the structure from different perspectives. As a result, the user increases its knowledge about the network's architecture. The development of the different visualizations, therefore, filled a gap in the literature, by producing more informative visualizations of the CM and making the interpretation of the results easier.

All in all, it was proven that the algorithm can reliably detect excitatory functional connections in electrophysiological data with high signal-to-noise ratio, such as in microfluidic compartmentalized cultures. The pipeline developed is also capable of revealing the underlying structure of the discovered network, by producing informative views of the excitatory CM and bridging the faults of traditional visualizations. Finally, the clustering coefficient proved to be an important metric to characterize network aggregation.

Chapter 5

Experimental Setup

The spinal cord is the information highway of the nervous system, moderating the communication between the outside world and the brain. Unlike the brain, the spinal cord has reduced spontaneous activity: neurons are mostly driven by external stimuli. Bearing this, the study of the electrophysiological activity in *ex vivo* spinal cord slices involves necessarily the stimulation of the sample. In theory, the stimulation will trigger neuronal responses, allowing for the uncover of local spinal circuits. MEAs are capable of performing simultaneous recording and stimulation, making it the ideal acquisition tool to study spinal cord connectivity. Experiments in the laboratory were carried out with hardware from MultiChannel Systems (MCS, Germany). MCS offers a wide range of tools to control data acquisition and stimulation. In fact, it provides an Application Programming Interface (API) that allows you to programmatically control the MCS devices using external software. This library was used to automate the stimulation of all electrodes of the MEA and the recording in between stimuli, with the objective of reducing the experience's duration and, therefore, increase the viability of the spinal slices.

This chapter overviews the experimental setup, explaining how the data acquisition/stimulation protocol was implemented and how the spinal slices can be prepared for use with the protocol. The chapter ends with the validation of the developed routine.

5.1 Experimental setup overview

The total experimental setup can be observed in Fig. 5.1. The acquisition and stimulation system is constituted by the computer with the MCS software connected to the MEA-2100 system. The MEA containing the spinal cord slice kept in artificial cerebrospinal fluid (ACSF) is inserted into the system, as shown in Fig.5.1. The slice should be put in the center of the ring to guarantee that the electrodes are right below the sample. Once the sample is put on the MEA and the oxygenation ceases, its deterioration starts, so it is of utmost importance that the experiment is performed as fast as possible, if perfusion is not available. With this in mind, the protocol was designed to fulfill this requirement, by eliminating the need for interaction with the system in the course of the experiment.

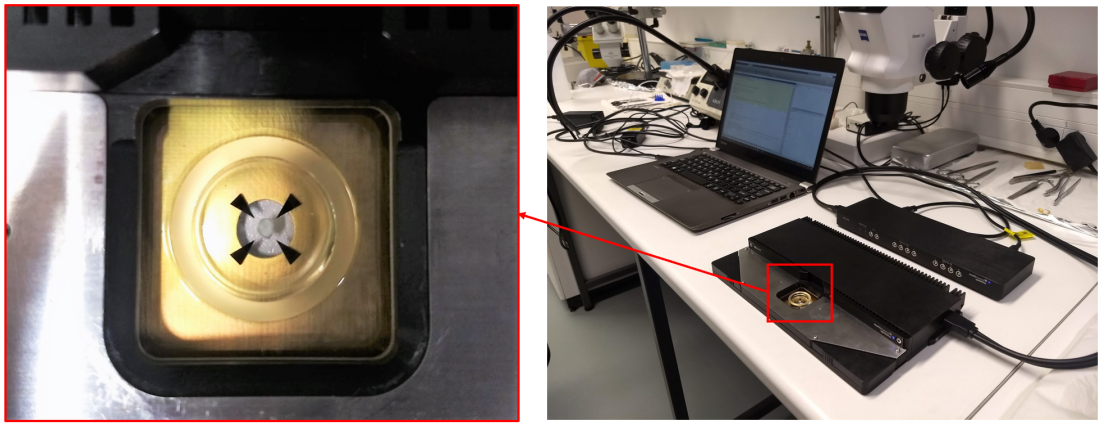

Figure 5.1: Experimental setup. The acquisition is carried out by the computer and the MEA-2100 system. The MEA containing the spinal cord slice is placed inside the headstage.

5.2 Spinal cord slice preparation

Laboratory Wistar rats (P14) were terminally anaesthetised (by intraperitoneal injection of Na+-pentobarbital) and decapitated, in accordance with national guidelines(Direcção Geral de Veterinária, Ministério da Agricultura) and the institutional Ethics Committee. The vertebral column was quickly cut out and immersed in ice-cold oxygenated artificial cerebrospinal fluid (ACSF). Slices from the lumbar enlargement were dissected and used as preparation. Given the unavailability of an appropriate tissue slicer, 1mm thick slices had to be cut manually with a blade (scalpel). Individual slices were kept in oxygenated ACSF, at room temperature, until used in the microelectrode array. All measurements were done at 22–24 °C. During the experiment the slices are kept in ACSF.

5.3 Data acquisition and stimulation routine

Given the objectives of the project, it was necessary to implement a custom-made data acquisition and stimulation protocol, using MCS available software tools. In this section, it is made an overview of the hardware and software used and a description of the routine. Finally, the implementation of the protocol was validated.

5.3.1 Electrophysiological system overview

The electrophysiological recordings performed in the present dissertation were carried out making use of MEA2100- System, a commercially available in vitro system for extracellular recordings using MEAs, provided by Multichannel Systems (MCS) [1]. The MEA2100 - System consists of several components: MEAs, headstage, interface board and PC with software, as depicted in Fig.5.2.

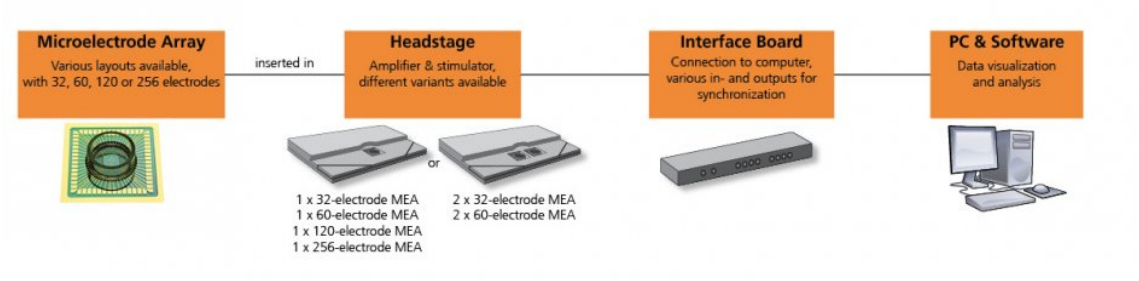

Figure 5.2: MEA-2100 system overview. The MEA100-System consists of several components: MEAs, headstage, interface board, PC with software. Adapted from [1].

The headstage is the core element of the system. It is where the MEA is placed and is responsible for data acquisition, signal amplification, and digitalization. Several MEAs are compatible with the headstage, however, in this work, it was only used a 256-electrode MEA. The headstage also provides an integrated stimulus generator, which can produce current or voltage stimulation signals on two independent channels for the MEA2100-256-Systems. The data acquisition is performed by an A/D converter integrated into the headstage, it is done on all channels simultaneously to ensure data quality. The acquisition parameters, such as the sampling rate, can be defined using the MCS software. More, the amplification system is designed in such a way that the recorded signals are amplified close to the signal source, which minimizes noise. The system has a fixed hardware gain of 10 and a resolution of 24 bits. Any MEAs' combination of electrodes can be selected for stimulation. The stimulus features such as the amplitude, duration, and frequency are implemented and controlled using the MCS software.

The interface board is the connecting element between the headstage and the computer. It receives the signal from the headstage and allows for real-time signal detection and feedback through a digital signal processor (DSP). This interface connects to the computer and has other digital and analog outputs for synchronization with other instruments. More detailed information can be found in the MEA2100-System brochure [65].

5.3.2 MCS software

MCS offers a software solution for the acquisition and analysis of electrophysiological data: the Multi Channel Suite. This package consists of three tools: the Multi Channel Experimenter - an interface that allows for online analysis and graphing of the signals acquired and control of data acquisition settings; the Multi-Channel Analyzer - an offline analysis tool and; the Multi Channel DataManager, which facilitates the data export for analysis with third-party programs.

The Multi Channel Experimenter enables the selection of the stimulation electrodes and the construction of the stimulation pattern through an interface that can be observed in Fig.5.3. After its design, the stimulus pattern is downloaded onto the DSP and can be triggered at any moment by clicking the *start stimulator* button. The data acquisition is also activated and stopped in the interface, by pressing the *Start/Stop DAQ* switch. Every time the stimulation electrode or the waveform changes, the stimulus needs to be downloaded and the user needs to activate the stimulator again,

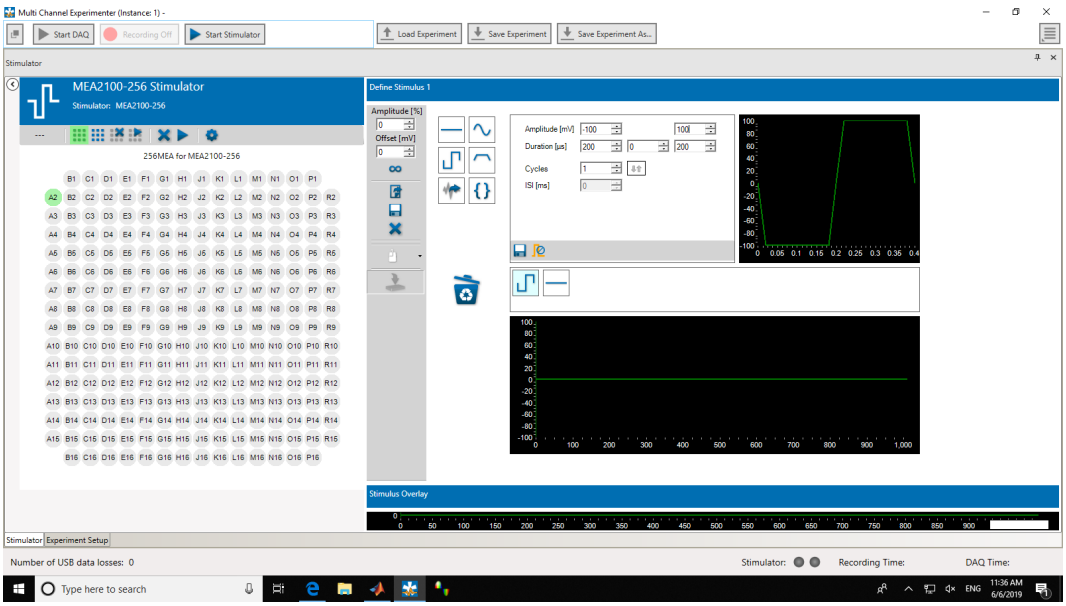

Figure 5.3: Multi Channel Experimenter: stimulus design interface. Easy-to-use drag and drop interface, you simply create your virtual experiment with e.g. data source, filters, spike detection, and recorder. The software indicates the battery level and signal quality and displays the data in real-time.

requiring a continuous interaction with the interface during the course of the experience, which may be time-consuming and unpractical. Despite Multi Channel Experimenter being a useful tool for the design and performance of simple experiments, it does not take full advantage of the hardware. So, MCS has made available an API through a dynamic link library (DLL) - a .NET interface to all MCS devices - which allows for the development of custom-made software with fine control over hardware settings.

The DLL is a collection of small programs that can be loaded and used by a larger program, letting it communicate with an MCS device, such as the stimulus generator, STG200x, or the data acquisition system, DAQ. The library is divided in classes dedicated to the control of different MCS devices. Thus, one can emulate the actions performed in the Multichannel Experimenter in a third party program, such as Matlab, and automate a stimulation/recording routine.

5.3.3 Stimuli/recording protocol

The purpose of the protocol is to automate the sequential stimulation of a set of electrodes and the data acquisition in between stimuli. The automation of the routine has the potential to reduce the experience's duration and, thereby increase the viability of live excised spinal cord samples since it eliminates the need for interaction with the software. The protocol was implemented in Matlab since it is a high-level programming language, which is widely used in the laboratory, allowing for future iterations in the code to be made by other members of the group. Fig.5.4 illustrates the flow chart that characterizes the sequence of actions encompassed by the routine.

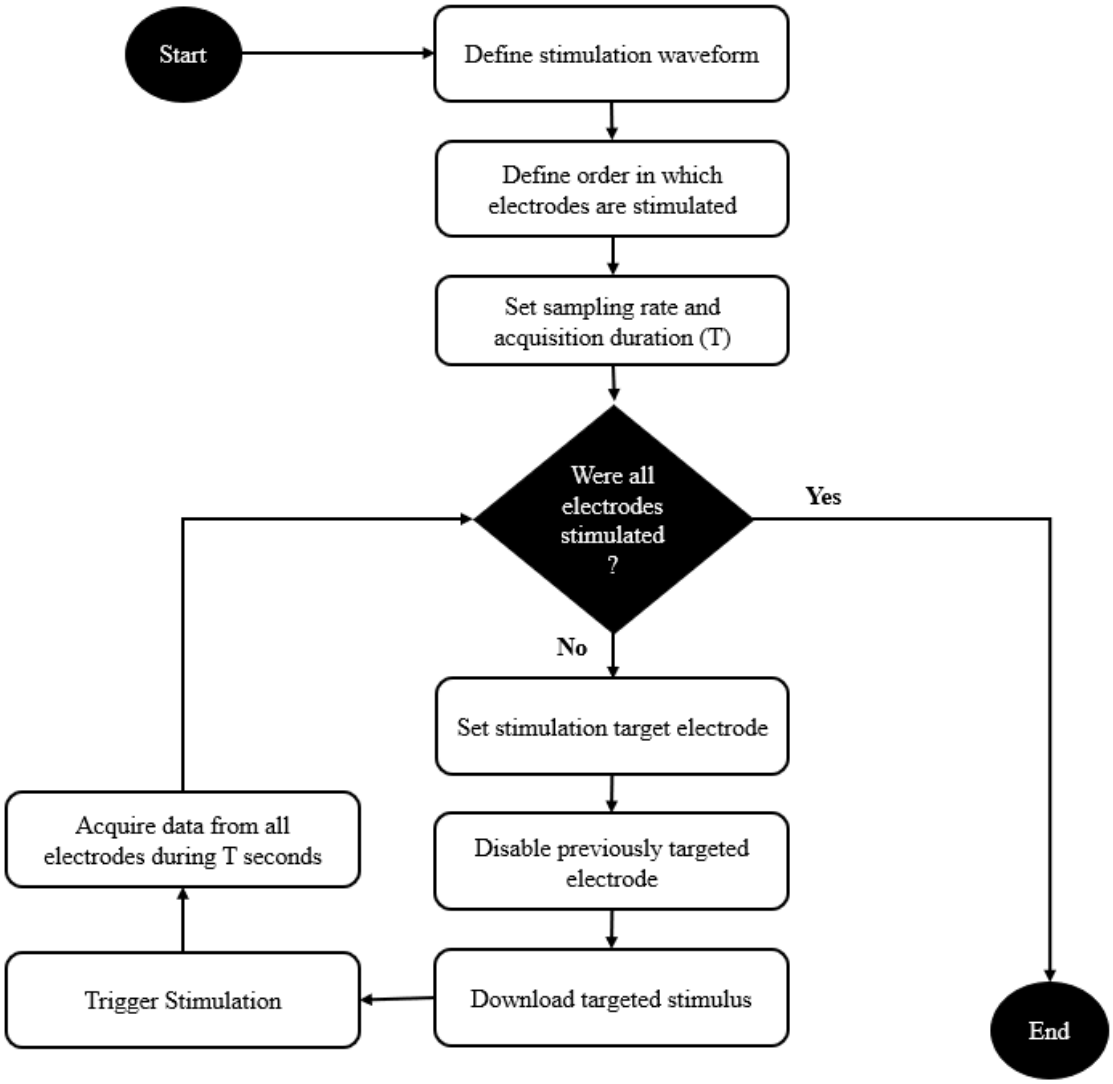

Figure 5.4: Flowchart explaining the sequence of actions that make the data acquisition and stimulation routine.

First, the user ought to define the stimulus waveform - its duration and amplitude - the number of repetitions of the stimulus and, the interval in between pulses. It is important to ensure that the stimulus does not damage the electrodes as positive pulses can lead to the formation of titanium oxide on the MEA surface. Only negative voltage pulses or biphasic current pulses applying the negative phase first should be applied. After that, the user specifies the order in which the electrodes will be stimulated and the sampling rate. Before the electrode scanning, all the electrodes need to be disabled for stimulation, to guarantee that no electrodes other than the required one are stimulated. At each stimulation iteration, the stimulation target electrode is enabled and the previously activated electrode disabled, the stimulus is, then, downloaded onto the DSP and the blanking activated. The blanking circuit disconnects the electrodes from the amplifiers, each time the stimulation is triggered, avoiding stimulus artifacts on the recording electrodes and the saturation of the amplifiers. The blanking period is approximately 600 μ before and after the stimulus.

Finally, the stimulation is triggered and the data acquisition is performed during T seconds.

In the experiments performed, the stimulation pulse was a square wave, with the first phase negative, a 2000 mV peak to peak amplitude and a period of 400 ms. Two repetitions with an interval of 500 ms were performed per electrode, the sampling rate was set to 5 kHz and the acquisition's duration was 2 seconds.

5.3.4 Validation

The validation of the routine developed was divided into two parts. First, the data acquisition was tested and its performance compared with the Multi Channel Experimenter then the stimulation procedure was verified by assessing if the stimulus is picked up by other electrodes submerged in a conductive fluid - phosphate-buffered saline (PBS). The validation step is essential to verify that the communication between the PC and the headstage is being performed correctly, assuring that the protocol fulfills its purpose.

5.3.4.1 Data acquisition

MSC provides an objective tool for testing data acquisition settings and MEA related software, without using biological samples - the 256MEA Signal Generator (MEA-SG). It can be used for training, controlling and troubleshooting purposes, reducing the number of animal experiments and saving laboratory equipment. The device, depicted in Fig.5.5, produces sine waves or real signals in a digitized form. These signals are read as analog signals by the MEA-System, enabling for the use and test of the complete MEA-System. The MEA-SG generates different signals depending on the dual in-line package (DIP) switches positions and the number of control button presses. For the validation of the data acquisition script, the MEA-SG was programmed to generate a sine wave with 1.25 Hz frequency and 3 mV peak-to-peak voltage.

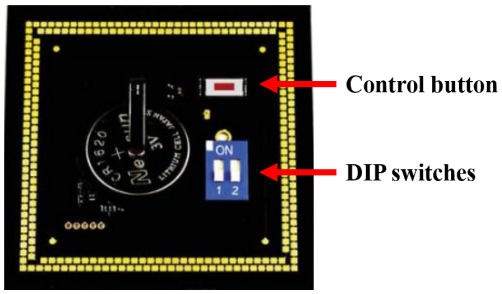

Figure 5.5: 256MEA Stimulus Generator. The position of the control button and the DIP switches determines which stimulus is generated.

Fig.5.7 depicts the signal recorded during 3 seconds. All electrodes recorded activity with a high signal-to-noise ratio (SNR), pointing to the hardware's good condition. Comparing the signal registered with the custom-made script by electrode H12, Fig.5.7 (a), with the recording made by

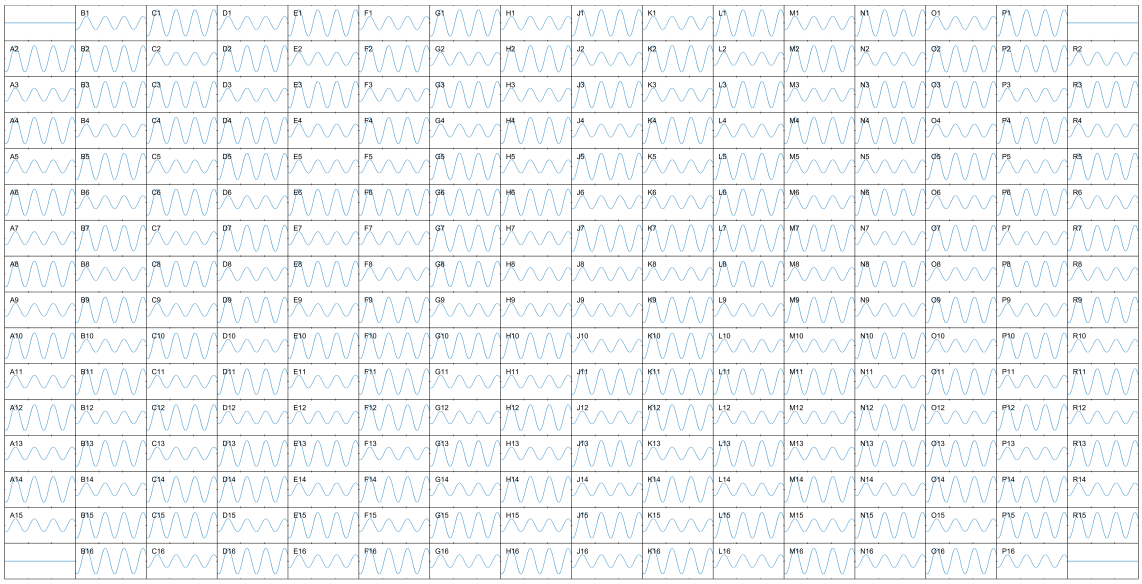

Figure 5.6: Signal read in each electrode with the MATLAB custom-made data acquisition protocol. The signal is acquired with a high signal-to-noise ratio.

Multi Channel Experimenter, Fig.5.7 (b), it is possible to confirm that the signal acquired by both methods has the same amplitude and frequency, hence validating the data acquisition protocol.

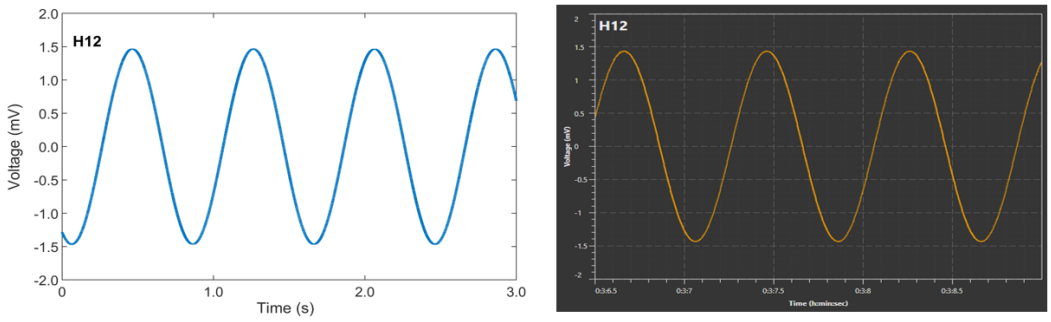

Figure 5.7: **(a)** H12 electrode signal read with the custom-made script.**(b)** H12 electrode signal read with Multichannel Experimenter.

5.3.4.2 Electrode scanning

The electrode scanning was tested in an MEA filled with PBS, a conductive solution. In the validation experiment, two electrodes (A2 and P16) were stimulated sequentially. The resulting recordings are shown in Fig.5.8 and Fig.5.9. One can observe that the signal is picked up by other electrodes other than the stimulation target electrode and that when one electrode is targeted for stimulation the previously activated electrode is disabled, corroborating the success of the

implementation of the protocol. In the recording of the stimulation electrode, Fig.5.8, the stimulus waveform is perceptible and zooming in it is possible to identify the blanking period.

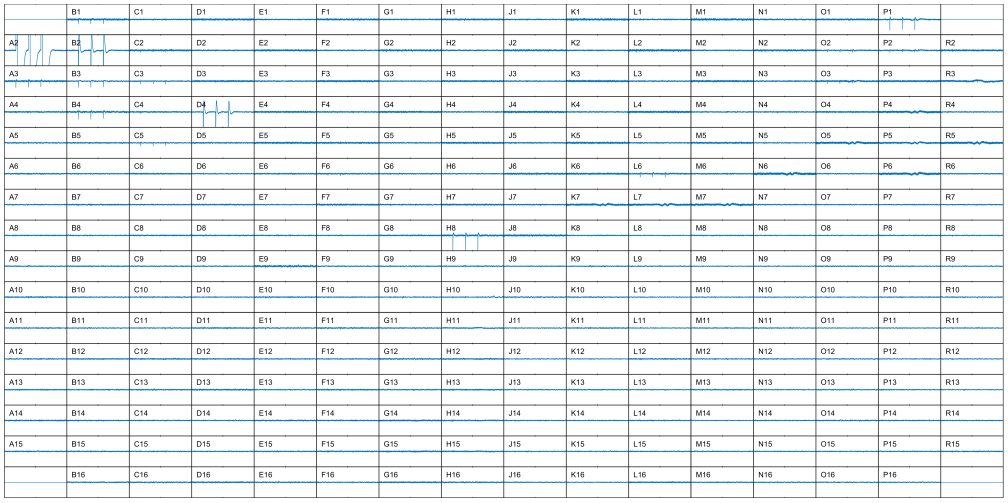

Figure 5.8: Signal read in each electrode after stimulation of A2 electrode. It is possible to see that the signal is picked up by nearby electrodes.

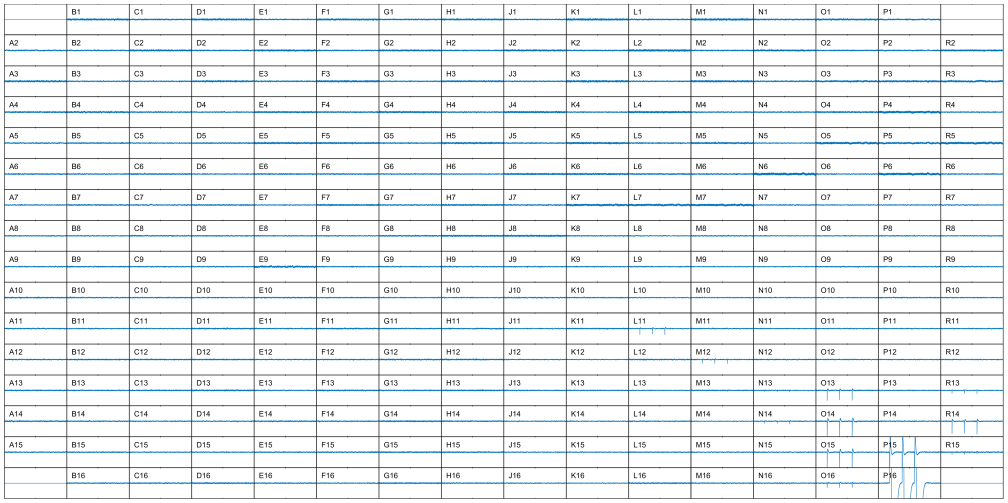

Figure 5.9: Signal read in each electrode after stimulation of P16 electrode.A stimulation artifact is recorded in nearby electrodes.

5.4 Results

The electrophysiological activity of the spinal cord slice was acquired with the protocol above described. For each channel, spikes were detected as being local maxima (or minima) with amplitude higher than the median of the signal plus 5 times the standard deviation, and a minimum separation in between peaks of 1 ms. The stimulation of each electrode produced a 40 mV artifact, as seen in Fig.5.10, which corrupts the signal and hinders spike detection. So, the stimulation period has been removed from each channel. Taking a closer look at two spikes identified in channel A2, Fig.5.11, it is possible to observe that they are detected immediately after the blanking period and to identify them as stimulation artifacts. The signal was filtered to remove these artifacts and optimize spike detection. First, a high-pass Butterworth filter with 200Hz cutting frequency and order 6 was applied to remove slow oscillations and correct the baseline, then, the signal was filtered with a low-pass Butterworth filter with 2000Hz cutting frequency and order 6 to eliminate rapid oscillations that characterize stimulation artifacts. Spikes were detected again using a threshold of 8 times the standard deviation plus the median of the signal. The resulting raster plot is depicted in Fig.5.12. Inspecting the voltage trace of the identified spikes, a specific shape, seen in Fig.5.13, is noticeable. The peak rises considerably above the threshold, reaching $600\mu V$.

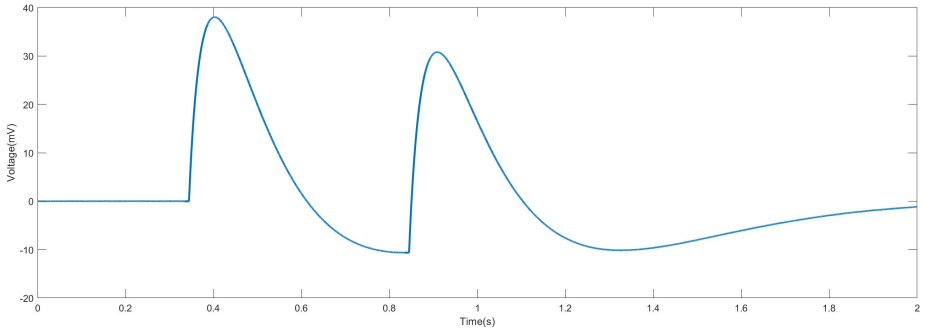

Figure 5.10: Voltage trace of the period of stimulation in channel A2. The stimulation produces a 40 mV artifact.

The excitatory connectivity map obtained from the functional connectivity analysis is shown in Fig.5.14. Since the objective was to detect functional connections between neurons, the maximum velocity threshold was set to 400 mm/s, whereas the minimum delay threshold was set to 1 ms. A total of seven excitatory links were identified. The average delay of the detected links is 10.00 ms, the average strength is 0.13 and the mean connection length is 0.80 mm. The average clustering coefficient is zero. No inhibitory connections were discovered.

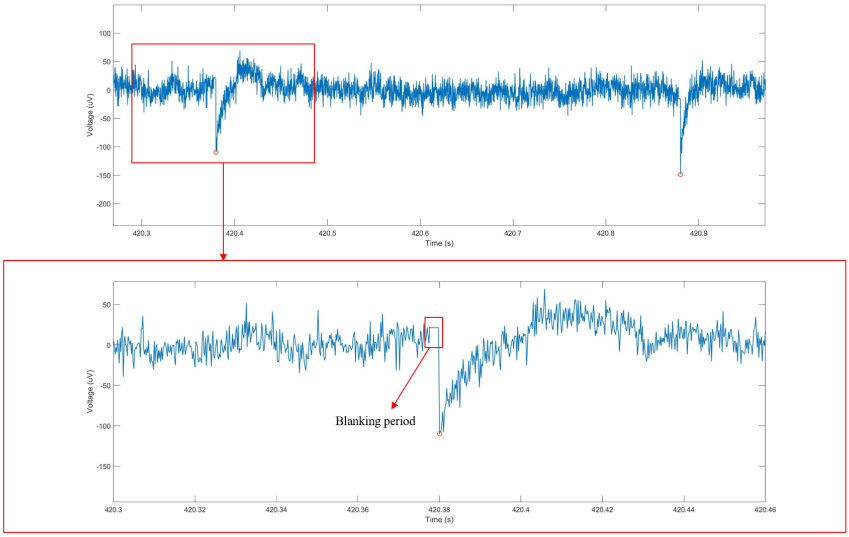

Figure 5.11: On top, voltage trace of a segment of the signal acquired on the channel A2 with the identified spikes marked. On the bottom, it is shown a zoomed view on the highlighted spike. It occurs immediately after the blanking period, suggesting that it is a stimulation artifact.

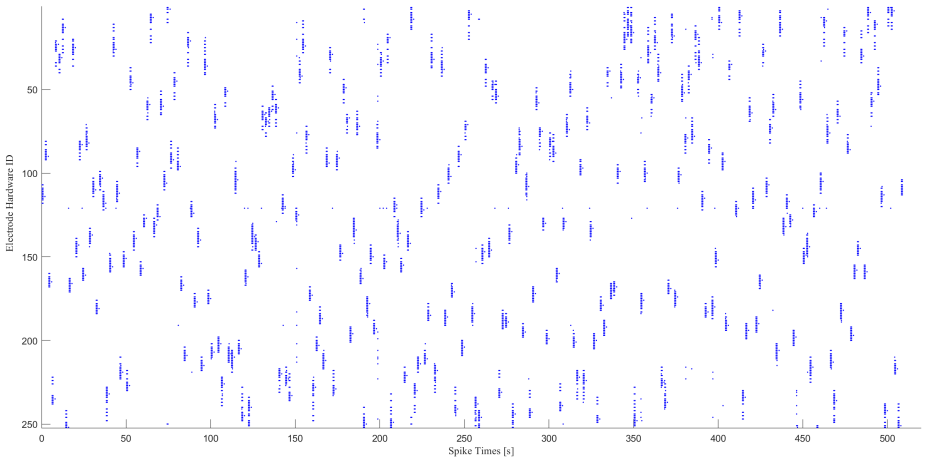

Figure 5.12: Raster plot of the spikes detected using the thresholding method. Spikes were detected as being local maxima (or minima) with amplitude higher than the median of the signal plus 8 times the standard deviation, and a minimum separation in between peaks of 1 ms.

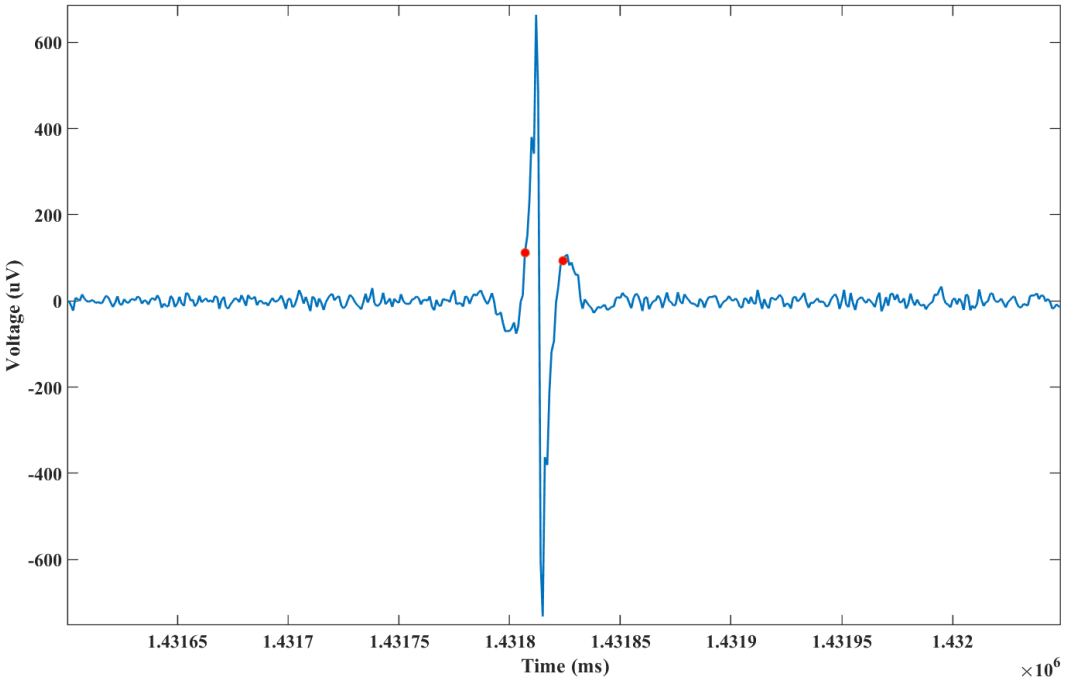

Figure 5.13: Filtered voltage trace of A2 channel with detected spikes(red markers). The spikes are identified near a peak of 600 μV, a value not compatible with that of action potentials.

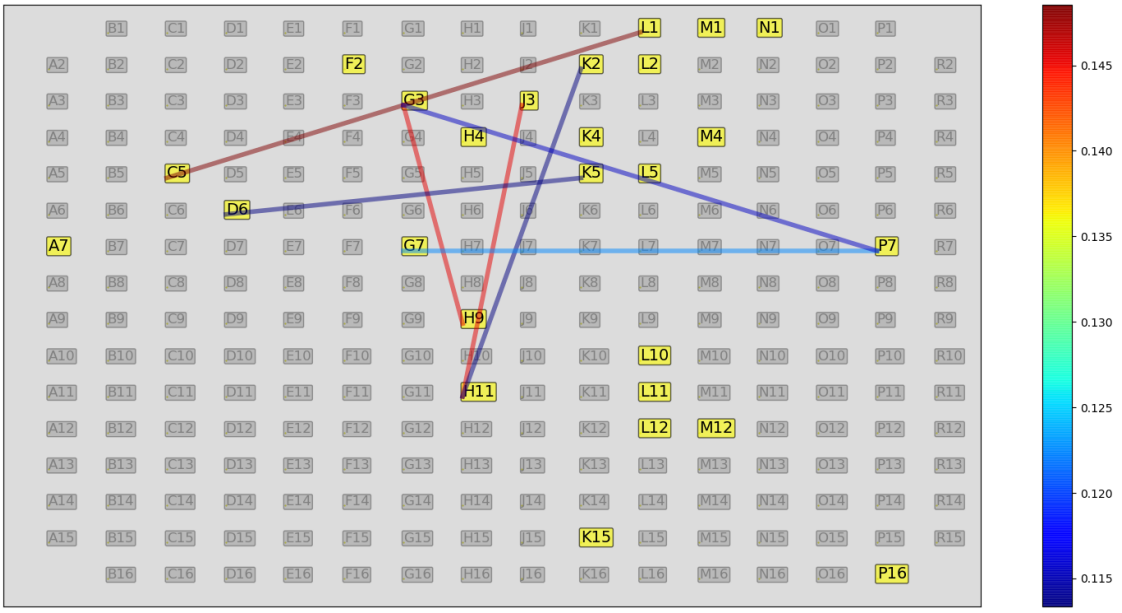

Figure 5.14: Excitatory links identified on the spinal cord slice recording. The average strength of the links is 0.13.

5.5 Discussion

The stimulation protocol was successfully implemented as it was capable of controlling the acquisition settings: all electrodes were randomly stimulated as the data was being recorded. Since no human intervention was necessary, it was possible to perform the experiment in 8.5 minutes, while the sample was still viable.

The signal acquired was corrupted by stimulation artifacts. Even though the filtering procedure was able to eliminate most of them, there was still some detected as spikes, as exemplified in Fig.5.13. The peak voltage, approximately 600 , and the waveform of the detected spikes in Fig.5.13 are not compatible with those of action potentials. Moreover, analyzing the raster plot, a pattern is noticeable: spikes occurring at stimulus delivery concentrate on groups of channels with successive hardware IDs, which may be a result of the wiring of the MEA hardware. This reinforces the idea that most of the spikes detected are stimulation artifacts. Their presence can be explained by the high conductance of the ACSF and potential contaminations on the MEA surface resulting from improper cleaning. This way, when an electrode is stimulated the signal is propagated to neighbor electrodes and the stimulation artifacts are observed. For this reason, the results from the connectivity inference analysis are inconclusive since the obtaining of a clean signal was not possible and the identified links are most probably a result of correlations between noise.

The absence of biological signals can be explained by the improper cutting of the sample. The spinal cord is surrounded by a set of membranes that has greater resistance than the spinal cord itself, which makes obtaining a clean cut with a scalpel a challenging task. This way, most cells die during slice preparation because the cut damages them. On the other hand, this cutting method makes it difficult to obtain a sample with a smooth surface, thereby, when the slice is put on top of the MEA some parts of the sample do not contact with the electrodes.

The quality of the signal acquired could be improved by using 3D MEAs, which are constituted by a set of needle electrodes that penetrate the tissue and acquire the signal locally with a high signal-to-noise ratio, thereby, assuring that the electrode is in contact with the slice. Moreover, the likelihood of triggering a neuronal response could be increased by stimulating directly the afferent pathways. This method would involve the usage of a microscope to localize the individual nerves targeted for stimulation.

Even though the acquisition of spinal activity was not possible, the custom-made protocol proved to be suitable for the precise control of the acquisition settings. The automatization of the routine permitted to reduce significantly the experience's duration and, as a consequence, increase the sample's yield. This way, it was possible to perform a complex stimulation protocol without compromising the viability of the sample. This work has paved the way for the development of custom-made protocols, by providing a framework to control the acquisition hardware.

Chapter 6

Conclusion

The spinal cord is an important structure in the central nervous system that conveys information from the outside world to the brain, allowing for the reaction to threats and the perception of changes in the environment. Patients with lesions in this structure are highly incapacitated, so, there has been a great deal of research mobilized to the development of therapies that aim to restore the function of the spinal cord, such as neuroprosthetics. The development of the said therapies requires a detailed description of the spinal circuitry and the underlying mechanisms of integration and transmission of information. This work focuses on the ascending tracts, the neural pathways by which sensory information from the peripheral nerves is transmitted to the cerebral cortex, whose coding mechanisms are still poorly described. In light of this, it was developed a library - SensorySimLib - which extends the functionalities of the NEURON simulation environment to construct a high-level, realistic representation of the ascending tracts. The model built can be used to test different architectures and coding strategies that may arise from experimental findings. In fact, it was demonstrated that the model can effectively code absolute temperature in the cooling range, by using a combinatorial code and stimulus location at the different levels of information integration. The model still presents limitations - it cannot code temperature change, for instance - but can be extended to encompass other coding mechanisms and stimulus modalities. Furthermore, the library provides methods for the testing of the model with real spiking data, allowing for the refinement of specific experimental parameters.

Electrophysiology has the potential to uncover spinal circuitry since the correlation between the electrical activity of neurons may indicate the existence of functional connections between them. With this in mind, it was implemented a pipeline to detect functional connections in data recorded with microelectrode arrays. The connections are detected using the FNCCH algorithm and the resulting connectivity matrix is filtered to obtain biologically plausible links. Three different views of the connectivity map were developed to highlight hidden connections and more easily visualize the structure of the network. The algorithm was successful in identifying the excitatory connections and structure imposed by microfluidic compartmentalization. However, the results obtained for the identification of inhibitory links were inconclusive.

Spinal cord slices have very limited spontaneous activity, thereby, the study of the electrophysiological activity in *ex vivo* spinal cord slices involves necessarily the stimulation of the sample. MEAs are capable of performing simultaneous recording and stimulation, making it the ideal acquisition tool to study the spinal cord connectivity. An acquisition and stimulation routine was designed to automate the stimulation of all electrodes of the MEA and the recording in between stimuli. Using the custom-made protocol, it was possible to record the activity of the slice. However, the signal acquired was corrupted with stimulation artifacts that resulted from the improper slicing of the sample. Only a few biologically realistic functional connections were identified, which were insufficient to reveal spinal circuits. Nevertheless, the custom-made protocol proved to be suitable for the precise control of acquisition settings, while reducing the experience's duration and, as a consequence, increasing the sample's yield.

Even though the work developed does not directly answer the research questions presented in the Introduction, it provides a set of tools that can be further explored to solve them. SensorySimLib provides a framework to test different mapping and coding hypotheses in the ascending tracts. The custom-made protocol allows for the development of complex automated routines compatible with spinal cord stimulation. The connectivity inference pipeline can reveal functional connections in high signal-to-noise ratio electrophysiological data and, hence, uncover the spinal circuitry.

All in all, the developed tools - the computational model of sensory integration, connectivity inference algorithms and visualization, and automated experimental protocols - paved the way for a better understanding of the mechanisms of information integration in the spinal cord, through the improvement of data acquisition and analysis methodologies of MEA electrophysiology experiments.

Chapter 7

Future Work

Even though this work allowed the development of pioneer tools for the study and analysis of sensory information integration mechanisms and spinal circuitry, there are some aspects that could be further improved. Concerning the model developed, its complexity was not sufficient to replicate all the results gathered from the literature. Therefore, additional mechanisms for neuronal information coding should be implemented. More, SensorySimLib could be extended to encompass other stimulus modalities. On the other hand, extra layers should be added to the model to represent the full extent of the ascending pathways, from the skin to the sensory cortex.

In theory, the connectivity inference framework should be able to detect both inhibitory and excitatory connections, however, it is more robust for the detection of excitatory links. As so, a new method for the detection of inhibitory links should be developed. Furthermore, the filtering procedure could be enhanced by implementing methods of greater complexity than the ones used, and other graph theory related metrics could be extracted to further characterize the network detected.

Another limiting aspect of this work was the irregular surface of the spinal cord slices, due to the use of an improper cutting tool. This could be improved by using an adequate slicer or by acquiring the data with 3D microelectrode-arrays since their needle electrodes penetrate the sample and ensure maximum surface contact. On the other hand, the stimulation of the ascending pathways during data acquisition could increase the probability of triggering activity in the spinal circuits and, as a consequence, increase the likelihood of detecting them with the connectivity inference framework. Finally, the removal of the stimulation artifacts either by reprogramming the acquisition settings or by doing post-processing of the signal could increase the quality of the data acquired and, consequently, improve spike detection. Through all the processes above mentioned the data acquired would have better quality and therefore could be used to test SensorySimLib with real data.

References

[1] MEA2100-Systems | www.multichannelsystems.com, 2019. URL https://www.multichannelsystems.com/products/mea2100-systems.

[2] Products | www.multichannelsystems.com, 2019. URL https://www.multichannelsystems.com/products.

[3] Somatosensory System Anatomy: Overview, Gross Anatomy, Microscopic Anatomy, 2019. URL https://emedicine.medscape.com/article/1948621-overview.

[4] The Ascending Tracts - DCML - Anterolateral - TeachMeAnatomy, 2019. URL https://teachmeanatomy.info/neuro/pathways/ascending-tracts-sensory/.

[5] What is neuron?, 2019. URL https://www.neuron.yale.edu/neuron/what_is_neuron.

[6] Victoria E. Abraira and David D. Ginty. The sensory neurons of touch. *Neuron*, 79(4): 618–639, 2013. ISSN 08966273. doi: 10.1016/j.neuron.2013.07.051. URL http://dx.doi.org/10.1016/j.neuron.2013.07.051.

[7] Dayo O Adewole, Mijail D Serruya, James P Harris, Justin C Burrell, Dmitriy Petrov, H Isaac Chen, John A Wolf, and D Kacy Cullen. The Evolution of Neuroprosthetic Interfaces. *Critical reviews in biomedical engineering*, 44(1-2):123–52, 2016. ISSN 1943-619X. doi: 10.1615/CritRevBiomedEng.2016017198. URL http://www.ncbi.nlm.nih.gov/pubmed/27652455http://www.pubmedcentral.nih.gov/articlerender.fcgi?artid=PMC5541680.

[8] P. Aguiar, M. Sousa, and D. Lima. NMDA Channels Together With L-Type Calcium Currents and Calcium-Activated Nonspecific Cationic Currents Are Sufficient to Generate Windup in WDR Neurons. *Journal of Neurophysiology*, 104(2):1155–1166, 8 2010. ISSN 0022-3077. doi: 10.1152/jn.00834.2009. URL http://www.physiology.org/doi/10.1152/jn.00834.2009.

[9] Andreoli, Thomas E., Charles C. J. Carpenter, and Russell L. *Andreoli and Carpenter's Cecil essentials of medicine*. Philadelphia: Saunders, 2007. ISBN 2013436106. doi: 10.1360/zd-2013-43-6-1064.

[10] Musa L Audu, Lisa M Lombardo, John R Schnellenberger, Kevin M Foglyano, Michael E Miller, and Ronald J Triolo. A neuroprosthesis for control of seated balance after spinal cord injury. *Journal of NeuroEngineering and Rehabilitation*, 12(1):8, 1 2015. ISSN 1743-0003. doi: 10.1186/1743-0003-12-8. URL http://www.jneuroengrehab.com/content/12/1/8.

[11] Bruno B. Averbeck, Peter E. Latham, and Alexandre Pouget. Neural correlations, population coding and computation. *Nature Reviews Neuroscience*, 7(5):358–366, 5 2006. ISSN 1471-003X. doi: 10.1038/nrn1888. URL http://www.nature.com/articles/nrn1888.

[12] Monya Baker. From promising to practical: tools to study networks of neurons. *Nature Methods*, 7(11):877–883, 11 2010. ISSN 1548-7091. doi: 10.1038/nmeth1110-877. URL http://www.nature.com/articles/nmeth1110-877.

[13] A. I. Basbaum. *The senses : a comprehensive reference.* Elsevier, 2008. ISBN 9780123708809. URL https://www.sciencedirect.com/referencework/9780123708809/the-senses-a-comprehensive-reference.

[14] Mark F. Bear, Barry W. Connors, and Michael A. Paradiso. *Neuroscience : exploring the brain*. Lippincott Williams & Wilkins, 2007. ISBN 0781760038.

[15] Rolfe Birch. *Surgical disorders of the peripheral nerves*. Springer US, second edi edition, 2011. ISBN 2013436106. doi: 10.1360/zd-2013-43-6-1064.

[16] Paolo Bonifazi, Maria Elisabetta Ruaro, and Vincent Torre. Statistical properties of information processing in neuronal networks. *European Journal of Neuroscience*, 22(11):2953–2964, 12 2005. ISSN 0953816X. doi: 10.1111/j.1460-9568.2005.04464.x. URL http://www.ncbi.nlm.nih.gov/pubmed/16324130http://doi.wiley.com/10.1111/j.1460-9568.2005.04464.x.

[17] S. Bourane, B. Duan, S. C. Koch, A. Dalet, O. Britz, L. Garcia-Campmany, E. Kim, L. Cheng, A. Ghosh, Q. Ma, and M. Goulding. Gate control of mechanical itch by a subpopulation of spinal cord interneurons. *Science*, 350 (6260):550–554, 10 2015. ISSN 0036-8075. doi: 10.1126/science.aac8653. URL http://www.ncbi.nlm.nih.gov/pubmed/26516282http://www.pubmedcentral.nih.gov/articlerender.fcgi?artid=PMC4700934http://www.sciencemag.org/cgi/doi/10.1126/science.aac8653.

[18] Daniel A Butts and Mark S Goldman. Tuning Curves, Neuronal Variability, and Sensory Coding. *PLoS Biology*, 4(4):e92, 3 2006. ISSN 1545-7885. doi: 10.1371/journal.pbio.0040092. URL http://dx.plos.org/10.1371/journal.pbio.0040092.

[19] Nicholas T. Carnevale and Michael L. Hines. *The NEURON book*. Cambridge University Press, 2006. ISBN 9780521115636. URL https://www.cambridge.org/us/academic/subjects/life-sciences/neuroscience/neuron-book.

[20] Jennifer. Carter, Matt C Shieh. *Guide to Research Techniques in Neuroscience*. Elsevier, 2015. ISBN 9780128005118. doi: 10.1016/C2013-0-06868-5. URL https://linkinghub.elsevier.com/retrieve/pii/C20130068685.

[21] Luísa Castro and Paulo Aguiar. Phase precession through acceleration of local theta rhythm: a biophysical model for the interaction between complex spike cells and theta cells. *BMC Neuroscience*, 12(S1):P2, 12 2011. ISSN 1471-2202. doi: 10.1186/1471-2202-12-S1-P2. URL https://bmcneurosci.biomedcentral.com/articles/10.1186/1471-2202-12-S1-P2.

[22] Daniel J Chew, Lan Zhu, Evangelos Delivopoulos, Ivan R Minev, Katherine M Musick, Charles A Mosse, Michael Craggs, Nicholas Donaldson, Stéphanie P Lacour, Stephen B McMahon, and James W Fawcett. A microchannel neuroprosthesis for bladder control after spinal cord injury in rat. *Science translational medicine*, 5(210):210ra155, 11 2013. ISSN 1946-6242. doi: 10.1126/scitranslmed.3007186. URL http://www.ncbi.nlm.nih.gov/pubmed/24197736.

[23] Marlene R Cohen and Adam Kohn. Measuring and interpreting neuronal correlations. *Nature Neuroscience*, 14(7):811–819, 7 2011. ISSN 1097-6256. doi: 10.1038/nn.2842. URL http://www.nature.com/articles/nn.2842.

[24] Peter Dayan and L F Abbott. *Theoretical neuroscience*. Massachusetts Institute of Technology Press, 2002. ISBN 1097-4199 (Electronic)\n0896-6273 (Linking). doi: 10.1016/j.neuron.2008.10.019.

[25] Ildefons Magrans de Abril, Junichiro Yoshimoto, and Kenji Doya. Connectivity Inference from Neural Recording Data: Challenges, Mathematical Bases and Research Directions. *Neural Networks*, 102:120–137, 2017. ISSN 08936080. doi: 10.1016/j.neunet.2018.02.016. URL http://arxiv.org/abs/1708.01888.

[26] Marian Cleeves Diamond, Arnold B. Scheibel, and Lawrence M. Elson. *The human brain coloring book*. Barnes & Noble Books, 1985. ISBN 9780064603065.

[27] Bo Duan, Longzhen Cheng, Steeve Bourane, Olivier Britz, Christopher Padilla, Lidia Garcia-Campmany, Michael Krashes, Wendy Knowlton, Tomoko Velasquez, Xiangyu Ren, Sarah E. Ross, Bradford B. Lowell, Yun Wang, Martyn Goulding, and Qiufu Ma. Identification of Spinal Circuits Transmitting and Gating Mechanical Pain. *Cell*, 159(6):1417–1432, 12 2014. ISSN 00928674. doi: 10.1016/j.cell.2014.11.003. URL http://www.ncbi.nlm.nih.gov/pubmed/25467445http://www.pubmedcentral.nih.gov/articlerender.fcgi?artid=PMC4258511https://linkinghub.elsevier.com/retrieve/pii/S0092867414014342.

[28] Peter E Latham and Yasser Roudi. Role of correlations in population coding. *Principles of Neural Coding*, 09 2011. doi: 10.1201/b14756-9.

[29] Edward C. Emery, Ana P. Luiz, Shafaq Sikandar, Rán Magnúsdóttir, Xinzhong Dong, and John N. Wood. In vivo characterization of distinct modality-specific subsets of somatosensory neurons using GCaMP. *Science Advances*, 2(11):e1600990, 11 2016. ISSN 2375-2548. doi: 10.1126/sciadv.1600990. URL http://advances.sciencemag.org/lookup/doi/10.1126/sciadv.1600990.

[30] Roger M. Enoka and Jacques Duchateau. Rate Coding and the Control of Muscle Force. *Cold Spring Harbor Perspectives in Medicine*, 7(10):a029702, 10 2017. ISSN 2157-1422. doi: 10.1101/cshperspect.a029702. URL http://perspectivesinmedicine.cshlp.org/lookup/doi/10.1101/cshperspect.a029702.

[31] A.G Fallis. HarrisoFallis, A. . (2015) "Harrison's Principles of Internal Medicine," Journal of Chemical Information and Modeling, II(9), hal. 1689–1699. doi: 10.1017/CBO9781107415324.004.n's Principles of Internal Medicine. *Journal of Chemical Information and Modeling*, II(9):1689–1699, 2015. ISSN 1098-6596. doi: 10.1017/CBO9781107415324.004.

[32] Philippe Faure. Combinatorial Coding. In Nobutaka Binder Marc D. }and Hirokawa and Windhorst Uwe, editors, *Encyclopedia of Neuroscience*, pages 800–803. Springer Berlin Heidelberg, Berlin, Heidelberg, 2009. ISBN 978-3-540-29678-2. doi: 10.1007/978-3-540-29678-2{_}1131. URL https://doi.org/10.1007/978-3-540-29678-2_1131.

[34] Felix Franke, David Jäckel, Jelena Dragas, Jan Müller, Milos Radivojevic, Douglas Bakkum, and Andreas Hierlemann. High-density microelectrode array recordings and real-time spike sorting for closed-loop experiments: an emerging technology to study neural plasticity. *Frontiers in Neural Circuits*, 6:105, 12 2012. ISSN 1662-5110. doi: 10.3389/fncir.2012.00105. URL http://journal.frontiersin.org/article/10.3389/fncir.2012.00105/abstract.

[33] Felix Franke, Michele Fiscella, Maksim Sevelev, Botond Roska, Andreas Hierlemann, and Rava Azeredo da Silveira. Structures of Neural Correlation and How They Favor Coding. *Neuron*, 89(2):409–422, 1 2016. ISSN 0896-6273. doi: 10.1016/J.NEURON.2015.12.037. URL https://www.sciencedirect.com/science/article/pii/S0896627315011393.

[35] Michael R Franz, Charles D Swerdlow, L Bing Liem, and Jochen Schaefer. Cycle Length Dependence of Human Action Potential Duration In Vivo and Different Steady-State Frequencies. *J. Clin. Invest,*, 82(September):972–979, 1988. URL https://dm5migu4zj3pb.cloudfront.net/manuscripts/113000/113706/JCI88113706.pdf.

[36] Flavio Fröhlich and Flavio Fröhlich. Optical Measurements and Perturbations. *Network Neuroscience*, pages 145–159, 1 2016. doi: 10.1016/B978-0-12-801560-5.00011-2. URL https://www.sciencedirect.com/science/article/pii/B9780128015605000112.

[37] Wainrib Gilles, Thieullen Michèle, and Pakdaman Khashayar. Intrinsic variability of latency to first-spike. *Biological Cybernetics*, 103(1):43–56, 7 2010. ISSN 0340-1200. doi: 10.1007/s00422-010-0384-8. URL http://link.springer.com/10.1007/s00422-010-0384-8.

[38] Henry Gray. *Anatomy of the human body, by Henry Gray. 20th ed., thoroughly rev. and re-edited by Warren H. Lewis.* Philadelphia: Lea & Febiger, 20 edition, 1918.

[39] Charles M. Greenspon, Emma E. Battell, Ian M. Devonshire, Lucy F. Donaldson, Victoria Chapman, and Gareth J. Hathway. Lamina-specific population encoding of cutaneous signals in the spinal dorsal horn using multi-electrode arrays. *The Journal of Physiology*, 597(2):377–397, 1 2019. ISSN 00223751. doi: 10.1113/JP277036. URL http://doi.wiley.com/10.1113/JP277036.

[40] Aviad Hai, Joseph Shappir, and Micha E. Spira. Long-Term, Multisite, Parallel, In-Cell Recording and Stimulation by an Array of Extracellular Microelectrodes. *Journal of Neurophysiology*, 104(1):559–568, 7 2010. ISSN 0022-3077. doi: 10.1152/jn.00265.2010. URL http://www.physiology.org/doi/10.1152/jn.00265.2010.

[41] Sungmin Han, Dong Hwee Kim, Joohwan Sung, Hwasun Yang, Jong Woong Park, and Inchan Youn. Electrical stimulation accelerates neurite regeneration in axotomized dorsal root

ganglion neurons by increasing mmp-2 expression. *Biochemical and biophysical research communications*, 508(2):348–353, 2019.

[42] Martin Häring, Amit Zeisel, Hannah Hochgerner, Puneet Rinwa, Jon E. T. Jakobsson, Peter Lönnerberg, Gioele La Manno, Nilesh Sharma, Lotta Borgius, Ole Kiehn, Malin C. Lagerström, Sten Linnarsson, and Patrik Ernfors. Neuronal atlas of the dorsal horn defines its architecture and links sensory input to transcriptional cell types. *Nature Neuroscience*, 21(6):869–880, 6 2018. ISSN 1097-6256. doi: 10.1038/s41593-018-0141-1. URL http://www.nature.com/articles/s41593-018-0141-1.

[43] Kristine Heiney, José C. Mateus, Cátia D. F. Lopes, Estrela Neto, Meriem Lamghari, and Paulo Aguiar. SpikeHunter: An advanced computational tool for the analysis of neuronal communication and action potential propagation in microfluidic platforms. *Scientific Reports*, 9(1):5777, 12 2019. ISSN 2045-2322. doi: 10.1038/s41598-019-42148-3. URL http://www.nature.com/articles/s41598-019-42148-3.

[44] M. L. Hines and N. T. Carnevale. The NEURON Simulation Environment. *Neural Computation*, 9(6):1179–1209, 8 1997. ISSN 0899-7667. doi: 10.1162/neco.1997.9.6.1179. URL http://www.mitpressjournals.org/doi/10.1162/neco.1997.9.6.1179.

[45] A. L. Hodgkin and A. F. Huxley. A quantitative description of membrane current and its application to conduction and excitation in nerve. *The Journal of Physiology*, 117(4): 500–544, 8 1952. ISSN 00223751. doi: 10.1113/jphysiol.1952.sp004764. URL http://doi.wiley.com/10.1113/jphysiol.1952.sp004764.

[46] Nari Hong, Sunghoon Joo, and Yoonkey Nam. Characterization of Axonal Spikes in Cultured Neuronal Networks Using Microelectrode Arrays and Microchannel Devices. *IEEE Transactions on Biomedical Engineering*, 64(2):492–498, 2 2017. ISSN 0018-9294. doi: 10.1109/TBME.2016.2567424. URL http://ieeexplore.ieee.org/document/7469329/.

[47] David Jäckel, Douglas J. Bakkum, Thomas L. Russell, Jan Müller, Milos Radivojevic, Urs Frey, Felix Franke, and Andreas Hierlemann. Combination of High-density Microelectrode Array and Patch Clamp Recordings to Enable Studies of Multisynaptic Integration. *Scientific Reports*, 7(1):978, 12 2017. ISSN 2045-2322. doi: 10.1038/s41598-017-00981-4. URL http://www.nature.com/articles/s41598-017-00981-4.

[48] Eric Kandel, James Schwartz, and Thomas Jessell. *Principles of Neural Science*. McGraw-Hill, 4th editio edition, 2000. ISBN 0-8385-7701-6 This.

[49] Marius A. Kemler, Henrica C. W. de Vet, Gerard A. M. Barendse, Frans A. J. M. van den Wildenberg, and Maarten van Kleef. Effect of spinal cord stimulation for chronic complex regional pain syndrome Type I: five-year final follow-up of patients in a randomized controlled trial. *Journal of Neurosurgery*, 108(2):292–298, 2 2008. ISSN 0022-3085. doi: 10.3171/JNS/2008/108/2/0292. URL http://www.ncbi.nlm.nih.gov/pubmed/18240925https://thejns.org/view/journals/j-neurosurg/108/2/article-p292.xml.

[50] Dhurgham Khudhair, Saeid Nahavandi, Hamid Garmestani, Asim Bhatti, D Khudhair, S Nahavandi, A Bhatti, au A Bhatti, and H Garmestani. Emerging Trends in Neuro Engineering and Neural Computation. *Springer Singapore*, 2018. doi: 10.1007/978-981-10-3957-7{_}2.

[51] Peter Kloppenburg and Martin Paul Nawrot. Neural Coding: Sparse but On Time. *Current Biology*, 24(19):R957–R959, 10 2014. ISSN 0960-9822. doi: 10.1016/J.CUB.2014.08.041. URL https://www.sciencedirect.com/science/article/pii/S0960982214010549.

[52] W. M. Knowlton, R. Palkar, E. K. Lippoldt, D. D. McCoy, F. Baluch, J. Chen, and D. D. McKemy. A Sensory-Labeled Line for Cold: TRPM8-Expressing Sensory Neurons Define the Cellular Basis for Cold, Cold Pain, and Cooling-Mediated Analgesia. *Journal of Neuroscience*, 33(7):2837–2848, 2 2013. ISSN 0270-6474. doi: 10.1523/JNEUROSCI.1943-12.2013. URL http://www.ncbi.nlm.nih.gov/pubmed/23407943http://www.pubmedcentral.nih.gov/articlerender.fcgi?artid=PMC3711390http://www.jneurosci.org/cgi/doi/10.1523/JNEUROSCI.1943-12.2013.

[53] Adam Kohn, Ruben Coen-Cagli, Ingmar Kanitscheider, and Alexandre Pouget. Correlations and Neuronal Population Information. *Annual Review of Neuroscience*, 39(1):237–256, 7 2016. ISSN 0147-006X. doi: 10.1146/annurev-neuro-070815-013851. URL http://www.annualreviews.org/doi/10.1146/annurev-neuro-070815-013851.

[54] Gabriel Kreiman. Neural coding: computational and biophysical perspectives. *Physics of Life Reviews*, 1:71–102, 2004. doi: 10.1016/j.plrev.2004.06.001. URL www.elsevier.com/locate/plrev.

[56] Jutta Kretzberg, Friederice Pirschel, Elham Fathiazar, and Gerrit Hilgen. Encoding of Tactile Stimuli by Mechanoreceptors and Interneurons of the Medicinal Leech. *Frontiers in Physiology*, 7:506, 10 2016. ISSN 1664-042X. doi: 10.3389/fphys.2016.00506. URL http://www.ncbi.nlm.nih.gov/pubmed/27840612http://www.pubmedcentral.nih.gov/articlerender.fcgi?artid=PMC5083904http://journal.frontiersin.org/article/10.3389/fphys.2016.00506/full.

[55] Jutta Kretzberg, Friederice Pirschel, Elham Fathiazar, and Gerrit Hilgen. Encoding of Tactile Stimuli by Mechanoreceptors and Interneurons of the Medicinal Leech. *Frontiers in physiology*, 7:506, 2016. ISSN 1664-042X. doi: 10.3389/fphys.2016.00506. URL http://www.ncbi.nlm.nih.gov/pubmed/27840612http://www.pubmedcentral.nih.gov/articlerender.fcgi?artid=PMC5083904.

[57] Krishna Kumar, Jefferson R. Wilson, Rod S. Taylor, and Shivani Gupta. Complications of spinal cord stimulation, suggestions to improve outcome, and financial impact. *Journal of Neurosurgery: Spine*, 5(3):191–203, 9 2006. ISSN 1547-5654. doi: 10.3171/spi.2006.5.3.191. URL http://www.ncbi.nlm.nih.gov/pubmed/16961079https://thejns.org/view/journals/j-neurosurg-spine/5/3/article-p191.xml.

[58] Ming-Gang Liu, Xue-Feng Chen, Ting He, Zhen Li, and Jun Chen. Use of multi-electrode array recordings in studies of network synaptic plasticity in both time and space. *Neuroscience Bulletin*, 28(4):409–422, 8 2012. ISSN 1673-7067. doi: 10.1007/s12264-012-1251-5. URL http://link.springer.com/10.1007/s12264-012-1251-5.

[59] Qiufu Ma. Labeled lines meet and talk: population coding of somatic sensations. *The Journal of clinical investigation*, 120(11):3773–8, 11 2010. ISSN 1558-8238. doi: 10.1172/JCI43426. URL http://www.ncbi.nlm.nih.gov/pubmed/21041959http://www.pubmedcentral.nih.gov/articlerender.fcgi?artid=PMC2964985.

[60] Qiufu Ma. Population coding of somatic sensations. *Neuroscience Bulletin*, 28(2):91–99, 4 2012. ISSN 1673-7067. doi: 10.1007/s12264-012-1201-2. URL http://link.springer.com/10.1007/s12264-012-1201-2.

[61] Alessandro Maccione, Matteo Garofalo, Thierry Nieus, Mariateresa Tedesco, Luca Berdondini, and Sergio Martinoia. Multiscale functional connectivity estimation on low-density neuronal cultures recorded by high-density CMOS Micro Electrode Arrays. *Journal of Neuroscience Methods*, 207(2):161–171, 6 2012. ISSN 0165-0270. doi: 10.1016/J.JNEUMETH.2012.04.002. URL https://www.sciencedirect.com/science/article/pii/S0165027012001252?via%3Dihub.

[62] Paolo Massobrio, Jacopo Tessadori, Michela Chiappalone, and Mirella Ghirardi. In vitro studies of neuronal networks and synaptic plasticity in invertebrates and in mammals using multielectrode arrays. *Neural Plasticity*, 2015, 2015. ISSN 16875443. doi: 10.1155/2015/196195.

[63] J McArthur and I W Husstedt. Peripheral nervous system. *Journal of neurovirology*, 8(3):32–33, 2002. ISSN 1355-0284. doi: 10.1080/13550280290049921.

[64] Arne F Meyer, Ross S Williamson, Jennifer F Linden, and Maneesh Sahani. Models of Neuronal Stimulus-Response Functions: Elaboration, Estimation, and Evaluation. *Frontiers in systems neuroscience*, 10:109, 2016. ISSN 1662-5137. doi: 10.3389/fnsys.2016.00109. URL http://www.ncbi.nlm.nih.gov/pubmed/28127278http://www.pubmedcentral.nih.gov/articlerender.fcgi?artid=PMC5226961.

[65] multichannel systems. Versatile in vitro recording system: MEA2100-System. Technical report, 2018. URL www.multichannelsystems.com.

[66] Oleh Mytakhir. 3-D Reconstruction of Spinal Lamina I Neurons, 2015. URL https://repositorio-aberto.up.pt/bitstream/10216/82719/2/37879.pdf.

[67] Zoltan Nadasdy. Binding by asynchrony: the neuronal phase code. *Frontiers in neuroscience*, 4, 2010. ISSN 1662-453X. doi: 10.3389/fnins.2010.00051. URL http://www.ncbi.nlm.nih.gov/pubmed/20859525http://www.pubmedcentral.nih.gov/articlerender.fcgi?artid=PMC2940453.

[68] Xavier Navarro, Thilo B Krueger, Natalia Lago, Silvestro Micera, Thomas Stieglitz, and Paolo Dario. A critical review of interfaces with the peripheral nervous system for the control of neuroprostheses and hybrid bionic systems. *Journal of the Peripheral Nervous System*, 258:229–258, 2005. ISSN 1085-9489. doi: 10.1111/j.1085-9489.2005.10303.x.

[69] Marie Engelene J. Obien, Kosmas Deligkaris, Torsten Bullmann, Douglas J. Bakkum, and Urs Frey. Revealing neuronal function through microelectrode array recordings. *Frontiers in Neuroscience*, 9(JAN):423, 2015. ISSN 1662453X. doi: 10.3389/fnins.2014.00423.

[70] Bruno A Olshausen and David J Field. Sparse coding of sensory inputs This review comes from a themed issue on Sensory systems Edited by Catherine Dulac and Benedikt Grothe. *Current Opinion in Neurobiology*, 14:481–487, 2004. doi: 10.1016/j.conb.2004.07.007. URL www.sciencedirect.com.

[71] Stefano Panzeri, Jakob H. Macke, Joachim Gross, and Christoph Kayser. Neural population coding: combining insights from microscopic and mass signals. *Trends in*

Cognitive Sciences, 19(3):162–172, 3 2015. ISSN 1364-6613. doi: 10.1016/J.TICS.2015.01.002. URL https://www.sciencedirect.com/science/article/pii/S1364661315000030.

[72] Michel Paré, Allan M Smith, and Frank L Rice. Distribution and Terminal Arborizations of Cutaneous Mechanoreceptors in the Glabrous Finger Pads of the Monkey. *J. Comp. Neurol*, 445:347–359, 2002. doi: 10.1002/cne.10196. URL https://onlinelibrary.wiley.com/doi/pdf/10.1002/cne.10196.

[73] Vito Paolo Pastore, Paolo Massobrio, Aleksandar Godjoski, and Sergio Martinoia. Identification of excitatory-inhibitory links and network topology in large-scale neuronal assemblies from multi-electrode recordings. *PLoS computational biology*, 2018. doi: 10.1371/journal.pcbi.1006381. URL https://doi.org/10.1371/journal.pcbi.1006381.

[74] Maria Antoniou. Patestas and Leslie P. Gartner. *A textbook of neuroanatomy*. Blackwell Pub, 2006. ISBN 140510340X.

[75] Friederice Pirschel and Jutta Kretzberg. Multiplexed Population Coding of Stimulus Properties by Leech Mechanosensory Cells. *The Journal of Neuroscience*, 36 (13):3636–3647, 3 2016. ISSN 0270-6474. doi: 10.1523/JNEUROSCI.1753-15.2016. URL http://www.ncbi.nlm.nih.gov/pubmed/27030751http://www.jneurosci.org/lookup/doi/10.1523/JNEUROSCI.1753-15.2016.

[77] Steven A Prescott and Stéphanie Ratté. Pain processing by spinal microcircuits: afferent combinatorics. *Current Opinion in Neurobiology*, 22(4):631–639, 8 2012. ISSN 09594388. doi: 10.1016/j.conb.2012.02.010. URL https://linkinghub.elsevier.com/retrieve/pii/S0959438812000323.

[76] Steven A Prescott, Qiufu Ma, and Yves De Koninck. Normal and abnormal coding of somatosensory stimuli causing pain. *Nature Neuroscience*, 17(2):183–191, 2 2014. ISSN 1097-6256. doi: 10.1038/nn.3629. URL http://www.nature.com/articles/nn.3629.

[78] Dale. Purves and S. Mark (Stephen Mark) Williams. *Neuroscience*. Sinauer Associates, 2001. ISBN 0878937420.

[79] Chen Ran, Mark A Hoon, and Xiaoke Chen. The coding of cutaneous temperature in the spinal cord. *Nature Neuroscience*, 19(9):1201–1209, 9 2016. ISSN 1097-6256. doi: 10.1038/nn.4350. URL http://www.nature.com/articles/nn.4350.

[80] Fred. Rieke. *Spikes : exploring the neural code*. MIT Press, 1997. ISBN 9780262181747.

[81] Christopher J. Rozell, Don H. Johnson, Richard G. Baraniuk, and Bruno A. Olshausen. Sparse Coding via Thresholding and Local Competition in Neural Circuits. *Neural Computation*, 20(10):2526–2563, 10 2008. doi: 10.1162/neco.2008.03-07-486. URL http://www.mitpressjournals.org/doi/10.1162/neco.2008.03-07-486.

[82] Marc Russo, Michael J. Cousins, Charles Brooker, Nathan Taylor, Tillman Boesel, Richard Sullivan, Lawrence Poree, Nastaran Hesam Shariati, Erin Hanson, and John Parker. Effective Relief of Pain and Associated Symptoms With Closed-Loop Spinal Cord Stimulation System: Preliminary Results of the Avalon Study. *Neuromodulation: Technology at the*

Neural Interface, 21(1):38–47, 1 2018. ISSN 10947159. doi: 10.1111/ner.12684. URL http://doi.wiley.com/10.1111/ner.12684.

[83] H. S. Seung and H. Sompolinsky. Simple models for reading neuronal population codes. *Proceedings of the National Academy of Sciences*, 90(22):10749–10753, 11 1993. ISSN 0027-8424. doi: 10.1073/pnas.90.22.10749. URL http://www.pnas.org/cgi/doi/10.1073/pnas.90.22.10749.

[84] Nebahat Sezer, Selami Akkuş, and Fatma Gülçin Uğurlu. Chronic complications of spinal cord injury. *World journal of orthopedics*, 6(1):24–33, 1 2015. ISSN 2218-5836. doi: 10.5312/wjo.v6.i1.24. URL http://www.ncbi.nlm.nih.gov/pubmed/25621208http://www.pubmedcentral.nih.gov/articlerender.fcgi?artid=PMC4303787.

[85] Maoz Shamir. Emerging principles of population coding: in search for the neural code. *Current Opinion in Neurobiology*, 25:140–148, 4 2014. ISSN 0959-4388. doi: 10.1016/J.CONB.2014.01.002. URL https://www.sciencedirect.com/science/article/pii/S0959438814000105.

[86] C Norman Shealy, J Thomas Mortimer, and James B Reswick. Electrical Inhibition of Pain by Stimulation of the Dorsal Columns: Preliminary Clinical Report. *Anesthesia and analgesia*, 46(4):489–491, 1967. ISSN 0003-2999. doi: 10.3109/15360288.2012.678473.

[87] Shafaq Sikandar, Irene Ronga, Gian Domenico Iannetti, and Anthony H. Dickenson. Neural coding of nociceptive stimuli—from rat spinal neurones to human perception. *Pain*, 154(8):1263–1273, 8 2013. ISSN 0304-3959. doi: 10.1016/j.pain.2013.03.041. URL http://www.ncbi.nlm.nih.gov/pubmed/23719576http://content.wkhealth.com/linkback/openurl?sid=WKPTLP:landingpage&an=00006396-201308000-00014.

[88] Nuno A. Silva, Nuno Sousa, Rui L. Reis, and António J. Salgado. From basics to clinical: A comprehensive review on spinal cord injury. *Progress in Neurobiology*, 114:25–57, 2014. ISSN 18735118. doi: 10.1016/j.pneurobio.2013.11.002.

[89] S. J. Slee. Two-Dimensional Time Coding in the Auditory Brainstem. *Journal of Neuroscience*, 2005. ISSN 0270-6474. doi: 10.1523/JNEUROSCI.2666-05.2005.

[90] Neil J. Smelser and Paul B. Baltes. *International encyclopedia of the social & behavioral sciences*. Elsevier, 2001. ISBN 9780080430768. URL https://www.sciencedirect.com/referencework/9780080430768/international-encyclopedia-of-the-social-and-behavioral-sciences.

[91] Micha E. Spira and Aviad Hai. Multi-electrode array technologies for neuroscience and cardiology. *Nature Nanotechnology*, 8(2):83–94, 2013. ISSN 17483395. doi: 10.1038/nnano.2012.265. URL http://dx.doi.org/10.1038/nnano.2012.265.

[92] David Sterratt, Bruce Graham, Andrew Gillies, and David Willshaw. *Princeples of Computational Modeling in Neuroscience*, volume 91. Cambridge University Press, 1 edition, 2011. ISBN 9780521877954.

[93] Felice T Sun and Martha J Morrell. Closed-loop neurostimulation: the clinical experience. *Neurotherapeutics : the journal of the American Society for Experimental NeuroTherapeutics*, 11(3):553–63, 7 2014. ISSN 1878-7479. doi: 10.1007/s13311-014-0280-3.

URL http://www.ncbi.nlm.nih.gov/pubmed/24850309http://www.pubmedcentral.nih.gov/articlerender.fcgi?artid=PMC4121459.

[94] Shuohao Sun, Qian Xu, Changxiong Guo, Yun Guan, Qin Liu, and Xinzhong Dong. Leaky Gate Model: Intensity-Dependent Coding of Pain and Itch in the Spinal Cord. *Neuron*, 93 (4):840–853, 2 2017. ISSN 08966273. doi: 10.1016/j.neuron.2017.01.012. URL https://linkinghub.elsevier.com/retrieve/pii/S0896627317300363.

[95] Peter Szucs, Liliana L Luz, Raquel Pinho, Paulo Aguiar, Zsófia Antal, Sheena Y X Tiong, Andrew J Todd, and Boris V Safronov. Axon diversity of lamina I local-circuit neurons in the lumbar spinal cord. *The Journal of comparative neurology*, 521(12):2719–41, 8 2013. ISSN 1096-9861. doi: 10.1002/cne.23311. URL http://www.ncbi.nlm.nih.gov/pubmed/23386329http://www.pubmedcentral.nih.gov/articlerender.fcgi?artid=PMC3738926.

[96] Can Tao, Guangwei Zhang, Ying Xiong, and Yi Zhou. Functional dissection of synaptic circuits: in vivo patch-clamp recording in neuroscience. *Frontiers in Neural Circuits*, 9:23, 5 2015. ISSN 1662-5110. doi: 10.3389/fncir.2015.00023. URL http://www.frontiersin.org/Neural_Circuits/10.3389/fncir.2015.00023/abstract.

[97] T. Tateno, A. Harsch, and H. P. C. Robinson. Threshold Firing Frequency–Current Relationships of Neurons in Rat Somatosensory Cortex: Type 1 and Type 2 Dynamics. *Journal of Neurophysiology*, 92(4):2283–2294, 10 2004. ISSN 0022-3077. doi: 10.1152/jn.00109.2004. URL http://www.ncbi.nlm.nih.gov/pubmed/15381746http://www.physiology.org/doi/10.1152/jn.00109.2004.

[98] Simon Thorpe and Jacques Gautrais. Rank Order Coding. In *Computational Neuroscience*, pages 113–118. Springer US, Boston, MA, 1998. doi: 10.1007/978-1-4615-4831-7{_}19. URL http://link.springer.com/10.1007/978-1-4615-4831-7_19.

[99] Andrew J. Todd. Neuronal circuitry for pain processing in the dorsal horn. *Nature Reviews Neuroscience*, 11(12):823–836, 12 2010. ISSN 1471-003X. doi: 10.1038/nrn2947. URL http://www.nature.com/articles/nrn2947.

[100] Simona Ullo, Thierry R. Nieus, Diego Sona, Alessandro Maccione, Luca Berdondini, and Vittorio Murino. Functional connectivity estimation over large networks at cellular resolution based on electrophysiological recordings and structural prior. *Frontiers in Neuroanatomy*, 8(November):1–15, 2014. ISSN 1662-5129. doi: 10.3389/fnana.2014.00137. URL http://journal.frontiersin.org/article/10.3389/fnana.2014.00137/abstract.

[101] Rubia van den Brand, Jean-Baptiste Mignardot, Joachim von Zitzewitz, Camille Le Goff, Nicolas Fumeaux, Fabien Wagner, Marco Capogrosso, Eduardo Martin Moraud, Silvestro Micera, Brigitte Schurch, Armin Curt, Stefano Carda, Jocelyne Bloch, and Grégoire Courtine. Neuroprosthetic technologies to augment the impact of neurorehabilitation after spinal cord injury. *Annals of Physical and Rehabilitation Medicine*, 58(4):232–237, 9 2015. ISSN 1877-0657. doi: 10.1016/J.REHAB.2015.04.003. URL https://www.sciencedirect.com/science/article/pii/S1877065715000500.

[102] Rufin VanRullen and Simon J Thorpe. Surfing a spike wave down the ventral stream. *Vision Research*, 42(23):2593–2615, 10 2002. ISSN 0042-6989. doi: 10.1016/S0042-6989(02)

00298-5. URL https://www.sciencedirect.com/science/article/pii/S0042698902002985.

[103] Sophie Veitinger. The Patch-Clamp Technique, 11 2011. URL https://www.leica-microsystems.com/science-lab/the-patch-clamp-technique/.

[104] Feng Wang, Erik Bélanger, Sylvain L. Côté, Patrick Desrosiers, Steven A. Prescott, Daniel C. Côté, and Yves De Koninck. Sensory Afferents Use Different Coding Strategies for Heat and Cold. *Cell Reports*, 23(7):2001–2013, 2018. ISSN 22111247. doi: 10.1016/j.celrep.2018.04.065.

[105] Alan D. Wickenden. Overview of Electrophysiological Techniques. *Current Protocols in Pharmacology*, 11(1):1–11, 12 2000. ISSN 19348282. doi: 10.1002/0471141755.ph1101s64. URL http://doi.wiley.com/10.1002/0471141755.ph1101s64.

[106] Richard E. Coggeshall (auth.) William D. Willis Jr. *Sensory Mechanisms of the Spinal Cord: Volume 1: Primary Afferent Neurons and the Spinal Dorsal Horn Volume 2: Ascending Sensory Tracts and their Descending Control*. Springer US, 3 edition, 2004. ISBN 978-1-4613-4893-1,978-1-4615-0035-3. URL http://gen.lib.rus.ec/book/index.php?md5=78564fcf7b3718fc90df3321ffd07857.

[107] World Health Organization. International Perspectives on Spinal Cord Injury. Technical report, World Health Organization, 2013. URL https://apps.who.int/iris/bitstream/handle/10665/94190/9789241564663_eng.pdf;jsessionid=FBD9AADBC237B5C0FA007A567F3D9179?sequence=1.

[108] Jijun Xu, Aijun Liu, and Jianguo Cheng. New advancements in spinal cord stimulation for chronic pain management. *Current Opinion in Anaesthesiology*, 30(6):710–717, 2017. ISSN 14736500. doi: 10.1097/ACO.0000000000000531.

[109] Fleur Zeldenrust, Wytse J. Wadman, and Bernhard Englitz. Neural Coding With Bursts—Current State and Future Perspectives. *Frontiers in Computational Neuroscience*, 12:48, 7 2018. ISSN 1662-5188. doi: 10.3389/fncom.2018.00048. URL https://www.frontiersin.org/article/10.3389/fncom.2018.00048/full.

[110] Y Zhao, S Inayat, D A Dikin, J H Singer, R S Ruoff, and J B Troy. Patch clamp technique: Review of the current state of the art and potential contributions from nanoengineering. *Proceedings of the Institution of Mechanical Engineers, Part N: Journal of Nanoengineering and Nanosystems*, 222(1):1–11, 3 2008. ISSN 1740-3499. doi: 10.1243/17403499JNN149. URL http://journals.sagepub.com/doi/10.1243/17403499JNN149.